University of Zurich[UZH]

Temporal evolution of soil erosion in the Geopark Estrela (Portugal)

GEO 511 Master's Thesis

Author
Samira Stauffer
16-730-863

Supervised by
Prof. Dr. Markus Egli

Faculty representative
Prof. Dr. Markus Egli

27.04.2022
Department of Geography, University of Zurich

Abstract

Soil erosion is expected to increase in the near future, especially in the Mediterranean region due to a higher frequency of estimated drought periods. This leads in combination with heavy precipitation events to a detachment of soil particles. The aim of this thesis is to reconstruct patterns of long-, mid- and short-term soil erosion in the past 15 ka in the Estrela UNESCO Geopark, Portugal. Short-term soil redistribution emphasises the last 60 years and was assessed by using the fallout radionuclides $^{239+240}$Pu as a tracer, whereas long-term soil redistribution is based on a soil formation model. The mid-term redistribution pattern is qualitatively defined with the relationship between δ^{13}C and C.

Volumetric soil samples were collected at five slope sites, located along an altitude gradient and at two flat reference sites. The hypothesis that the sites distributed along the altitude gradient resembles a chronosequence with sites located at a higher altitude having a less developed soil state had to be rejected. Moreover, the modelled long-term soil redistribution resulted in soil erosion rates of up to 14 t ha^{-1} a^{-1}. Even though the mid-term pattern indicates soil disturbances such as cryoturbation or erosion, other sites are affected in comparison with the long-term data. The results for the short-term soil redistribution show contrary to the expectation material accumulation instead of soil erosion.

This thesis was able to show that soils are influenced by many different disturbances, which also change depending on the time-period one views. In the past, mainly changes in climate lead to soil erosion, whereas today, the anthropogenic influence is leading to higher soil redistribution rates.

Table of Contents

Table of Figures

List of Tables

Abbreviation

a	Year (lat. = annus), ka = 1000 a
AAS	Atomic Absorption Spectroscopy
Bq	Unit: Becquerel
Cs	Caesium
D_{50}	Median grain size
FAO	Food and Agriculture Organisation of the United Nations
FRNs	Fallout Radionuclides
IM	Inventory Method
LOI	Loss on Ignition
MODERN	Modelling Deposition and Erosion rates with Fallout radionuclides
P	particle size correction factor
PDM	Profile Distribution Model
Pu	Plutonium
QC	Quality Control
WI	Weathering Index
XRF	X-Ray Fluorescence

1. Introduction

1.1 Relevance

At a global scale, soil erosion is increasing and therefore classified as one of the main soil degradation processes (Borrelli et al., 2014; Panagos et al., 2019). The FAO (2015) defined soil erosion as an accelerated removal of topsoil from a land surface. This definition involves two processes: the detachment of soil particles by an external source such as by precipitation and the subsequent gravitational transport of the removed particles. The latter process is mostly driven by wind and water (Ferreira et al., 2022, Shakesby, 2011). However, today the main driver of soil erosion can be attributed to anthropogenic influences. Some of these are related to improper agricultural activities, which lead to a disturbance of the surface cover, for example by overgrazing or tillage (Borrelli et al., 2017). In addition, wildfires lead to the loss of vegetation cover (Borrelli et al., 2017), which does not only expose the soil surface to the force of nature but also results in a change of soil properties (Caon et al., 2014).

In Europe, around 70% of the overall soil erosion occurs in only 15% of Europe's land area (Cerdan et al., 2010). The soils located in the Mediterranean region are threatened the most by soil degradation processes, which include soil erosion (Ferreira et al., 2022). This is partly due to the Mediterranean climate. It is known to have very strong interannual variability with hot and dry summers, while the winters are humid and mild. This in turn influences the soil moisture, resulting in very dry soils over the summer period, which can lead to a higher susceptibility of wind erosion (Borrelli et al., 2014; Ferreira et al., 2022). In addition, drier soils are less stable and thus increasing the risk of erosion (Nunes, 2011). Consequently, the highest soil erosion rates in the European Union are estimated to occur in this region (Panagos et al., 2020). For instance, Cerdan et al. (2006) stated that soil erosion from a bare soil is around 32 t ha^{-1} a^{-1}, whereas erosion for the rest of Europe is about 17 t ha^{-1} a^{-1}. They related this difference in erosion of almost 50 % to the different rainfall regimes (Cerdan et al., 2006). Soils in the Mediterranean area are very shallow. The high pressure of human activities on the soils as well as the area being classified as one of the hotspots for climate change is resulting in very vulnerable soils (Ferreira et al., 2022). Thus, Figure 1 shows no surprise despite the fact that data used to generate the map is from 1985 to 1990 (EEA, 2009).

There are many environmental impacts not only at the site where soil erosion occurs, but also at sites where material is accumulating, leading to impacts on various biochemical processes such as the carbon cycle. However, there are still many unknown parameters in this equation (Ferreira et al., 2022). In addition, erosion also influences the amount of nutrients and organic material within a soil and thus its fertility (Alewell et al., 2020).

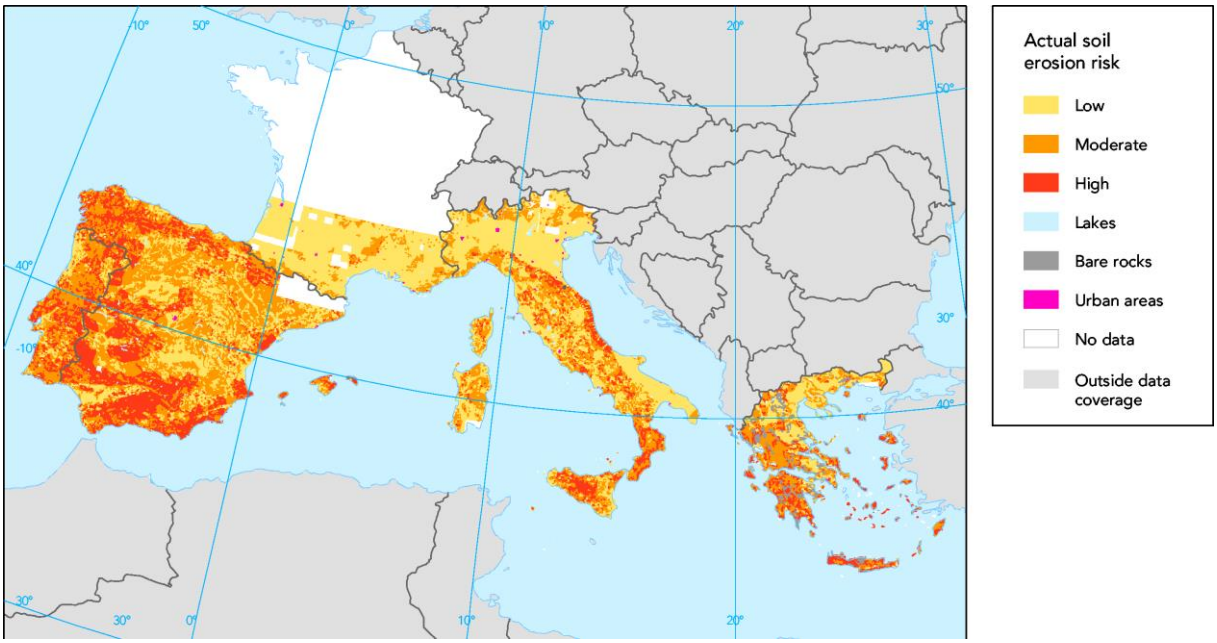

Figure 1: Actual soil erosion risk of the Mediterranean area (EEA, 2009).

Due to off-site effects such as damage to infrastructure and recreation facilities, it is important to understand how the redistribution of an eroded soil over a landscape as well as into a waterbody is (Ferreira et al., 2022).

1.2 Fallout radionuclides

To better understand the short-term soil erosion processes, fallout radionuclides (FRNs) ^{137}Cs or $^{239+240}$Pu can be used as a tracer. FRNs originated from the thermonuclear weapon testing in the 1950s and 1960s as well as during nuclear accidents such as Chernobyl in 1986 (Alewell et al., 2014; IAEA, 2014). Since the traditional soil erosion estimation approaches are very labor-intensive in combination with the need of long-term monitoring programs, FRNs are a good alternative for the quantification of how much soil has been eroded (Arata et al., 2016b; Meusburger et al., 2016). Especially, ^{137}Cs (half-life = 30.2 a) was used very often on a global scale. In the last few years, Plutonium was suggested to be used as an alternative, due to the nuclear accident of Chernobyl and the low half-life of ^{137}Cs. The isotopic composition of $^{239+240}$Pu deposited by the Chernobyl accident and the global fallout is different. Based on the ^{240}Pu/^{239}Pu atom ratio, the fallout from Chernobyl and the nuclear weapon testing can easily be distinguished (Alewell et al., 2014; Matisoff and Whiting, 2011). $^{239+240}$Pu can be categorised as non-volatile fraction of a reactor release, leading to only very short transport ranges (Arata et al., 2016a). In addition, ^{239}Pu and ^{240}Pu have a very long half-life (^{239}Pu = 42110 a and ^{240}Pu = 6561 a), which guarantees their long-term availability in a soil (Arata et al., 2016a).

After the fallout from the atmosphere, the FRNs attach to fine soil particles such as the organic matter, sesquioxide's or clay minerals (Loba et al., 2022). The binding is very strong, which is why most of $^{239+240}$Pu can be found at the surface of a soil or within the first few centimetres

(Arata et al., 2016a). They primarily move across a landscape by physical processes of soil redistribution including bioturbation and translocation (Alewell et al., 2014; Matisoff and Whiting, 2011). In addition, a lower content in the first few centimetres of the soil might be related to plant up-take right after the deposition (Chawla et al., 2010).

The key concept behind their use as a tracer for soil erosion is based on a comparison of the $^{239+240}$Pu inventory of a flat reference site and a slope site. Because of the long half-life of $^{239+240}$Pu and the knowledge that they were mostly deposited around the 1950s and 1960s, the assumption is that a lower $^{239+240}$Pu inventory is due to material being eroded, while a higher inventory can show soil accumulation (Alewell et al., 2014).

1.3 Research Question and Objectives

This thesis is imbedded in the TERRA NOVA project by Gerald Raab. TERRA NOVA is the abbreviation for “Tor Exhumation Rates and soil erosion: Relation between non-glaciated and formerly vastly glaciated areas”. In addition, it is a follow up thesis based on the master thesis by Wasja Dollenmeier, in which he compared the soil erosion rate of a former glaciated area with a non-glaciated one in the Geopark Estrela.

The emphasis is on the use of $^{239+240}$Pu as a tracer for soil erosion. The main research question is how the short-term erosion rate of the last 60 years differs between five sites, which are located in a former glacier valley. Furthermore, if there is a difference, to what extent does the erosion rate differ and what are possible reasons for this variation?

In addition, long- and mid-term trends of soil redistribution will be analysed and related to the short-term soil redistribution.

The main idea is based on a soil chronosequence, which can be described as genetically related groups of soils that evolved under comparable conditions such as climate, topography or vegetation. Spatial difference between the soils are due to the different temporal evolution of the soils (Huggett, 1998).

1.4 Hypothesis

The sampling sites are located in a valley, which was covered by glaciers, leading to the assumption that not all soils have had the same amount of time to evolve and become a stabilized soil system. Sites located near the former terminus or generally in the ablation area of the glacier should have had more time to evolve, due to the glacier’s retreat. In contrast, sites situated in the accumulation area were covered by ice for a longer time period, leading to a shorter soil formation period. Thus, the erosion rate on sites further down the valley should be smaller in comparison with sites located at higher altitude.

2. General information about the sampling location

2.1 Estrela UNESCO Global Geopark

The research location is situated in the Geopark Estrela, which is in Central Portugal, approximately 300 km north of Lisbon (see Figure 2). The total area of the Geopark is 2216 km^2. In the core of the Geopark, a mostly plateau-type mountain terrain with steep slopes can be found, known as Serra da Estrela. The top of the plateau mountain is called Alto da Torre and reaches an altitude of 1993 m a.s.l, which is the highest point of Portugal's mainland. The area of the Geopark does not only cover the mountainous region but also spans into the lowlands, where traditional villages or castles are located (Vieira et al., 2020; Vieira and Nieuwendam, 2020).

Figure 2: Location of the Geopark Estrela in Portugal (image source: Google maps)

In the Geopark Estrela there are many glaciation relicts. For instance, moraines, roches mountonnées and glacial scouring are visible. It is estimated that the glaciers covered an area of 66 km^2 during the maximum ice extent (MIE) of the last glaciation period of the Pleistocene (Vieira et al., 2021). The MIE was around 30 ka ago (Vieira and Nieuwendam, 2020). Figure 3 shows the glacier extent and among others the Candieira glacier, which formed the valley of the sampling location (Vieira et al., 2020). Overall, seven glacier tongues were reconstructed, of which the longest one had a length of 13 km. Today, this glacier is known as the Zézere glacier and the valley formed by the glacier is thus called Zézere valley (Jansen, 1998).

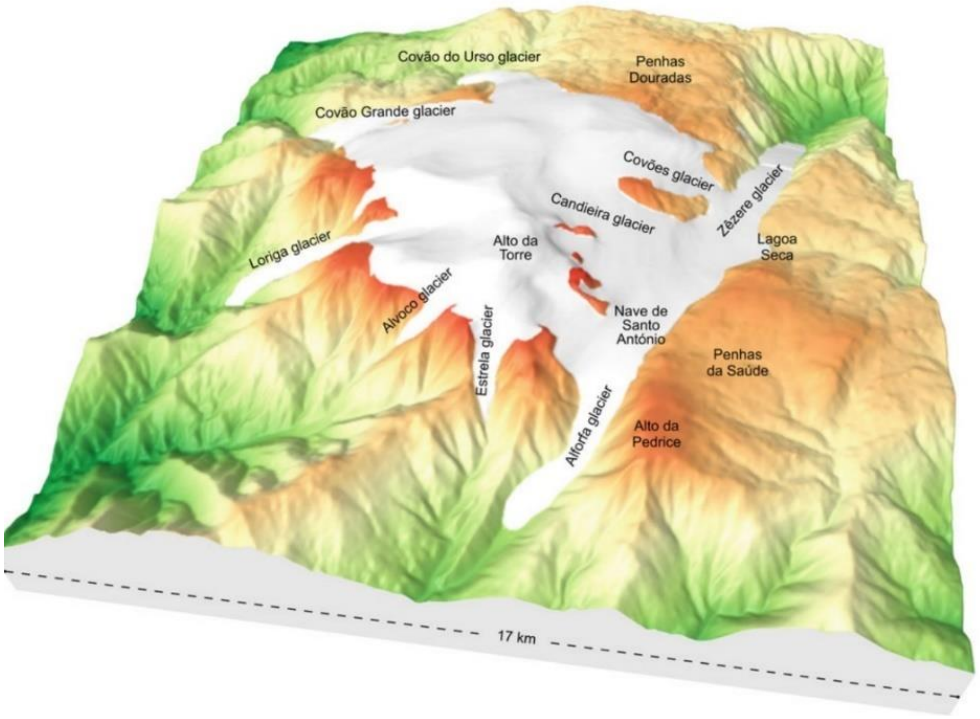

Figure 3: Estimated extent of the area covered by glaciers during the MIE in the Geopark Estrela (image source: Vieira and Nieuwendam, 2020)

Nowadays, the Geopark Estrela is one of the largest in Portugal and it serves various purposes such as the geoconservation of the landscape or as a recreation area. Until the 1980s the Candieira valley was used for agricultural purposes. Besides sheep cultivation, which did decrease over the years, there was also rye cultivation (e-mail source: José Conde). Generally, the areas used for agriculture are at slope sites below 1600 m a.s.l. Here, they also cultivated potatoes. Below 800 m a.s.l, the cultivation has its emphasis on vineyards, orchards and olive groves (Vieira et al., 2005). Moreover, in 2020 the Geopark Estrela received the UNESCO world heritage label (Vieira et al., 2020).

2.2 Climate of the Geopark

The climate can be described as Mediterranean with warm and dry summers (Vieira et al., 2005). The mean annual temperature at the Alto da Torre (1993 m a.s.l) is around 4°C and the average yearly precipitation is approximately 2500 mm at the top (Mora, 2010). During October to March the wet season occurs, where snow is not unlikely (Vieira et al., 2005). The western part of the mountain has a higher number of precipitation days. Although the eastern site has less days of precipitation, it receives in total the higher amount of precipitation (Vieira et al., 2005). In the lower areas of the park at an altitude of 1300 m a.s.l the mean annual temperature increases towards 8 – 10 °C, whereas an annual precipitation of 2000 mm can occur (Mora, 2010).

2.3 Geology of the Geopark

The geological area in which the Geopark is located is known as the Central Iberian Zone, which is a part of the Iberian Massif (Vieira et al., 2020; Vieira and Nieuwendam, 2020). It developed due to the continental collision of Laurentia and Gondwana (Ayarza et al., 2021). The geological history can be dated back to the Neoproterozoic, resulting in ages of over 650 Ma (Gomes et al., 2019). This dating is based on the Duoro-Beiras Super Group, which in turn can be described as a terrigenous sequence containing turbidites (De Castro, 2021). In addition, the Duoro-Beiras Super-Group is known as Schist-Greywacke Complex (Vieira and Nieuwendam, 2020). It can be characterised by its turbiditic lithofacies, in which the sediments show deformation and metamorphism by the Variscan orogeny leading to the development of various granites (Ferreira et al., 1987; Vieira and Nieuwendam, 2020). Some of these granites can be classified as granodiorite, biotitic granites as well as peraluminous leucogranites, biotitic granite series or two-mica granites (Vieira and Nieuwendam, 2020).

The geographical location of the Geopark is on a horst system subjected to an ongoing uplift since the Middle to Late Miocene (Martín-González, 2009) with a peak of the alpine compression in the Tortonian (Vieira and Nieuwendam, 2020). This compression leads to a pop-up like structure of the plateau mountain. The plateau is extended in a SW-NE direction and restricted by two fault-generated ridges.

2.4 Vegetation of the Geopark

Depending on the location different vegetation forms can be found as precipitation, relief and altitude changes have a strong influence on its establishment (Hu et al., 2019). Vieira et al. (2005) defined five landform groups with different vegetation. One of these landforms is the central plateau, where grasslands, bogs and dwarf shrubs formation can be found. Another group contains the slopes, which form a gradient from one vegetation to another. While the highest slopes (approximately 1600 – 1900 m a.s.l) contain a unique primary grassland, the slopes further down (i.e., from 1200 – 1600 m a.s.l) have a different vegetation. Here, it is possible to have degraded Pyrenean oak species as well as other tree species such as birch or yew (see Figure 4). In the valleys, hay meadow and riparian vegetation can be found. Due to the arid summers and human activities, wildfires occur quite frequently, resulting in a vegetation change (Shakesby, 2011).

Figure 4: Example of the vegetation of the geopark. Note that elderflower at the lower left is not a native species of the area. Image source: own image

2.5 Location of research sites

Five sites in the Candieira valley were selected as sites of interest. Additionally, two reference sites, one on top of the valley and one on the opposite side of it were defined as well. The five sites were chosen by accessibility (i.e., not covered with shrubs) and are distributed along various slopes. The reference sites are located on a flat area in order to be able to neglect erosion. Figure 5 shows the map of the sampling location. The surroundings of the first site of interest can be seen in Figure 6. Table 1 contains the coordinates as well as if available the local name of the sampling areas. In addition, sites 1 – 3 and reference site 1 are located close to small lakes or ponds.

Since the glacier retreated from the bottom of the valley to the top, older sites are supposed to be located at a lower altitude in the valley. As a result, a chronosequence with the youngest soils supposably located on the top of the valley (i.e., sites 1 and 2) and the oldest towards the lower end (i.e., sites 4 and 5) is expected. The altitude ranges from 1873 m a.s.l towards 1412 m a.s.l and the average slope gradient is 18°. Furthermore, the sites are covered with grassland. Additionally, the exposition of the different sites is covering almost each cardinal direction.

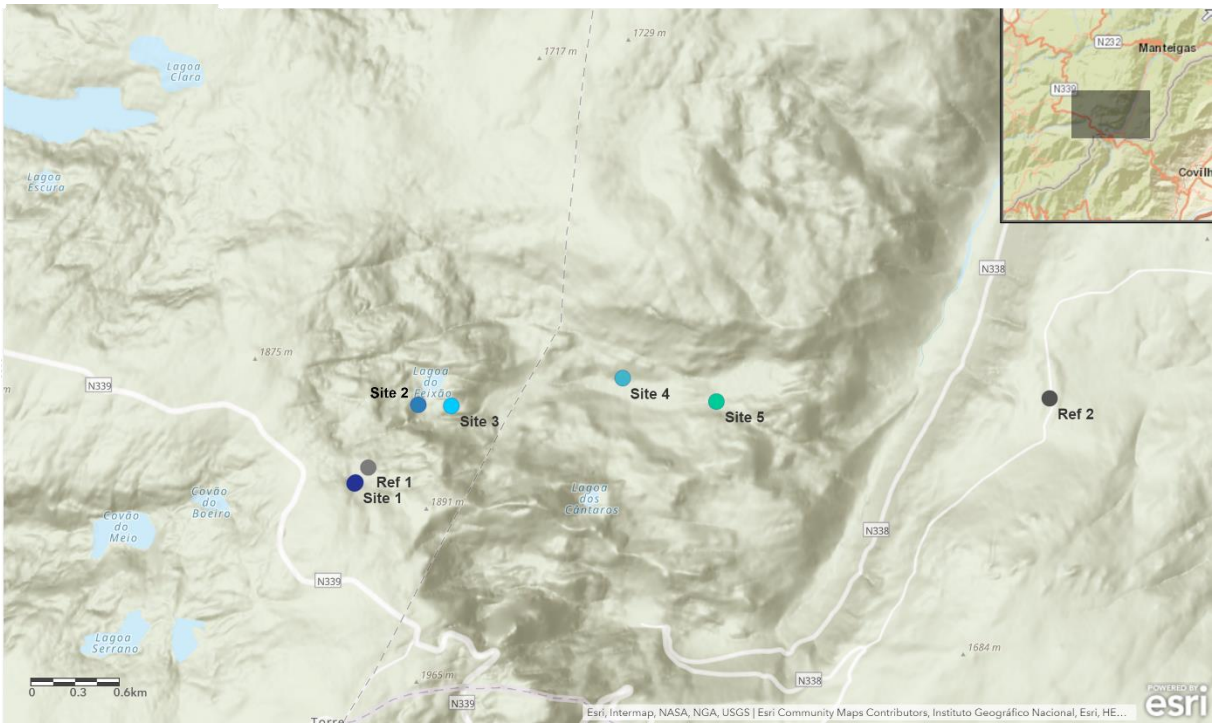

Figure 5: Map of the sampling locations in the Candieira valley. Note: reference site 2 is located at Lagoa Seca. Image source: arcmap online

Figure 6: Surroundings of the first site of interest. Image source: own image

Table 1: Information about the sampling locations

Site	Area name	Coordinates (WGS 84)	Elevation m a.s.l	Exposition °N	Slope °	Vegetation	Land use
Site 1	Salgadeiras	40.33688 N, 7.61171 W	1873	30	30	Grassland	national park
Site 1	Salgadeiras	40.33688 N, 7.61171 W	1873	45	30	Grassland	national park
Site 2	Lagoa do Peixao	40.34174 N, 7.60658 W	1645	80	12	Grassland	national park
Site 2	Lagoa do Peixao	40.34174 N, 7.60658 W	1645	60	18	Grassland	national park
Site 3	Lagoa do Peixao	40.34167 N, 7.60392 W	1582	222	10	Grassland	national park
Site 3	Lagoa do Peixao	40.34167 N, 7.60392 W	1582	230	9	Grassland	national park
Site 4	Candieria Valley	40.34201 N, 7.59009W	1429.1	190	21	Grassland	national park
Site 4	Candieria Valley	40.34201 N, 7.59009W	1429.1	185	20	Grassland	national park
Site 5	Candieria Valley	40.34192 N, 7.58252 W	1412	0	18	Grassland	national park
Site 5	Candieria Valley	40.34192 N, 7.58252 W	1412	0	12	Grassland	national park
Reference Site 1	Salgadeiras	40.33789 N, 7.61063	1848	0	0	Grassland	national park
Reference Site 1	Salgadeiras	40.33789 N, 7.61064	1848	0	0	Grassland	national park
Reference Site 2	Lagoa Seca	40.34212N, 7.55570 W	1424	0	0	Grassland	national park
Reference Site 2	Lagoa Seca	40.34212N, 7.55570 W	1424	0	0	Grassland	national park

3. Material and Methods

3.1 Field work

The field work was done in June, 2021. The sampling strategy was the same for the reference sites and the sites of interest. The only difference between the two is that the reference sites are located on a flat surface, while the sites of interest are on a slope. At each site two soil pits, within close proximity, were dug by hand. Within each pit, two replicate rows of samples were extracted. There is one exception, namely the first reference site, where one pit (R1ABC) had three replicate sample rows. The samples were collected using a volumetric cylinder (volume: 100 cm^3). Every five centimetres a sample was taken, resulting in four to seven samples per replicate row depending on the depth of the pit (see Figure 7 for a sampling illustration). The depth of the pits varies between 20 to 45 cm. Additionally, top- and if possible subsoil samples were sampled as well by collecting soil straight out of the pit with a small shovel. This results in a total of 19 soil pits in which 162 samples were collected. 111 samples are from the sites of interest and 51 from the reference sites. In addition, the pH was measured with the pH Hellige method. The soil profiles were sketched and their horizons noted. Coordinates and altitude were measured with a GPS device, while the slope angle and exposition were observed as well.

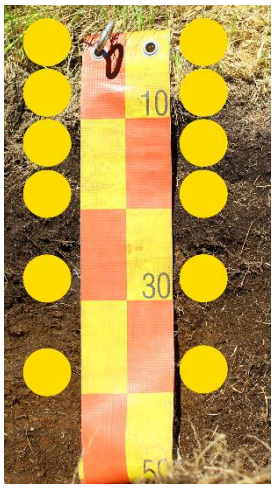

Figure 7: Sketch of the sampling, replicate rows indicated by yellow dots

3.2 Laboratory work

3.2.1 Sample preparation

In the laboratory of the University Zurich, the samples were oven-dried at 70°C for 48 hours (Egli et al., 2021). Afterwards, their dry weight was noted, followed by sieving and extraction of the skeleton part of the soil (i.e., roots and stones). The weight of the resulting fine earth (< 2 mm) was used to calculate the corresponding bulk density. For the FRN analysis, 10 g of fine earth was milled in a carbide mill (Retsch® MM400, Germany) using a tungsten cylinder with three tungsten beads for 5 minutes with a frequency of 28. In addition, for other analysis, where milled samples are required such as the XRF analysis, 10 g of fine earth was milled for 12 minutes with a frequency of 30, leading to a grain size < 63 µm (Egli et al., 2021). When the samples did not have enough fine earth to be able to mill a total of 20 g, only 6 g per frequency was milled with two instead of three beads. A common feature of these samples was their strong organic smell and thus, high organic content. Yet, enough material was milled to conduct each measurement once.

3.2.2 Chemical and physical analysis

3.2.3 pH

pH values can be used as an indication of the acidity of a soil. While already measured in the field with the pH-Hellige method, it is more precise when done in the laboratory. 5 g of fine earth was combined with 12.5 ml of 0.01 mol l^{-1} $CaCl_2$, resulting in a 1:2.5 ratio. After gently stirring for 30 minutes, followed by a 30 minutes resting period, the glass electrode was dipped into the $CaCl_2$ soil mixture and the pH of each sample was measured (Egli et al., 2021). Note that nine of the 162 samples had a very high organic content and the liquid was soaked up. In these cases, the doubled amount of liquid was used to be able to measure the pH of the soil $CaCl_2$ solution (see Table A1.1 and A1.2, values marked with a * received twice the amount of liquid).

3.2.4 Loss on Ignition

By measuring the loss on ignition (LOI) of a sample, the amount of organic material can be indirectly estimated. During the combustion, high temperature and oxygen destroy the organic particle in the sample (Pansu and Gautheyrou, 2006), leading to oxidation of the organic matter to CO_2 (Salehi et al., 2011). This results in a lower amount of sample material after the combustion. Thus, by re-weighing the sample the loss of organic carbon can be calculated (Salehi et al., 2011).

$$\frac{Sample\ weight\ after\ combustion\ [g] - dry\ sample\ before\ combustion\ [g]}{dry\ sample\ before\ combustion\ [g]} \times 100 \quad \textit{Equation 1}$$

The higher the LOI, the more organic material has been in the sample as only the inorganic material remains after the ignition.

In addition, this is the first step of the Plutonium sample preparation (see Chapter 3.4). The amount of used material as well as the duration of the ashing is based on Ketterer (2015). Even though the Plutonium analysis did not take the top- and subsoil samples into account, all samples were used for the LOI analysis. Overall, 5 g of milled fine earth material was burned for 16 hours at 550 °C in a muffle furnace (here: Nabertherm 30-3000°C).

3.2.5 C, N and $\delta^{13}C$ measurements

To determine the carbon and nitrogen content as well as the isotopic composition of $\delta^{13}C$, the Flash HT Plus elemental analyser was used, which is connected to the Delta V Plus isotope ratio mass spectrometer (eaIRMS). Each of the 162 samples was analysed. Note that all samples were measured once, except the sub- and topsoil samples. These were measured twice to ensure a more precise result. Based on the colour, smell and depth of the sample, a different amount of milled fine earth was filled in a tin capsule. Generally, for samples from a soil depth below 10 cm, 5 mg were used, whilst samples from 0 to 10 cm were only filled with 2 mg. Lastly, if the sample had a strong organic smell such as samples SSP57,

SSP58 or SSP62 only 1 mg was filled into the tin capsule.
The amount of carbon and nitrogen content is given in percent. The unit of the stable isotope $\delta^{13}C$ is permille V-PDB, in relation of the heavy ($\delta^{13}C$) towards the lighter ($\delta^{12}C$) isotope. V-PDB stands for Vienna Pee Dee Belemnite, which is the international standard (Rijk and Ekblad, 2020). For quality control a standard soil classified as Chernozem was used.

The measurement was conducted by Aline Hobi, one of the technicians of the Geography Department at UZH.

3.2.6 AAS: Oxalate extraction

To determine the chemical forms of Fe, Al and Mn in a soil, dissolution methods such as an oxalate extraction can be applied. It gives information about the soil genesis as well as it can be used as chemical criteria for classifying soil. Amorphous inorganic forms of Al, Fe and Mn, non-crystalline aluminium silicates and organically complex forms of the same elements can be removed by acid ammonium oxalate. In addition, it can dissolve poorly ordered phases such as imogolite and allophane and can be used to determine their amount in a soil (Courchesne & Turmel, 2008).

To measure the concentration of atoms, atomic absorption spectroscopy (AAS) uses the absorption of light in a flame, which is proportional to the number of atoms passing the light. To guarantee a long pathway, which in turn covers a higher absorbance, a slow type burner is used. For this measurement, the atoms need to be gaseous, which they become by passing the high-temperature flame (Bashour and Sayegh, 2007). For quality control (QC), two QC samples were measured after eight measurements and if they did not pass the control values, the samples before were re-measured.

As the method is rather time-consuming, only the 17 top- and subsoil samples were analysed. Each sample was measured twice. 2 g of sieved fine earth was used per measurement. 5 litre of an acid ammonium oxalate solution was prepared as followed: $(NH_4)_2C_2O_4 * H_2O$ (0.11 mol) and 10.9 g oxalic dihydrate $H_2C_2O_4 * 2H_2O$ (0.087 mol) was combined and topped with distilled water. The pH was adjusted to pH 3.0 (Courchesne & Turmel, 2008).

Afterwards, 100 ml of the oxalate solution was added to the samples, followed by them being covered by aluminium foil and placed on a shaker for 2 hours. Then, the sample solution was filtered. The measurement was done by Yves Brügger with an Atomic Absorption Spectrometry (AAS) (Atomabsorptions – Spektrometer contra 100BU).

The result was calculated as follows:

$$\frac{Measured\ value\ [mg\ l^{-1}] * 100\ ml\ (sample\ volume)}{sample\ weight\ [g] * dilution\ factor\ (here: 5)} \qquad \textit{Equation 2}$$

3.2.7 Total elemental concentration

To measure the total elemental concentration of the samples X-ray Fluorescence analysis (XRF) can be used. Generally, if the X-ray hits an atom, the state of the atom changes. It is now excited, leading to the release of an inner electron, which is rapidly replaced by an outer electron. This results in energy being emitted. This emittance is known as fluorescence and can be used to detect the elements in the sample. Based on the concept that each atom reacts element specifically, when the X-ray radiation hits it, its amount in the soil sample can be determined (Egli et al., 2021). Furthermore, due to the emittance of fluorescence being element specific, overlaps can be minimized. Yet, if the amount of an element in the sample is too small, it can lay below the detection limit (Brouwer, 2003).

5 g of milled fine earth was weight into tiny measuring cups. The measurement was conducted with the SPECTRO X-LAB 2000 (by SPECTRO Analytical Instruments, Germany). A standard (NCS DC 73326) was measured frequently as well and calibrations were done every third day of the measuring period. Due to the long measurement time, the measuring was supported by Yves Brügger.

All 162 samples were measured. Yet, 60 of them had a very high silicon concentration leading to erroneous results. Using an internal regression calibration curve, these 60 samples with their too high concentration could be corrected.

The acquired total contents were used to generate weathering indexes to estimate the relative soil age (Ban et al., 2017).

3.2.8 Weathering indexes

Weathering indexes (WI) are used to quantitively estimate the severity of weathering. These can be used to assess the relative age of a soil by comparing it with another soil (Ban et al., 2017). The main principle behind the applied indexes is similar, as it is based on the ratio of base cations such as Ca, K or Na to Si and/or Al (Egli et al., 2015).

Based on the XRF data the major elements (Al, Ca, Fe, K, Mg, Mn, Na, P, S, Si and Ti) were calculated into their corresponding oxide form, followed by a normalisation to 100%, where the LOI values have been taken into account as well. The oxide form was used to calculate the WI. Generally, with advanced weathering, the amounts of SiO_2, Na_2O as well as CaO decreases, whilst an increase in Al_2O_3 and TiO_2 can be seen (Ban et al., 2017).

The following chemical indexes have been applied in this thesis:

i) A-Index by Kronberger and Nesbitt, 1981

$$A = \frac{SiO_2 + CaO + K_2O + Na_2O}{Al_2O_3 + SiO_2 + CaO + K_2O + Na_2O}$$ *Equation 3*

ii) B-Index by Kronberger and Nesbitt, 1982

$$B = \frac{CaO + K_2O + Na_2O}{Al_2O_3 + CaO + K_2O + Na_2O}$$ *Equation 4*

iii) Chemical Index of Alteration (CIA) by Nesbitt and Young, 1982

$$CIA = 100\left[\frac{Al_2O_3}{Al_2O_3 + CaO + Na_2O + K_2O}\right]$$ *Equation 5*

iv) Molar ratio of (Ca+K)/Ti by Harrington and Whitney, 1987

v) Molar ratio of (Na+K)/Ti by Egli et al., 2020

vi) Weathering Index of Parker (WIP) by Parker, 1970

$$\mathrm{WIP} = 100\left[\frac{2\mathrm{Na_2O}}{0.35} + \frac{\mathrm{MgO}}{0.9} + \frac{2\mathrm{K_2O}}{0.25} + \frac{\mathrm{CaO}}{0.7}\right]$$ *Equation 6*

For the A- and B- Index, WIP as well as the molar ratios of (Ca+K)/Ti and (Na+K)/Ti the interpretation is as follows: the lower the index the more advanced the weathering. In case of the CIA it is the other way around: The higher the index the more weathered the soil is.

3.2.9 Grain size

To get a general view of the soil characteristics, the grain size can be analysed. It can be used to estimate different soil properties such as the air and water balance or the exchange capacity (Egli et al., 2021).

Before the analysis of the different grain sizes can be conducted, the fine earth needs to be pre-treated to dissolve the bounding strengths of the individual mineral grains. To dissolve them 50 g of dry fine earth is mixed with hydrogen peroxide (H_2O_2). The suspension is heated until boiling is reached. The pre-treatment is finished when the foaming stops (Egli et al., 2021).

To determine the grain size fractions of 2 mm – 32 µm, wet-sieving is used. The analysis set-up consists of a sieve tower with eight sieves, in which water flows through leading to fractionation. The fractions > 32 µm stay in their respective sieves, while the smaller ones are caught in a bucket. The fraction < 32 µm is analysed with an X-ray monitored gravity sedimentation i.e., an X-ray sedimentometer (micromerticis, SediGraph III Plus V1.02). However, this can only be done after at least 24 hours have passed as the particles in the bucket need to sink to the ground first. Thus, sedimentation needs to occur to be able to remove the water in the bucket. Note that due to the time-consuming preparation only ten out of the 17 top- and subsoil samples were analysed. Nevertheless, the grain size was determined for one soil pit of each site. If available, always the pit with top- and subsoil samples was chosen for the analysis.

3.2.10 Bulk density

Bulk density was calculated for the dry volumetric samples. It is an indirect measurement of the total pore space. It is also affected by the structure and texture of a soil. Generally, the bulk density of a sandy soil ranges from 1.3 to 1.7 g cm^{-3}, whereas the one of a fine texture mineral soil ranges from 1.0 to 1.3 g cm^{-3}. Additionally, if a soil contains a high amount of organic material, its bulk density is much lower. For instance, mineral soils can have a bulk density of only 0.4 g cm^{-3} (Bashour and Sayegh, 2007).

The calculation of the bulk density is shown in equation 7:

$$\frac{Fine\ earth,dry\ (g) + skelett,dry\ (g)}{volume\ of\ zylinder\ (g\ cm^{-3})} \qquad \textit{Equation 7}$$

3.3 Soil formation modelling for long-term soil erosion estimation

Soil formation is dependent on climate, parent material, topography, organisms and time (Jenny, 1941). It can be seen as a continuous process, during which the soil depth is increasing. This is known as a progressive process, where among other things a soil deepening occurs due to chemical weathering, in which rocks are chemically decomposed (Ban et al., 2017; Raab et al., 2018). However, if erosion occurs, a soils depth can become less deep as material from the surface has been removed (Egli et al., 2018; Yu and Hunt, 2018). This phase is called regressive soil formation (Raab et al., 2018).

Chemical weathering is restricted by solute transport and thus strongly affected by water fluxes in a soil (Egli et al., 2018). The theory behind it is based the percolation theory by Hunt and Ghanbarian (2016). Based on equation 8, the soil depth can be modelled.

$$\frac{dx}{dt} = R - E(t) = \frac{1}{1.87} * \frac{I(t)}{\Phi} * \left(\frac{x}{x_0}\right)^{-0.87} - E(t) \qquad \textit{Equation 8}$$

Where

- R: soil production function
- E(t): Erosion rate over time
- $\frac{I(t)}{\Phi}$: net infiltration rate over time
- Φ: pore volume
- x_0: median particle size known as d_{50}

The pore volume is important to know, as it influences the water flow in a soil (Egli et al., 2018). The factor - 0.87 is used as the soil formation rate decreases over time and depth, whilst d_{50} is based on the median particle size of the analysed grain size. The infiltration rate is set to be one third of the yearly precipitation.

Due to the strong altitude dependency of the yearly precipitation amount (see Mora (2010)), the precipitation input data has been calculated for each site individually based on Equation 9 (Espinha Marques et al., 2006):

$$y = 0.99x + 542.22 \qquad \textit{Equation 9}$$

where

- x: sampling location [m a.s.l]

With these input parameters, soil erosion can be modelled by using the R-Code of Egli et al. (2018) (see Appendix for more information). By iterating the amount of erosion, the theoretical modelled soil depth can be compared with the one measured in the field. As a result, the long-term soil erosion is known as soon as the two soil depths are equal.

3.4 Fallout radionuclides:

3.4.1 Extraction and Measurement of $^{239+240}$Pu

The extraction of $^{239+240}$Pu is based on Ketterer (2015). The first step is to remove the organic matter in the sample. 5 g of milled fine earth was ignited for 16 h at 550°C in the muffle furnace (here: Nabertherm 30-3000°C). Afterwards, elements such as U and Pu are extracted. This is done by adding 10 ml of 65% HNO_3. After a reaction time of two hours, 1 ml of a ^{242}Pu standard solution is added, which has a content of 0.00413 Bq g^{-1} in 2M HNO_3. To guarantee a well-mixed solution, the samples are put on a shaker and then heated in an oven for 16 h at 80°C. Afterwards, Mili-Q H_2O is added, followed by a few rounds of shaking and then the samples were centrifuged. All these steps are needed to be able to leach out the aforementioned elements from the solid soil into a liquid. The leachate is filtered and 1 ml ferrous sulphate heptahydrate ($FeSO_4$ * 7 H_2O) is added to change the species of Pu to Pu(IV). Afterwards, 1 ml of sodium nitrite ($NaNO_2$) is added as well. After shaking the samples to ensure a well-mixed solution, they are placed on a hot plate (75°C) for two hours. After the reaction occurred, 1 ml of TEVA resin is added. The Pu atoms attach to this resin and stay in the solution while all other elements such as Th or U are washed out during the following filtration process. The filtration is based on various rinses with different acids like 2 M HNO_3 or 8 M HCl. To be able to remove Pu from the TEVA resin 0.05 M ammonium oxalate is used.

The samples were measured with the 8800 ICP-MS Triple Quad at the Chemistry Department of the University of Zurich by Dr. Dmitry Tikhomirov. The measured $^{239+240}$Pu activity was corrected by Dr. Dmitry Tikhomirov to the IAEA-447 standard, by multiplying the measured activity with the correction factor of 1.1421. By comparing the $^{239+240}$Pu inventory of the flat reference sites with the slope sites, soil erosion can be assessed.

3.4.2 Soil erosion quantification

Soil erosion can be estimated by using the $^{239+240}$Pu content in the soil. Based on the two assumption that a) non-eroding sites only lose $^{239+240}$Pu by radioactive decay and b) eroding sites lose $^{239+240}$Pu by erosion (Lal et al., 2013). Thus, by comparing the $^{239+240}$Pu inventory between a reference site and a site of interest, erosion as well as accumulation can be determined. The latter is the case, when the $^{239+240}$Pu inventory is higher compared to the reference site. Currently, there are different methods used to estimate the amount of erosion. One is the Profile Distribution Model (PDM) by Walling and Quine (1990) and Zhang et al. (1990), another one is known as Inventory Method (IM) by Lal et al. (2013), whilst the third one is based on a modeling approach called MODERN by Arata et al. (2016b). These will be looked at in this thesis and are therefore, explained in more detail below.

3.4.3 Profile Distribution Model for erosion estimation

It is assumed that the amount of $^{239+240}$Pu within an undisturbed soil has an exponential decline with depth. This decline can be calculated with equation 10 (Walling and Quine, 1990; Zhang et al., 1990).

$$A'(x) = A_{Ref}\,(1 - e^{\frac{-xm}{h_0}}) \qquad \textit{Equation 10}$$

Where

- A'(x): cumulative amount of $^{239+240}$Pu until the investigated depth [Bq m^{-2}]
- A_{Ref}: mean $^{239+240}$Pu inventory of the reference site [Bq m^{-2}]
- Xm: takes the depth from soil surface and mass into account [kg m^{-2}]
- h_0: coefficient describing the profile shape [kg m^{-2}] and thus the depth trend of $^{239+240}$Pu

Generally, the higher h_0 is, the deeper $^{239+240}$Pu has penetrated into the soil. Based on the two assumptions that i) the depth distribution of $^{239+240}$Pu within a soil profile is independent of time and ii) the total fallout occurred in 1963 (i.e., the year in which the nuclear testing peaked), the erosion rate can be calculated (see equation 11) (Walling and He, 1999; Walling and Quine, 1990; Zhang et al., 1990).

$$Y = \frac{10}{t-1963} * ln\left(1 - \frac{X}{100}\right) * h_0 \qquad \textit{Equation 11}$$

Where

- Y: erosion rate [t ha^{-1} yr^{-1}]
- t: Sampling year (here: 2021)
- X: reduction of the total $^{239+240}$Pu inventory [%]
- h_0: coefficient describing the profile shape [kg m^{-2}] and thus the depth trend of $^{239+240}$Pu

3.4.4 Inventory Method for erosion estimation

Another way to estimate the erosion is by applying the Inventory Method by Lal et al. (2013). Generally, they defined the Invenotry I of a $^{239+240}$Pu fallout as followed:

$$I = \int_0^{Z_{max}} N(z)dz \qquad \text{Equation 12}$$

Where

- I = Inventory [mBq cm^{-2}]
- z_{max}: depth towards bottom of the soil pit
- N(z): content of Pu [mBQ cm^{-1}] at this depth (z[cm])

The loss of $^{239+240}$Pu is calculated like this:

$$I_{loss} = I_{Reference} - I_{Site\ of\ Interest} \qquad \text{Equation 13}$$

Depending on the history of the site two land-use scenarios with ploughed and unploughed soil can be distinguished. This thesis only looks at the unploughed scenario. Here, the $^{239+240}$Pu depth profile should remain more or less exponential, due to material loss from the surface. Additionally, during the process of erosion, finer-graded material is preferably removed. This is exactly the material, which has because of its larger surface to volume ratio also a higher $^{239+240}$Pu content. Especially, in comparison with the bulk material. Thus, a particle size correction factor needs to be taken into account (Arata et al., 2016a; IAEA, 2014).

$$I_{loss} = \int_0^L N(0)e^{-\alpha z}dz \qquad \text{Equation 14}$$

$$with: L = -\frac{1}{\alpha P} * ln\left(1 - \frac{I_{loss}}{I_{ref}}\right) \qquad \text{Equation 15}$$

Where

- L: loss of soil / erosion
- P: particle size correction factor (P > 1)
- α: exponential factor for the shape of the $^{239+240}$Pu depth profile (Arata et al., 2016a)

3.4.5 MOdellig Deposition and Erosion rates with RadioNuclides (MODERN)

MODERN was developed by Arata et al. (2016b). It can be used to convert fallout radionuclides into soil redistribution processes. Thus, it is able to quantitively estimate how much soil erosion or accumulation occurred. In comparison with the above-mentioned methods, this modelling is independent on the depth function shape, which is an advantage. In addition, it can also be used for different land use scenarios such as ploughed and unploughed soils. This allows the comparison of the reference site with the total inventory of the site of interest. The main assumption behind the modelling is that both sites have the same development in regards of the depth distribution of the FRNs (Arata et al., 2016b).

The model of the depth profile of the reference site is based on a step function *g(x).* At each increment (*inc*) the function returns a value Inv_{inc} [Bq m^{-2}]. In the end, the result *Inv* contains the total inventory of the FRN of a site of interest, measured for the depth of the soil profile *d* [cm]. Moreover, the model focuses on the soil level x*[cm] from x* to x* + d [cm]. Here, the cumulative FRN inventory of the reference site is equal to the cumulative FRN inventory of the site of interest (Arata et al., 2016b). Based on this, the authors defined that x* must fulfil Equation 16:

$$\int_{x^*}^{x^*+d} g(x)dx = Inv \qquad \textit{Equation 16}$$

By adding a number of simulated layers above and below the reference site, possible soil redistributions can be found. This can be modelled with Equation 17:

$$S(x) = \int_{x}^{x+d} g(x')dx \qquad \textit{Equation 17}$$

Where

- S(x) = Simulated total inventory of FRN of the reference site [Bq m^{-2}]

This function can be solved by using the primitive function G of the original distribution function *g(x)*:

$$S(x) = G(X + d) - G(x) \qquad \textit{Equation 18}$$

As MODERN returns the amount of soil erosion or accumulation in cm, the results can be converted to annual soil losses or gains Y [t ha^{-1}] for easier interpretation of the data. Equation 19 shows the conversion.

$$Y = 10 * \frac{x^* * xm}{d * (t_1 - t_0)} \qquad \textit{Equation 19}$$

Where

- xm: mass depth of the site of interest [kg m^{-2}]
- d: total depth increment of the site of interest
- t_1: sampling year (here: 2021)
- t_0: reference year (here: 1963, peak of nuclear weapon testing)

3.5 Statistics

To assess if there is a difference between the different input data (i.e., the two reference sites) as well as how the measured $^{239+240}$Pu data is distributed within and along the sites, statistical tests such as a t-test for normally distributed data or a Wilcoxon-test for not normally distributed data with dependent samples are used. In addition, different correlations are applied to see if there is a statistical relationship between the data.

4. Results

4.1 General information about the soil profiles

The soils from all analysed sites can be characterised as Cambisols and Umbrisols. Figure 8 shows one pit per site of interest. A common feature of all the soils is the deep rooting systems of the grass vegetation, which can be seen on some pictures. Generally, the soils have a relatively thick organic layer consisting of a Rhizic Moder, which known as “Wurzelfilzmoder” in the German classification system (Kneisel et al., 2015). Site 4, where the organic layer can be classified as “Mull”, is an exception. Furthermore, this site has the least amount of visible roots in the soil (see Figure 8) and the darkest soil colour. The depth of the pits varies, even within the same location (see Table 2). During the sampling, the C horizon was often not reached. In addition, the above-ground vegetation is very similar between all sites as it consists of grass species. Based on the sample depth, the soil was divided into top- and subsoil. Topsoil includes the first 20 cm and the subsoil the samples from a depth below 20 cm.

Table 2: Information about the soil pits

Site	**Soil Type WRB**	**Soil Horizons**	**Pit depth**
Site 1	Cambisol	OR - Ah - AC - C	45 cm
Site 1	Cambisol	OR - Ah - Ac - bA - AB	35 cm
Site 2	Cambisol	OR - Ah - AhE - Bw	40 cm
Site 2	Cambisol	OR - Ah – Bw	20 cm
Site 3	Cambisol	OR – Ah	30 cm
Site 3	Cambisol	OR – Ah	30 cm
Site 4	Umbrisol	OC – C	35 cm
Site 4	Umbrisol	OR – OC	25 cm
Site 5	Cambisol	OR - Ah – AC	30 cm
Site 5	Cambisol	OR- Ah – Ac	30 cm
Reference Site 1	Cambisol	OR - Ah – BC	40 cm
Reference Site 1	Cambisol	OR - Ah - Ac - bOh	25 cm
Reference Site 2	Cambisol	Ah – Bw	30 cm
Reference Site 2	Cambisol	Ah-Bw	30 cm

Site 1 (Pit 6AB)

Site 2 (Pit 2AB)

Site 3 (Pit 3AB)

Site 4 (Pit 7AB)

Site 5 (Pit 10AB)

Reference Site 1
(Pit R1ABC)

Reference Site 2
(Pit R3AB)

Figure 8: Soil pits of each site

As mentioned in Chapter 3.1, two replicate values per depth were measured for each soil pit. Therefore, usually four values per depth are available at each site. These were used to calculate a mean value per depth for each of the five sites of interest as well as for the two reference sites. The raw values can be seen in Table A1.1 and A1.2.

4.2 Chemical characteristics

4.2.1 pH

Generally, the pH values are in a range of 3.0 to 4.1 (see Figure 9). The most acidic soils can be found at site 1, respectively at reference site 1, with values between 3 and 3.8. Site 2 and 4 are very similar in the topsoil, while they vary around 0.4 in the subsoil. Site 3 mirrors these two sites. Thus, its measured pH decreases, followed by an increase and then another decrease. In theory, the pH should increase with depth, which is visible at some sites but not at all of them (Habte, 1999). Furthermore, site 5 can still be characterised as acidic. However, in comparison with the other sites of interest it is the least acidic and has the highest variation. Again, a decrease can be seen in the subsoil. This time it is about 0.2. Reference site 2 resembles site 3. Yet, it is slightly less acidic and instead of a decrease an increase is measured.

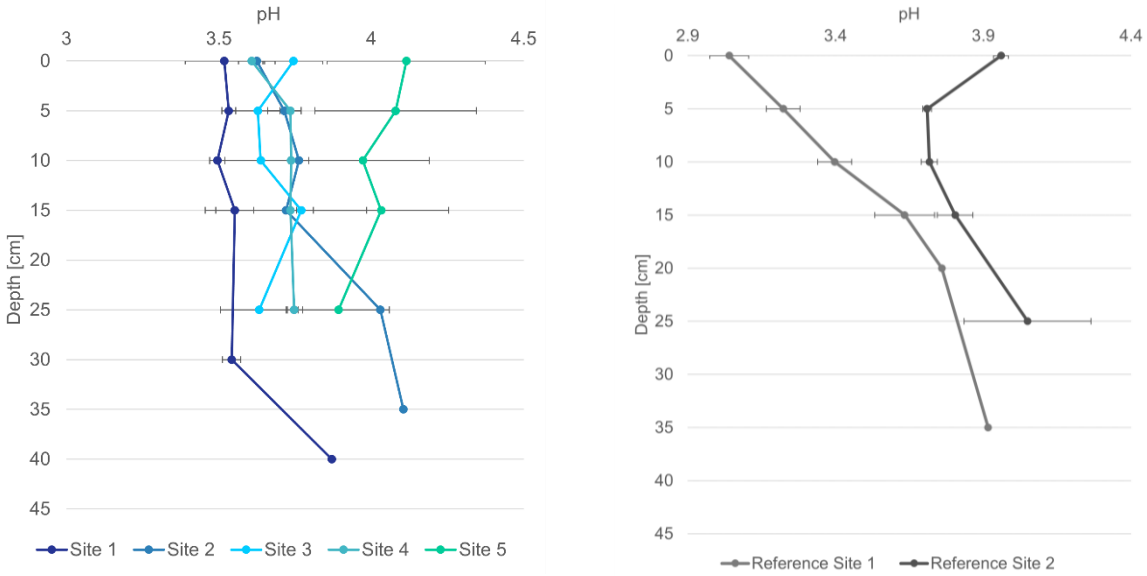

Figure 9: pH distribution with depth. Left: sites of interest, right: reference sites

4.2.2 Loss on ignition

Figure 10 shows the LOI for each site of interest and the reference sites. Overall, a decreasing LOI with depth is visible. The variation between the sites is rather high as it ranges from 12% loss of organic material at site 4 to almost 50% loss at site 1. Yet, site 1 has a very high standard deviation for the depths of 0 to 5 cm (48.80 ± 13.10%) and 5 to 10 cm (29.08 ± 10.73%). Sites 3 and 5 have a similar pattern. Furthermore, for the depth range of 10 to 15 cm all samples except the ones from site 1 show a comparable decrease. The subsoil samples variate more. Site 1 follows the same trend as it is the case for reference site 1. Moreover,

reference site 1 has for the whole depth distribution a very high standard deviation. Reference site 2 has less loss of organic material than reference site 1 and is overall most similar to site 4.

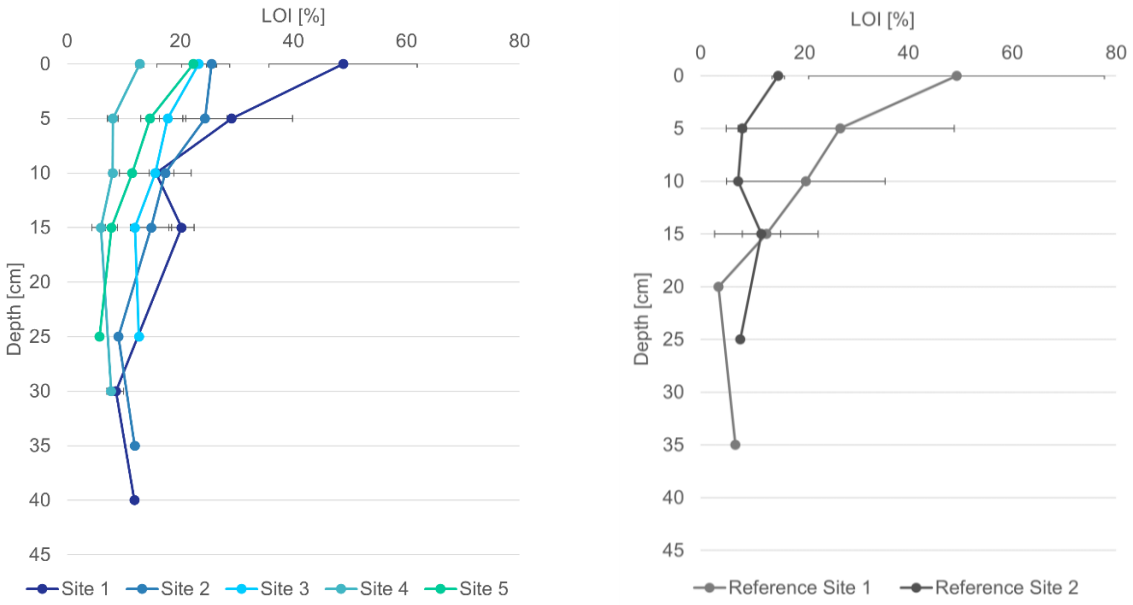

Figure 10: LOI with depth. Left: sites of interest, right: reference sites

4.2.3 Carbon content

The carbon content of the soils varies between 6 and 23% within the first 5 cm (see Figure 11). Afterwards, a strong decrease with depth can be seen. The highest amount of C can be found in the samples from site 1, whereas site 4 has the lowest C content on average. Sites 3 and 5 seem to mirror each other regarding the C content development with depth. For the top 10 cm, reference site 1 follows a similar pattern like site 1. However, the C content for the sample depth of 10 to 15 cm at site 1 increases, while there is a decrease at the first reference site. Another similar depth trend can be seen at site 4, site 5 and the second reference site. Yet, the amount of C in the soil at site 5 is higher compared with site 4 and reference site 2. At the subsoil level, the C content levels off at around 5%. However, this is only the case for both reference sites as well as the first, second and fourth site of interest. Site 5 has a lower C content with only 1.5% C at a depth of 25 cm. In contrast, site 3 has a higher C content with 6.5% C at the same depth.

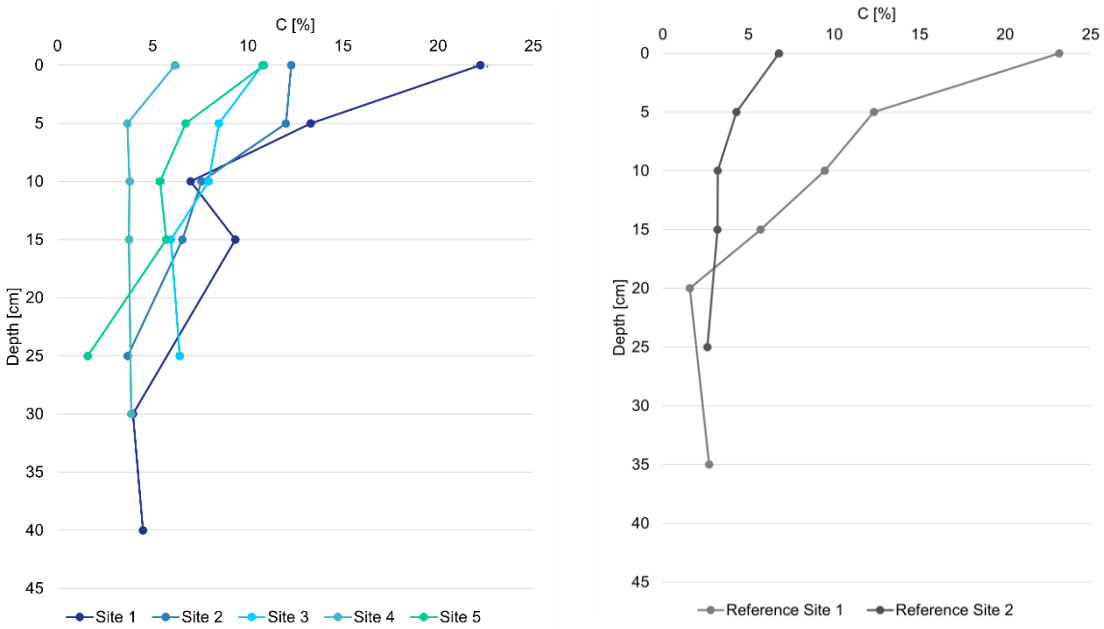

Figure 11: C content [%] with with depth. Left: sites of interest, right: reference sites

4.2.4 Nitrogen content

Generally, the nitrogen content decreases with depth. The first reference site as well as the first site of interest have a very high standard deviation within the topsoil. The lowest N concentration is found at the fourth site of interest with values in the range of 0.39 ± 0.94% in the topsoil and 0.20 ± 0.01% in the subsoil, followed by the fifth site (0.81 ± 0.20%). Sites 2 and 3 seem to have an opposite trend, i.e., high N concentration at site 2, whilst a lower N concentration can be seen at the same depth in the samples of site 3. The first interest site shows a strong decrease like the first reference site. However, as the decrease continues at the reference site, a slight increase can be seen at the first site of interest (see Figure 12).

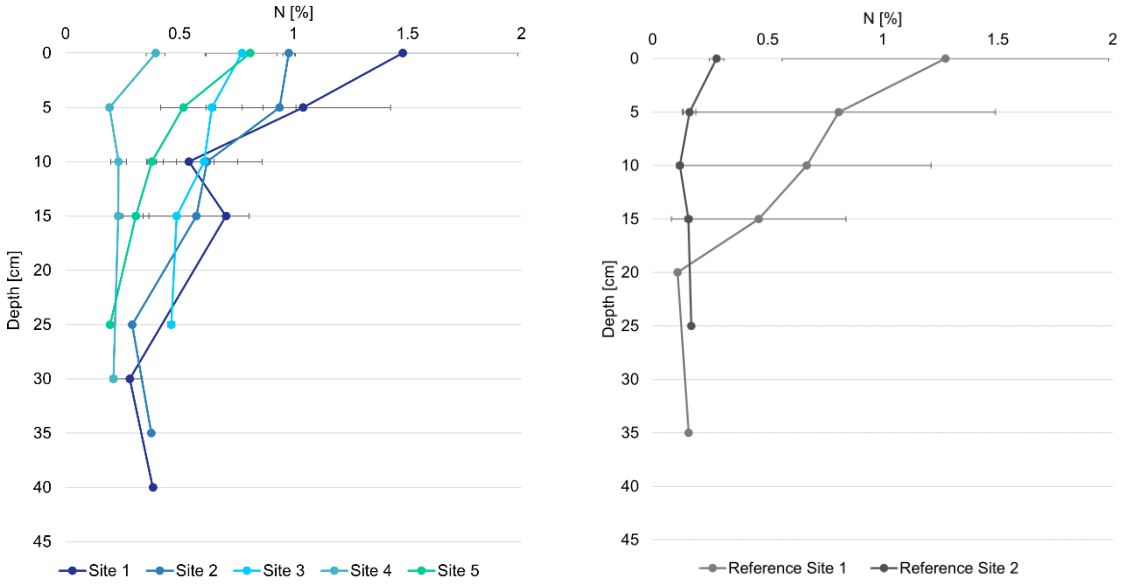

Figure 12: N [%] distribution with depth. Left: sites of interest, right: reference sites

4.2.5 Carbon and nitrogen ratio

Figure 13 shows the CN ratio of all sites. Overall, the CN ratio of the first, second and third site of interest have a similar pattern, while site 4 and 5 mirror each other within the first 15 cm. A strong decrease of is 10 visible at site 5 in the subsoil, whereas site 4 increases again. The second reference site has the highest CN ratio, with a decreasing trend after the first 10 cm, whilst the ratio of the first reference site decreases, followed by an increase resulting in a similar ratio at the subsoil of 35 cm as it had at the start at 0 cm.

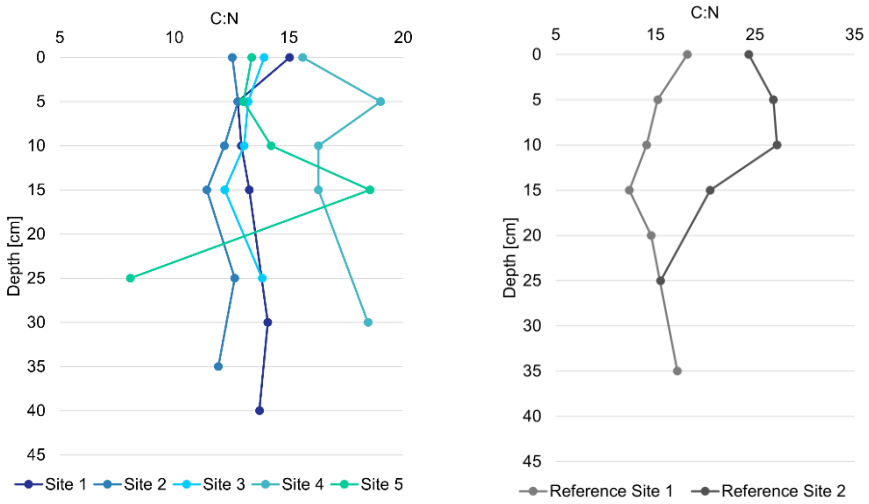

Figure 13: CN development with depth. Left: sites of interest, right: reference sites

4.2.6 $\delta^{13}C$ and C as erosion proxy

Overall, the $\delta^{13}C$ values are in the range of -28‰ to -25.5‰ V-PDB. Moreover, an increase in the depth of the first 20 cm can be seen (see Table A1). The main idea behind the use of $\delta^{13}C$ and C as a proxy for erosion is based on the consideration that in an undisturbed oxic soil system the carbon content decreases with depth, whilst the $\delta^{13}C$ values increase and become less negative (Meusburger et al., 2013). A high correlation between these two variables can reflect an enrichment of the isotope ^{13}C, due to the decomposition of the organic carbon in an undisturbed and thus, non-eroded soil (Portes et al., 2018). To conduct a correlation between the $\delta^{13}C$ values and the C content in the samples a Shapiro-Wilk test is applied to test if the data is normally distributed. This is the case for the second and third site of interest ($p > 0.05$), which is why a Pearson correlation was conducted. All other sites including the reference sites have at least one variable, which is not normally distributed. In these cases, a Spearman correlation was applied. Table 3 shows the correlation values, while Figure 14 shows the relationship graphically.

Table 3: Correlation values of $\delta^{13}C$ values C

Site	Site 1	Site 2	Site 3	Site 4	Site 5	Ref. Site 1	Ref. Site 2
Correlation	-0.51	-0.14	-0.46	-0.62	-0.79	-0.85	-0.93

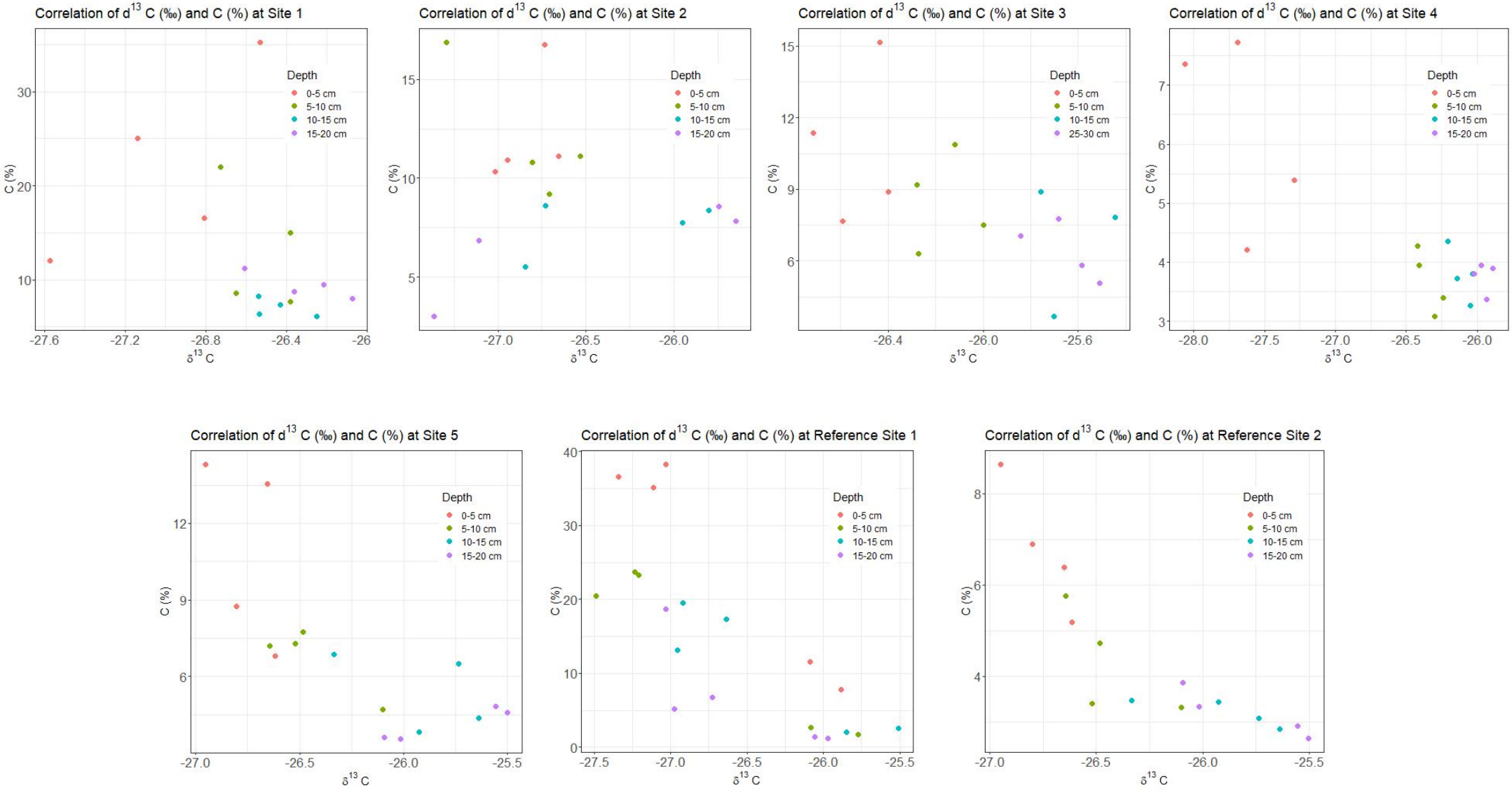

Figure 14: Correlation of $\delta^{13}C$ with C for the first 20 cm. Note that only the first 20 cm were looked at to have approximately the same amount of input data. An exception is site 4, where no samples for the depth 15 – 20 cm were collected. Here, the depth 20 – 25 cm was used. In addition, due to three replicate sample rows at one of the soil pits at reference site 1, each depth contains one more data point.

4.2.7 Oxalate extraction

Only the top- and subsoil samples have been used for the oxalate extraction. Table 4 shows the respective mean value per site. Four values are considered for the mean and standard deviation as each site has two soil pits and each sample was measured twice. Overall, the oxalate extraction gives an indication about how many weathering products were formed over time. Thus, the higher the number, the more weathered products there are (Dahms et al., 2012).

Generally, it is visible that the topsoil from site 2 has the highest values of all sites of interest. The second reference site has the overall highest Fe_o and Al_o values. The Mn_o values are in the range of 0.013 – 0.025 g kg^{-1}, with two possible outliers. One at site 5 (0.0528 g kg^{-1}) and another one at reference site 2 (0.0357 g kg^{-1}). Yet, one is found in the topsoil and the other one in the subsoil, respectively. The Fe_o concentration varies even more. For example, within the three subsoil samples there is a difference of almost 4 g kg^{-1}. In addition, the expectation is that topsoil samples contain a higher number of weathered products as soil formation starts at the surface (Dahms et al., 2012). However, this is not the case, when the few top- and subsoil samples are compared.

Table 4: Mean values the oxalate extraction with the top- and subsoil samples

Site	Fe_o mean [g kg^{-1}]	Fe_o sd [g kg^{-1}]	M_o mean [g kg^{-1}]	Mn_o sd [g kg^{-1}]	Al_o mean [g kg^{-1}]	Al_o sd [g kg^{-1}]
Site 1 Topsoil	0.7598	0.2228	0.0148	0.0002	2.6134	0.0684
Site 2 Topsoil	1.2380	0.4803	0.0180	0.0003	4.0788	0.0085
Site 2 Subsoil	0.0764	0.0000	0.0130	0.0000	5.9300	0.0000
Site 3 Topsoil	0.7233	0.2980	0.0146	0.0001	2.6319	0.0356
Site 4 Topsoil	0.6793	0.1917	0.0135	0.0000	2.1489	0.0166
Site 5 Topsoil	0.4867	0.1553	0.0528	0.0012	2.9805	0.0798
Reference Site 1 Topsoil	0.2299	0.1188	0.0187	0.0019	2.4958	0.0852
Reference Site 1 Subsoil	0.1111	0.0000	0.0134	0.0000	2.6625	0.0000
Reference Site 2 Topsoil	1.8706	0.0541	0.0255	0.0000	2.3240	0.0293
Reference Site 2 Subsoil	4.0318	0.0000	0.0357	0.0000	7.2150	0.0000

4.2.8 Major oxide forms based on the total elemental concentration

SiO_2 is most abundant over all samples, followed by Al_2O_3. The third most common oxide is K_2O, except for site 1 and site 2, where more MgO than K_2O can be found. Generally, SiO_2, Al_2O_3 and K_2O are the oxides, which are most abundant in granite (Amelung et al., 2018). In addition, TiO_2 is used as an immobile element in the molar ratio of two weathering indexes.

4.2.8.1 SiO_2

The SiO_2 concentration increases until a depth of 15 cm, where a slight decrease can be seen (see Figure 15). Reference site 2 and the third site of interest have a similar development, with

reference site 2 having a slightly higher concentration as long as the emphasis is on the topsoil. Afterwards, site 3 has the higher concentration. Site 1 and reference site 1 have the lowest amount of SiO_2 in the first 5 cm with +/- 35%. The other sites start at around 55 – 65%.

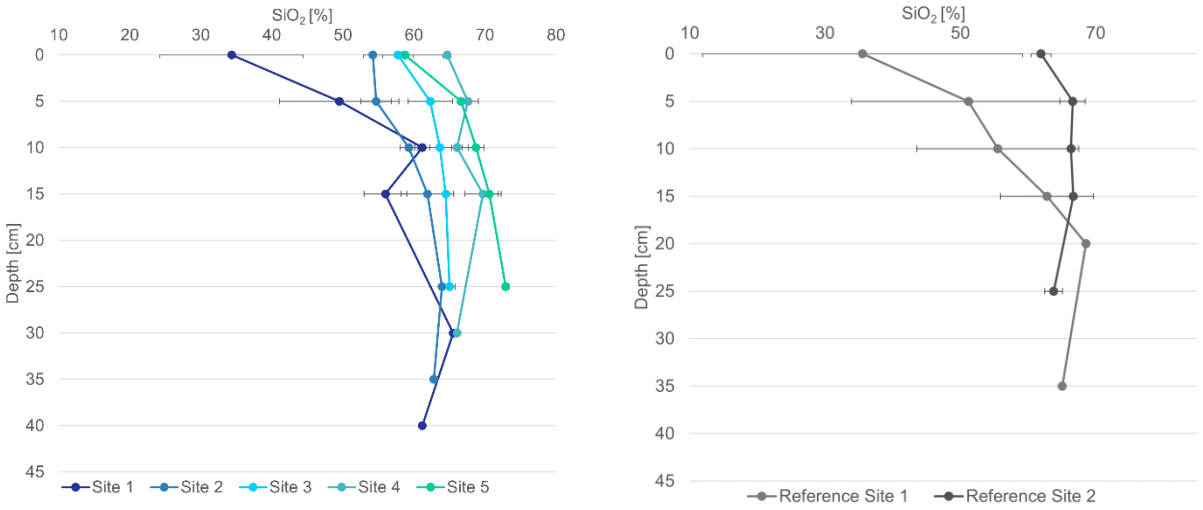

Figure 15: SiO_2 distribution with depth Left: sites of interest, right: reference sites

4.2.8.2 Al_2O_3

As shown in Figure 16 the concentration of Al_2O_3 is for all samples between 8 - 16%. Moreover, an increase with depth can be seen at each site. Site 1 and reference site 1 are again very similar in their depth trend, just as site 4 and reference site 2 are. The lowest Al_2O_3 concentration was found at site 5 and the highest one is at the second reference site.

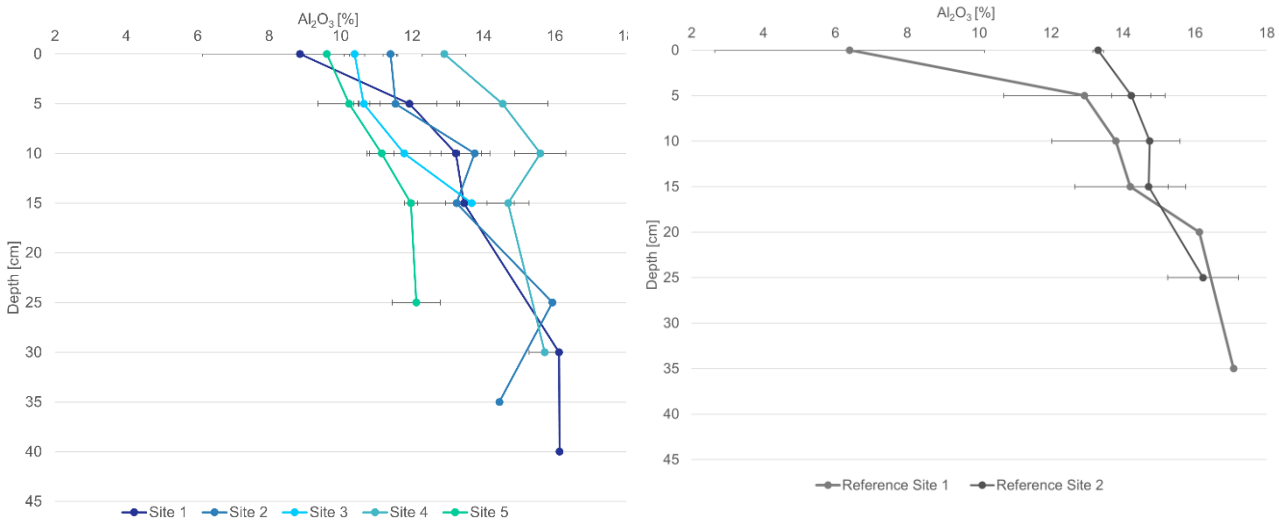

Figure 16: Al_2O_3 distribution with depth. Left sites of interest, right: reference sites

4.2.8.3 K_2O

K_2O does have a range of 2 – 6%, which is lower in comparison with SiO_2 and Al_2O_3. In Figure 17 a slight increase with depth can be seen as well. Site 1 and site 3 show a similar development. Yet, site 1 has a lower concentration in the first 5 cm. The strongest increase

with depth can again be seen in the data from reference site 1. Site 4 and reference site 2 also have a similar pattern as observed above.

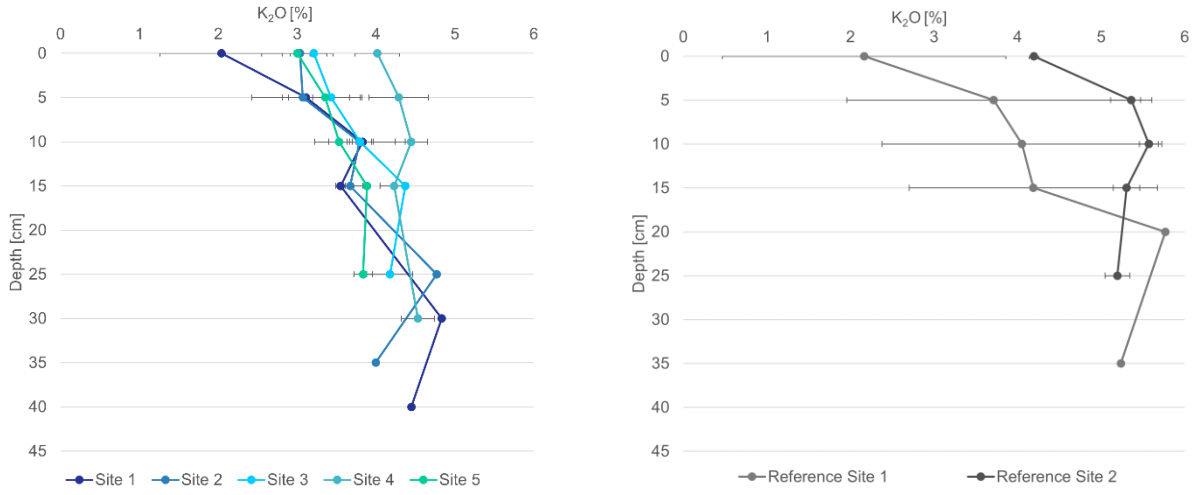

Figure 17: K2O distribution with depth. Left: sites of interest, right: reference sites

4.2.8.4 MgO

The lowest amount of MgO can be found at the fifth site of interest (0.49 ± 0.01), whereas the highest one is at site 2 (0.61 ± 0.06) (see Figure 18). A decreasing pattern with depth is visible at sites 1, 2 and 5, while sites 3 and 4 have a slight increase. This is also the case at the reference sites, where again an increase with depth can be observed. However, while there is an increase until a depth of 15 cm at reference site 1, the second reference site does have a decrease, followed by an increase in the subsoil.

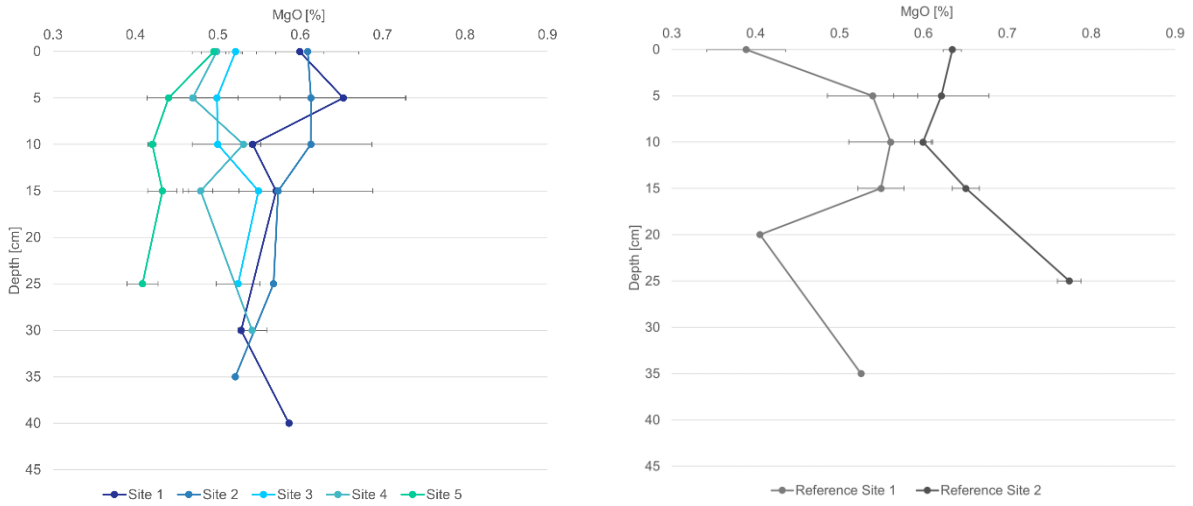

Figure 18: MgO distribution with depth. Left: sites of interest, right: reference sites

4.2.8.5 TiO_2

TiO_2 is an important oxide for the weathering indexes. Yet, it is not really abundant in comparison with the other oxides. Its values range from 0.01 – 0.40%. As seen in Figure 19 the highest concentration can be found in the second reference site (0.30 – 0.40%), whilst the

lowest one is at site 4. The development of reference site 1 resembles a semi-circle. After an increase of 0.10%, it still increases but only lightly, followed by a decrease of 0.07%. As far as the data shows, it is constant in the subsoil for the next 15 cm. The first site of interest shows a zigzag development, while the values for the subsoil seem more or less constant with depth. Sites 3 and 5 are mirroring each other.

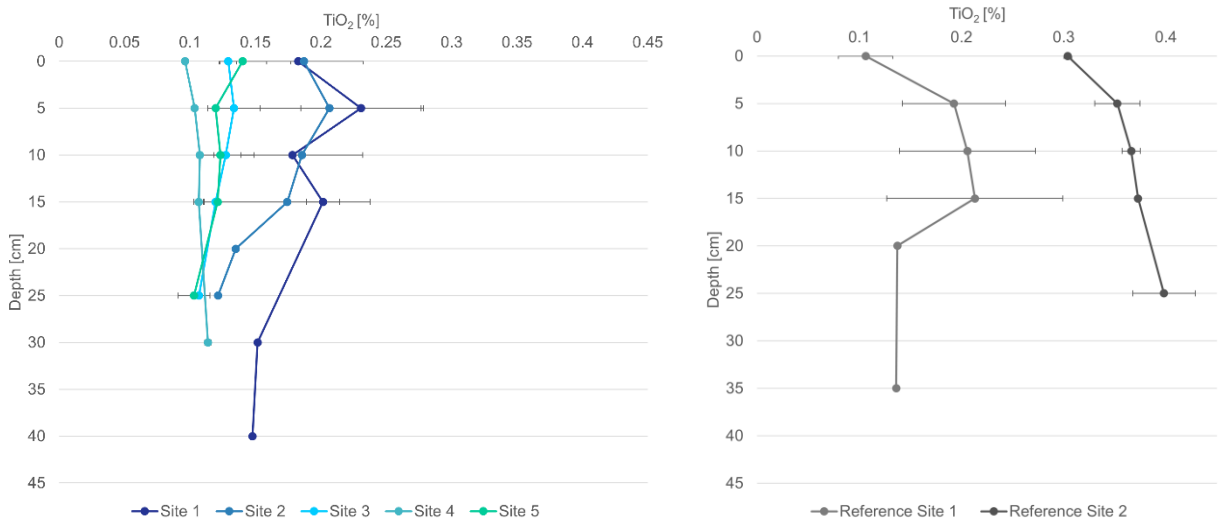

Figure 19: TiO_2 distribution with depth. Left sites of interest, right: reference sites

4.2.9 Weathering indexes

4.2.9.1 A-Index

Figure 20 shows the ratio of the A-Index, which is between a range of 0.88 and 0.92 for top- and subsoil. This is true for both the sites of interest as well as the two reference sites. The development of sites 3 and 5 is very similar, with an increasing edge at a depth of 5 cm, followed by a decrease until a depth of 15 cm, where again an increase can be seen. The pattern of sites 1 and 4 seem to mirror each other until a depth of 15 cm. Site 2 has a very similar ratio as site 4 for the soil depth of 5 to 15 cm. At reference site 1, a strong decrease within the first five centimetres can be seen. Afterwards, the ratio increases until a decrease in the subsoil can be observed. The ratio for the second reference site is smaller. Yet, a decrease occurs at the top- and subsoil border. Reference site 1 and the first site of interest have the highest variation (see Table A 3.1 & A 3.2).

Kronberg and Nesbitt, 1981 stated that the smaller the ratio, the more advanced the weathering is. This leads to the following ranking: Site 5 is based on this index the least weathered site, followed by site 3, site 4 and site 2. The most weathered site is therefore site 1. In addition, reference site 2 is less weathered than reference site 1.

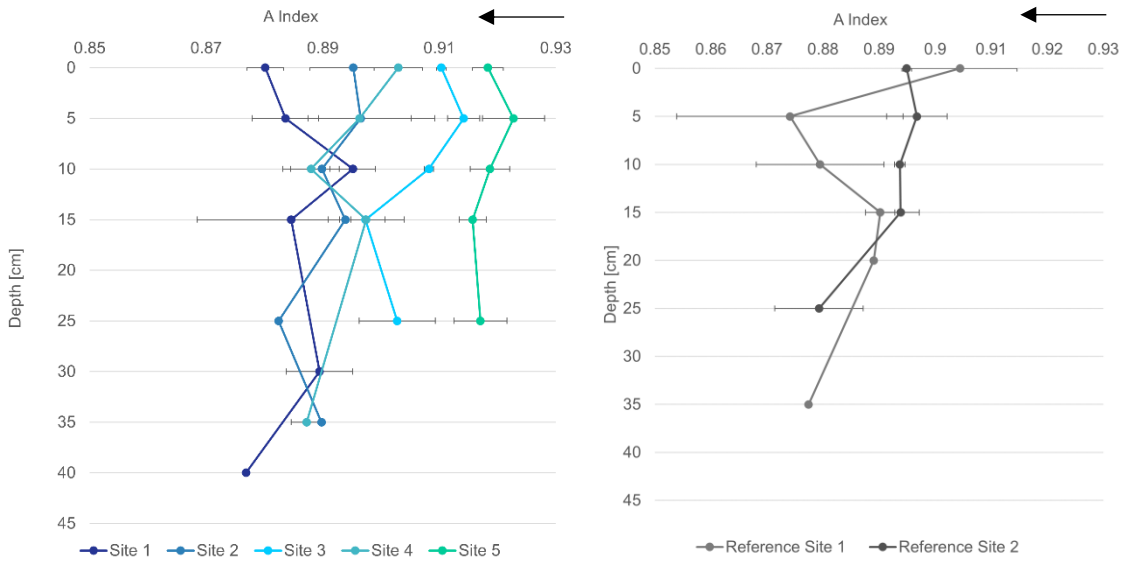

Figure 20: Depth distribution of the A-Index Left: sites of interest, right: reference sites. Arrow indicates increased weathering.

4.2.9.2 B – Index

The B – Index is similarly calculated as the A-Index. However, it is important to note that here SiO_2 is not taken into consideration. This results in lower index values and gives a slightly different impression regarding the weathering degree. The index range is between 0.38 and 0.47 (see Figure 21). Thus, around half of the A-Index. Here, the development of the individual site is more distinguishable than before. Site 3 and 4 seem to mirror each other, while there is a zigzag pattern at site 1 and site 2. Site 5 has again the highest ratio. A mirrored pattern can also be observed in the data from the reference sites. The strong increase at reference site 1, was also found in the A-Index. Moreover, this site has the highest data variation.

As before, the smaller the index, the more weathered a soil is. Thus, site 5 is again the least weathered site. There is a shift as site 4 seems to be less weathered than site 3. Followed by site 1 and site 2. It is not as straight forward, when the emphasis is on the reference sites. Depending on the depth one site is more weathered than another, especially by considering the standard deviation at reference site 1. Thus, no clear statement can be made at this point.

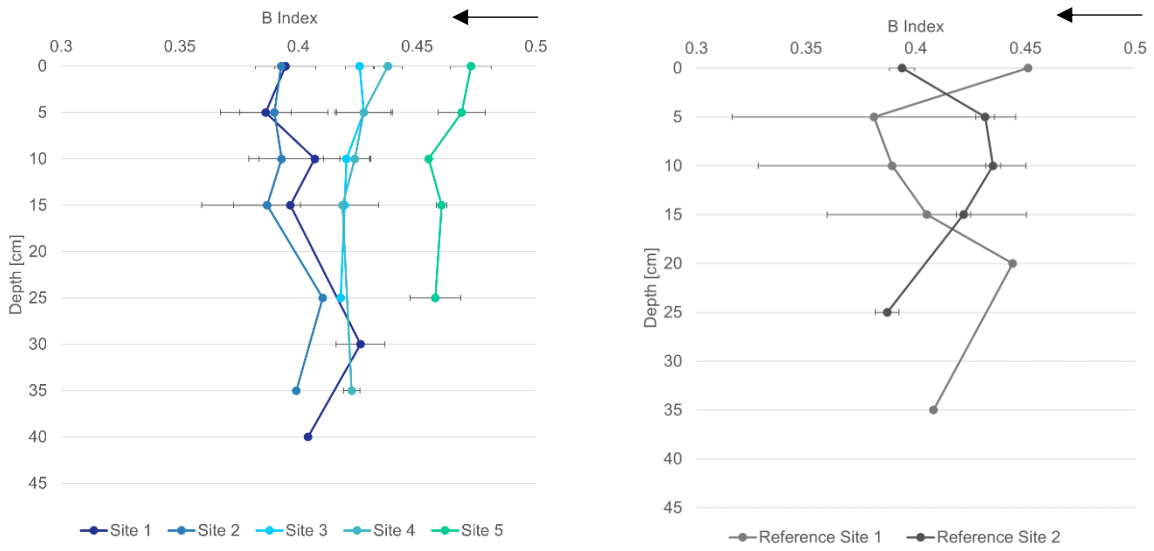

Figure 21: Depth distribution of the B-Index. Left: sites of interest, right: reference sites. Arrow indicates increased weathering.

4.2.9.3 (Ca+K)/Ti

The ratio of the sites of interest is very broad as it ranges from around 20 to slightly over 70 (see Figure 22). The highest ratio can again be seen at site 5. Site 1 and 2 exhibit topsoil ratios between 20 to 30, whereas it increases towards 50 to 60 for the subsoil samples. Sites 3 and 4 show again a mirroring pattern and lie between 40 and 60. In addition, this is the first index where the pattern of the first site of interest and the first reference site is similar within the first 10 cm. However, the ratio of the reference site is higher as well as it has again a high standard deviation. This can be attributed to the difference between the two soil pits from this site. As an example: For the soil depth of 0 to 5 cm the index value for one pit is around 11, while it is around 45 for the other pit (see Table A 3.2). Moreover, the second reference site has overall the smallest ratio and it decreases slightly with depth as the first reference site increases. Like before a smaller index indicates a more advanced weathering. Therefore, site 5 weathered the least, followed by site 3 and site 4. Reference site 1 is slightly more weathered. The second site of interest shows again a higher degree of weathering, followed by the first site. Based on the consideration that this site has a stronger index increase with depth compared with the second reference site, the latter is assumed to be the most weathered one.

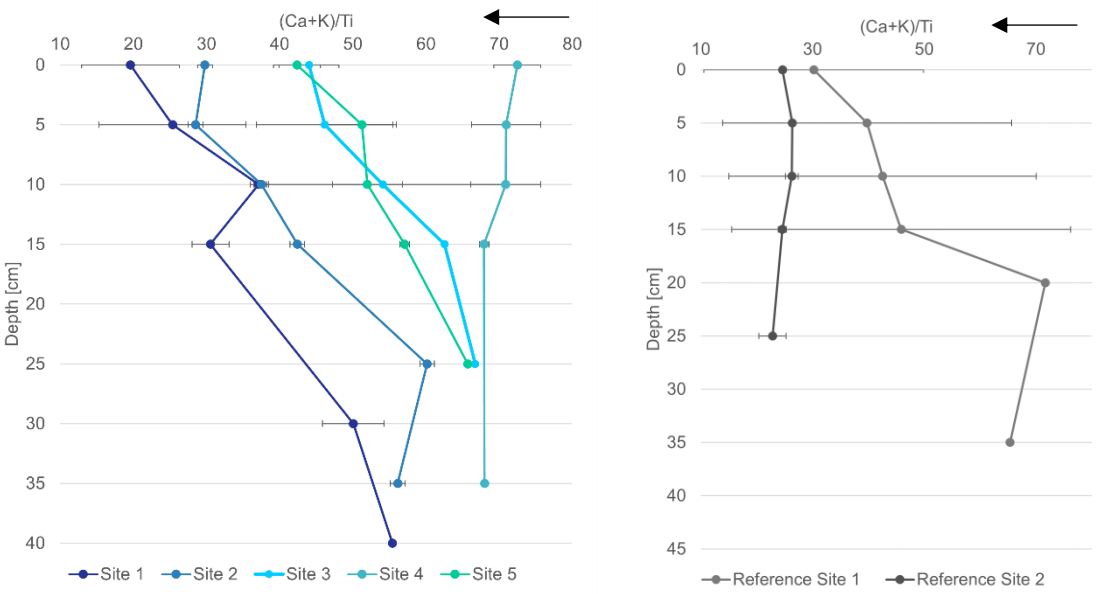

Figure 22: Depth distribution of the molar ratio of (Ca+K)/Ti. Left: sites of interest, right: reference sites. Arrow indicates increased weathering.

4.2.9.4 CIA

This index indicates changes in alkali elements in comparison with Al_2O_3, which has a lower mobility. The assumption is that a high index number represents a greater amount of weathering. Typical values for fresh granite are around 50, whereas they increase if the granite is already weathered (Ban et al., 2017).

The values from the sites of interest as well as from the reference sites are in a range of 52 to 61. Similar patterns as seen in the other weathering indexes are visible in Figure 23. This time site 5 has the lowest ratio, whilst site 3 and 4 are again mirroring each other. Site 1 has a slightly lower ratio in comparison with site 2, which has the highest one. The two reference sites are again intersecting each other with an opposite pattern. In addition, the second reference site and the first site of interest seem to have a similar development of the index. However, the index range at reference site 2 is higher.

This leads to the following weathering of the sites: Site 5 is again the least weathered site, followed by site 4 and site 3. Site 1 is the second most weathered site while site 2 shows the most weathered conditions. It is more complicated with the two reference sites. The first five centimetres of reference site 1 seem less weathered than the one of the second reference site. Based on the topsoil development reference site 2 is more weathered than reference site 1. Yet, depending on the emphasis (i.e., subsoil development), the opposite could also be the case.

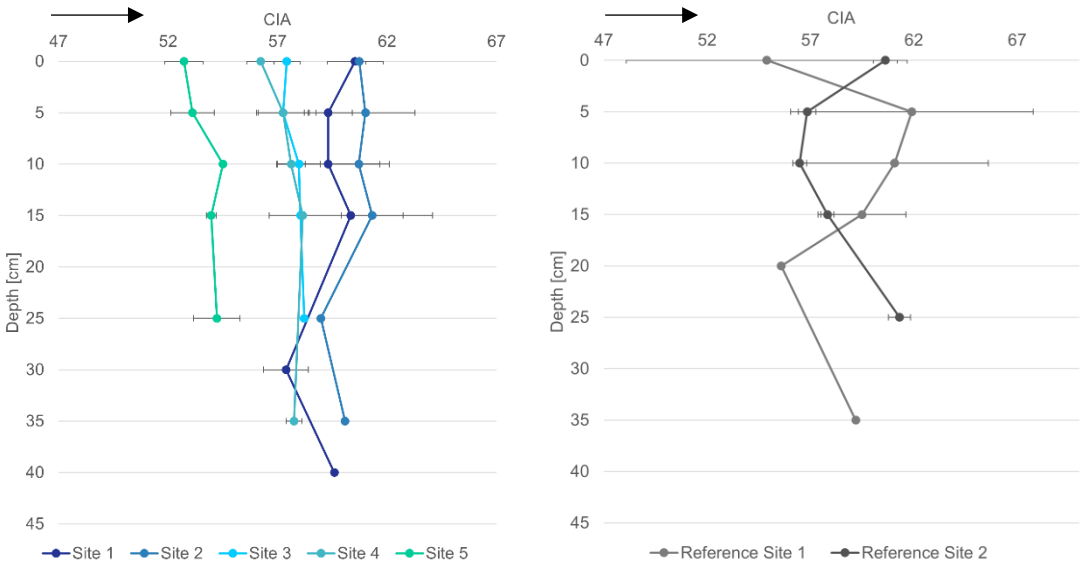

Figure 23: Depth distribution of the CIA. Left: sites of interest, right: reference sites. Arrow indicates increased weathering

4.2.9.5 (Na+K)/Ti

The molar ratio increases with depth for all sites of interest except site 4 (see Figure 24). Site 1 has the lowest ratio of 46, whereas the ratio of site 4 starts at 160. Thus, the data range is extremely broad. Sites 1 and 2 as well as sites 3 and 5 show a similar development, while the latter have a zig zagging pattern, the one of sites 1 and 2 is more alike. Again, the highest standard deviation can be found at reference site 1. This can again be attributed to the major difference between the two soil pits from this site (see Table A 3.2).

As with the molar ratio of (Ca+K)/Ti the idea is that a higher ratio indicates lower weathering. Thus, the following weathering pattern can be seen. The first site of interest is the most weathered, followed by the second, third and fifth site, while site 4 is the least weathered. The second reference site seems to have a slightly higher weathering degree than the first site of interest, whilst the first reference site can be assigned between the second and third site of interest. Yet, when the standard deviation is taken into account, it could be assigned differently.

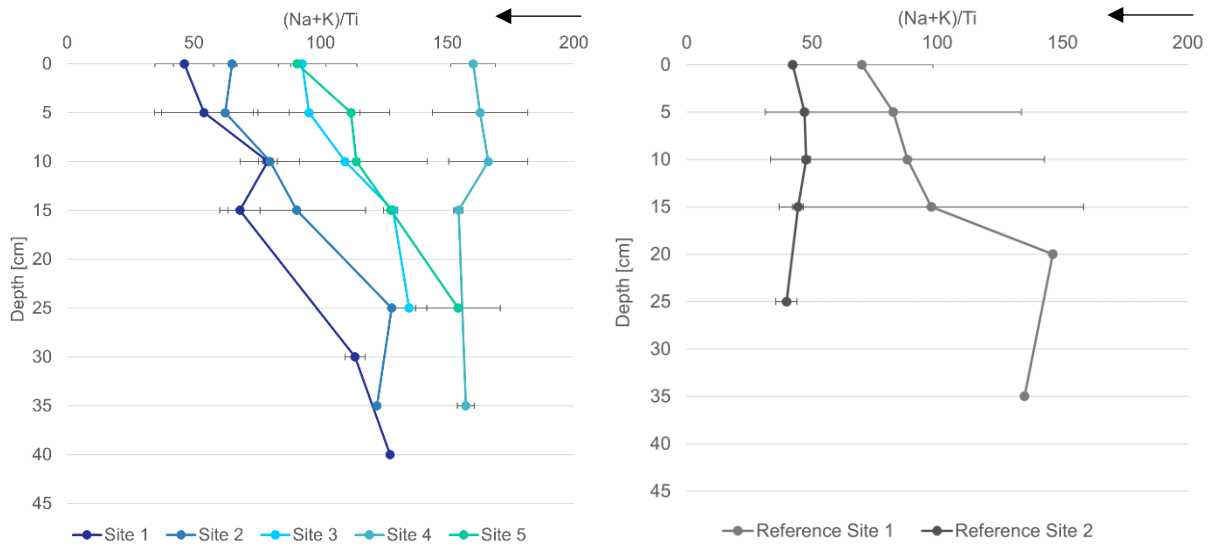

Figure 24: Depth distribution of the molar ratio of (Na+K)/Ti. Left: sites of interest, right: reference sites. Arrow indicates increased weathering.

4.2.9.6 WIP

The weathering index by Parker is based on the analysis of quartz rocks, which contain alkaline elements. If a soil has already lost a high amount of alkaline elements, because it is strongly weathered it might not be suitable. This is due to the dependence of the index on the mobility of the alkaline elements (Ban et al., 2017). A smaller index indicates more advanced weathering. The index range is between 35 to 86 as seen in Figure 25. Therefore, it is again quite broad. Within the depth of 5 to 15 cm the sites 1 to 4 are quite close together. Sites 3 and 5 are mirroring each other as sites 1 and 2 have a similar development. However, site 2 has slightly lower values. With this index, site 4 has the highest values within the five sites of interest. Overall, the second reference site has the highest index. Reference site 1 gradually increases with depth, until a decrease in the subsoil. The high standard deviation at reference site 1 can be attributed to the difference between the two soil pits from this site as it can be seen in Table A 3.2, where the values range from 13 at a depth 0 to 5 cm in one pit to 56 at the same depth in the other pit.

Consequently, site 4 and the second reference site are the least weathered, followed by site 5, 3 and 2. Site 1 on the other hand is more difficult to classify, as it has the lowest index at the top. However, with depth its index increases, leading to a lower weathered soil in comparison with sites 2, 3 and 5. At the topsoil to subsoil border sites 3 and 5 have a higher index, followed by a shift after which site 1 has the higher index. Moreover, until a depth of 15 cm reference site 1 shows a lower index and thus a more weathered soil in comparison with reference site 2. Yet, after a depth of 20 cm there is also a shift, which would lead to the conclusion that here reference site 2 is more weathered than reference site 1.

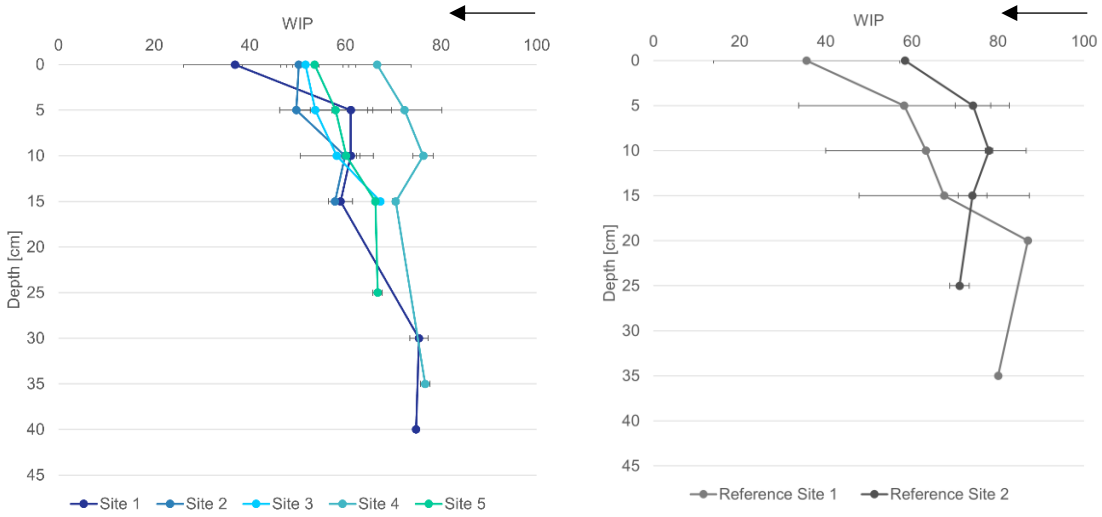

Figure 25: Depth distribution of the WIP. Left: sites of interest, right: reference sites. Arrow indicates increased weathering.

4.3 Physical characteristics

4.3.1 Bulk density

Table A1.1 and A1.2 show the calculated bulk density for each replicate row and depth. Again, the mean value per site and the standard deviation have been calculated and can be seen in Figure 26. Generally, the bulk density increases with depth. This is true for almost all sites of interest, except site 4, where a decrease can be observed. Moreover, the bulk density of the organic layer varies between 0.37 g cm^{-3} and 0.90 g cm^{-3}. Interestingly, the pattern at reference site 1 and the first site of interest is not as similar as it was before (such as pH or LOI). Whereas there is a linear increase at the first reference site, the topsoil of site 1 shows an increase followed by a decrease of around 0.2 g cm^{-3}. Generally, the subsoil samples have a higher density, than the topsoil samples.

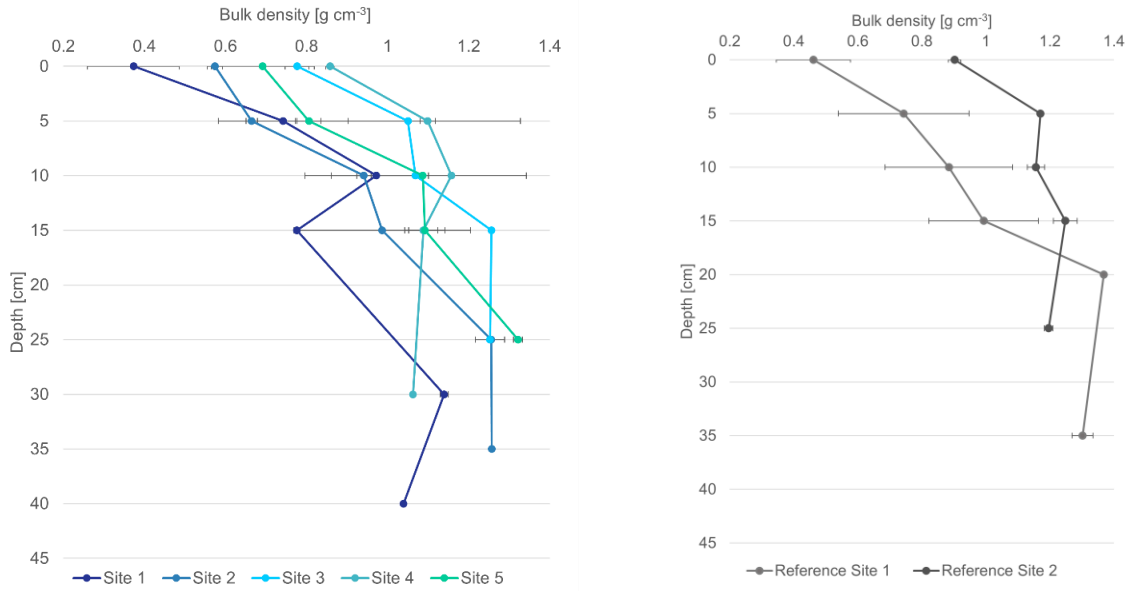

Figure 26: Depth distribution of the bulk density [g cm^{-3}]. Left: sites of interest, right: reference sites

4.3.2 Grain size

10 out of the 17 top- and subsoil samples were used for the grain size analysis. As the material was stored in a plastic bag to differentiate between top or subsoil, no accurate depth trend can be visualised. Figure 27 shows the cumulative grain size distribution of each site summed up to 100% as well as the assigned classes of sand, silt and clay. The clay fraction is smaller than 2 µm. Silt has a grain size between 63 µm – 2 µm. Sand is classified to range from 2 mm to 63 µm. All samples contain more than 50% of sandy material and the amount of clay is almost always less than 10%. In addition, the three sites where both top- and subsoil samples were analysed have a higher amount of sand in the subsoil samples. The subsoil samples from the second site of interest and the first reference site only contain around 2% of clay.

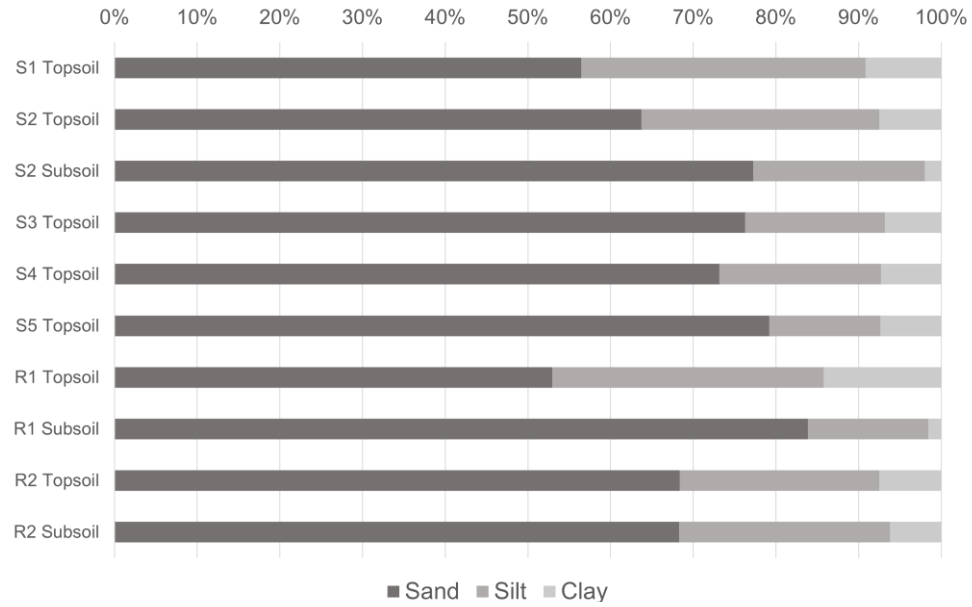

Figure 27: Relative amount of grain size summed up to 100%

4.4 Correlation between WI and grain size

Due to missing surface age measurements based on for example ^{10}Be samples, no accurate surface age and thus maximum soil age can be verified with field data. To quantify the relative age estimation based on the WI, a correlation between the weathering indexes and the median grain size was calculated. The idea behind it is that a more weathered soil should have a smaller medium grain size (Amelung et al., 2018). For WIP a Spearman correlation was used (p: 0.004606). All other correlations were calculated with a Pearson correlation, due to them being normally distributed ($p > 0.05$).

A- and B-Index as well as the CIA did yield a high (negative) correlation with the medium grain size value (see Table 5). A correlation per individual site could not be calculated due to a missing grain size value distributed with depth.

Table 5: Correlation values based on the correlation between the WI and the median grain size

Site	Ca	A Index	B Index	CIA	WIP	Na
Correlation	0.42	1.00	0.88	-0.88	0.10	0.36

4.5 Soil formation modelling

Based on the study by Vieira et al. (2021), where they stated that around 14.2 ka ago the plateau ice field has disappeared, the soil age is assumed to be 15 ka. The amount of precipitation depends on the altitude (see Chapter 3.3). It is assumed that one third of precipitation infiltrates into the soil and two thirds are lost by evapotranspiration.

Table 6 shows the result of the long-term soil erosion modelling. It is visible that the calculated precipitation decreases along the sites. The modelled annual soil erosion ranges from 2.10 t ha^{-1} at site 1 to 13.89 t ha^{-1} at the fifth site of interest. Yet, no linear increase over the sites can be seen as the pattern is strongly influenced by the particle size of the soils. The higher the median particle size (d_{50}), the higher is the amount of soil erosion.

Table 6: Input values for the long-term soil erosion modelling

Site	Soil age [a]	Precipitation [mm a^{-1}]	Evapotranspiration [mm a^{-1}]	Infiltration [mm a^{-1}]	d_{50} [µm]	Porosity	Erosion [t ha^{-1} a^{-1}]
Site 1	15000	2396	1598	799	50	0.5233	2.10
Site 2	15000	2171	1447	724	145	0.5894	5.37
Site 3	15000	2108	1406	703	230	0.6730	9.83
Site 4	15000	1957	1305	652	170	0.6556	6.21
Site 5	15000	1940	1293	647	370	0.6224	13.89

Soil erosion assessment based on the percolation theory did yield extremely high soil erosion rates. They are strongly influenced by the median grain size value as it can be seen by the correlation factor of 0.992 based on a Pearson correlation due to both variables being normally distributed (d_{50}: p = 0.8845, erosion: p = 0.8957). Figure 28 shows the correlation between the two variables. Overall, the higher the median grain size is, the more erosion was modelled.

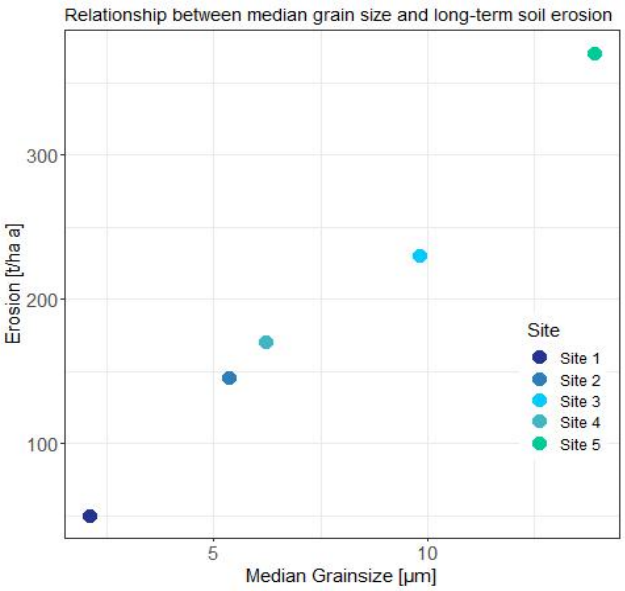

Figure 28: Visualisation of the relationship between erosion [t ha^{-1} a^{-1}] and median grain size [µm]

Bakker et al. (2004) stated that increased soil erosion rates are linked to a decrease of soil thickness, which in turn influences the weathering degree of a soil. This is due to the consideration that already weathered material could be eroded, resulting in a less weathered soil (Brosens et al., 2021). Therefore, a correlation between the WI and the amount of long-term soil erosion has been calculated. Table 7 shows the results. They are extremely similar to the correlation values of d_{50} and WI (see Table 5).

Table 7: Correlation values for the relationship between long-term soil erosion and WI

Site	Ca	A Index	B Index	CIA	WIP	Na
Correlation	0.44	0.98	0.90	-0.90	0.10	0.39

4.6 Fallout radionuclides

4.6.1 $^{239+240}$Pu activity and inventories

Note that SSP112 has been contaminated during the last filtration process. However, as the contaminated material was from the same soil pit and depth as well as the resulting values were in range with the values from the replicate samples (SSP117 and SSP124, see Table A 8; A9) it was used in the erosion calculation.

Figure 29 shows the mean cumulative $^{239+240}$Pu inventory for each depth and site as well as the standard deviation. The reference site consists of the combined $^{239+240}$Pu inventory of reference site 1 and reference site 2. Even though only the first reference site is located within the Candieira valley, both sites are chosen as a reference to cover the altitude range of the sites of interest. As stated in Table 1, reference site 1 is located at 1848 m a.s.l and reference site 2 is at 1424 m a.s.l.

The $^{239+240}$Pu inventory of the reference site decreases with depth, whereas the $^{239+240}$Pu inventory of the sites of interest shows a big range. The total inventory of the combination of both reference sites is 160.97 ± 43.71 Bq m^{-2}. The highest amount of $^{239+240}$Pu was detected in the soil depth of 0 to 5 cm at the first site of interest (337.7 ± 207.25 Bq m^{-2}), followed by the third site of interest (136 ± 42. Bq m^{-2}). The fifth site of interest has 79.9 ± 24. Bq m^{-2}, whilst the lowest amounts in the same soil depth are 60.8 ± 12.56 Bq m^{-2} and 48.4 ± 19.3 Bq m^{-2} for the second and fourth site of interest, respectively. A decrease of the $^{239+240}$Pu content in the topsoil can be seen at all sites, except the second site of interest. Interestingly, three out of the five sites of interest show an increase in the subsoil.

Yet, when considering the standard deviation, which is really high at site 1 for the depths of 0 to 5 cm and 5 to 10 cm as well as it is rather high at site 3 for the depth 0 to 5 cm a different picture could result. Moreover, the measured $^{239+240}$Pu activity for these samples is really high as it can be seen in Tables A6 – A9.

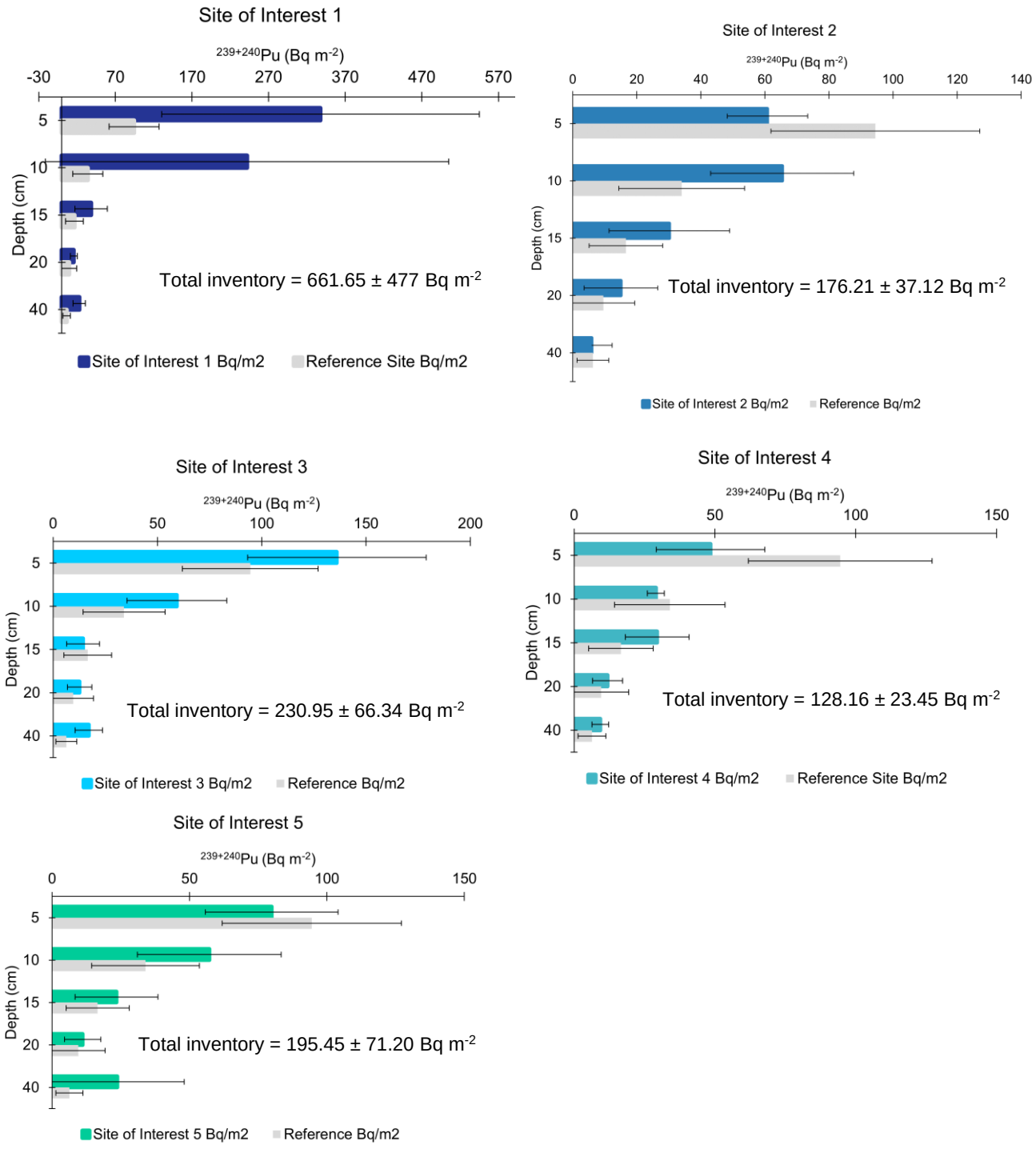

Figure 29: $^{239+240}$Pu inventory of each site of interest in comparison with $^{239+240}$Pu inventory of both reference sites

The average corrected $^{239+240}$Pu activity for all samples is 2.2051 ± 5.61 Bq kg^{-1}. Based on a Shapiro-Wilk test, the $^{239+240}$Pu activity is not normally distributed within a site, independent of the samples being from a reference site or site of interest. The combined samples for each depth are also not normally distributed for the depths of 0 to 5 cm, 5 to 10 cm, 10 to 15 cm and 25 to 30 cm ($p < 0.05$). In contrast, the samples from the depths of 15 to 20 cm, 20 to 25 cm and 30 to 35 as well as 35 to 40 cm are normally distributed ($p > 0.05$). Based on their

distribution a paired t-test or Wilcoxon rank sum test was used to look for significant differences in the data.

The only results that yield a significant difference between the samples were the depths of 20 to 25 cm with 25 to 30 cm (p: 0.125) and 25 to 30 cm with 30 to 35 cm (p: 0.1094), thus subsoil samples. Figure 30 shows the $^{239+240}$Pu activity per depth and site for the first 20 cm. Afterwards, the samples were not taken consistently at the same depth, which is why these are not shown. It is visible that the activity in the samples from the first site of interest have a very broad data range. Yet, this depth did not show a significant difference between the samples, which can be related to the high data variation.

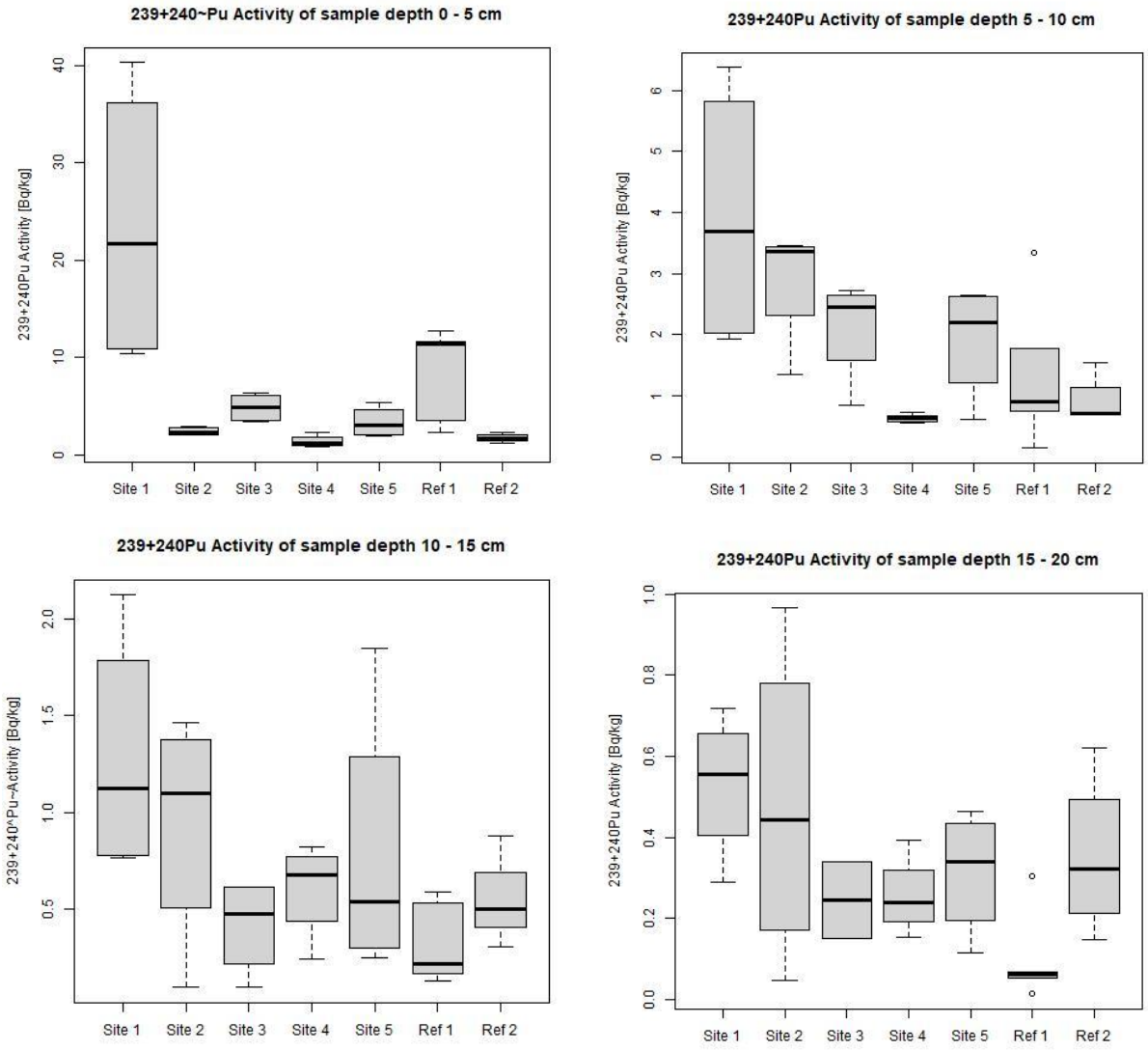

Figure 30: $^{239+240}$Pu activity [Bq kg^{-1}] with depth for each site

4.6.2 Estimation of short-term erosion rate based on $^{239+240}$Pu

To determine if and how much soil erosion occurred in the last 60 years, the $^{239+240}$Pu inventory of the reference sites and the sites of interest is compared. Table 8 shows the comparison of the soil redistribution between the sites as well as within a site by using either reference site

1, reference site 2 or both reference sites as reference inventory. In addition, different scenarios are based on the introduced models in Chapter 3.4. For the Inventory Method by Lal et al. (2013) three particle size correction factors were used ranging from P = 1 to P = 1.2 and P = 1.5.

Table 8: Comparison of soil redistribution based on different reference inventories and models

		IM P=1		IM P=1.2		IM P=1.5		PDM		MODERN	average	
Reference	Site	t ha^{-1} a^{-1}	sd	t ha^{-1} a^{-1}	sd	t ha^{-1} a^{-1}	sd	t ha^{-1} a^{-1}	sd	t ha^{-1} a^{-1}	t ha^{-1} a^{-1}	sd
With R1	Site 1	17.04	± 8.57	14.2	± 7.15	11.36	± 5.72	3.41	± 1.58	4.25	10.05	± 5.4
	Site 2	0.9	± 2.46	0.75	± 2.05	0.6	± 1.64	0.27	± 0.6	0.55	0.61	± 0.21
	Site 3	4.9	± 4.89	4.08	± 4.07	3.27	± 3.26	0.94	± 0.86	1.61	2.96	± 1.49
	Site 4	-3.03	± 2.55	-2.52	± 2.12	-2.02	± 1.7	-0.56	± 0.48	-1.71	-1.97	± 0.84
	Site 5	2.15	± 4.6	1.79	± 3.83	1.43	± 3.07	0.47	± 0.92	1.19	1.41	± 0.57
With R2	Site 1	16.85	± 8.9	14.04	± 7.41	11.23	± 5.93	15.84	± 7.73	4.16	12.42	± 4.55
	Site 2	0.2	± 2.64	0.17	± 2.2	0.13	± 1.76	0.47	± 2.95	0.32	0.26	± 0.12
	Site 3	4.14	± 5.07	3.45	± 4.22	2.76	± 3.38	3.73	± 4.22	1.41	3.1	± 0.96
	Site 4	-4.13	± 2.67	-3.44	± 2.23	-2.75	± 1.78	-3.57	± 2.33	-3.99	-3.58	± 0.49
	Site 5	1.39	± 4.8	1.16	± 4	0.92	± 3.2	1.44	± 4.48	0.91	1.17	± 0.22
With R1&2	Site 1	17.77	± 9.14	14.81	± 7.61	11.85	± 6.09	7.96	± 3.77	4.18	11.31	± 4.83
	Site 2	0.65	± 2.8	0.54	± 2.33	0.43	± 1.87	0.45	± 1.44	0.36	0.49	± 0.1
	Site 3	4.78	± 5.21	3.99	± 4.34	3.19	± 3.47	2.05	± 2.06	1.45	3.09	± 1.22
	Site 4	-3.45	± 2.56	-2.88	± 2.13	-2.3	± 1.71	-1.52	± 1.14	-2.83	-2.59	± 0.65
	Site 5	2.15	± 4.6	1.79	± 3.83	1.43	± 3.07	1.03	± 2	0.97	1.47	± 0.45

Figure 31 shows the data of Table 8 in a graphical way, whereas from left to right the inventory of the first reference site, then of the second reference site and lastly the $^{239+240}$Pu inventory of both sites are used to compare the $^{239+240}$Pu inventory of each site.

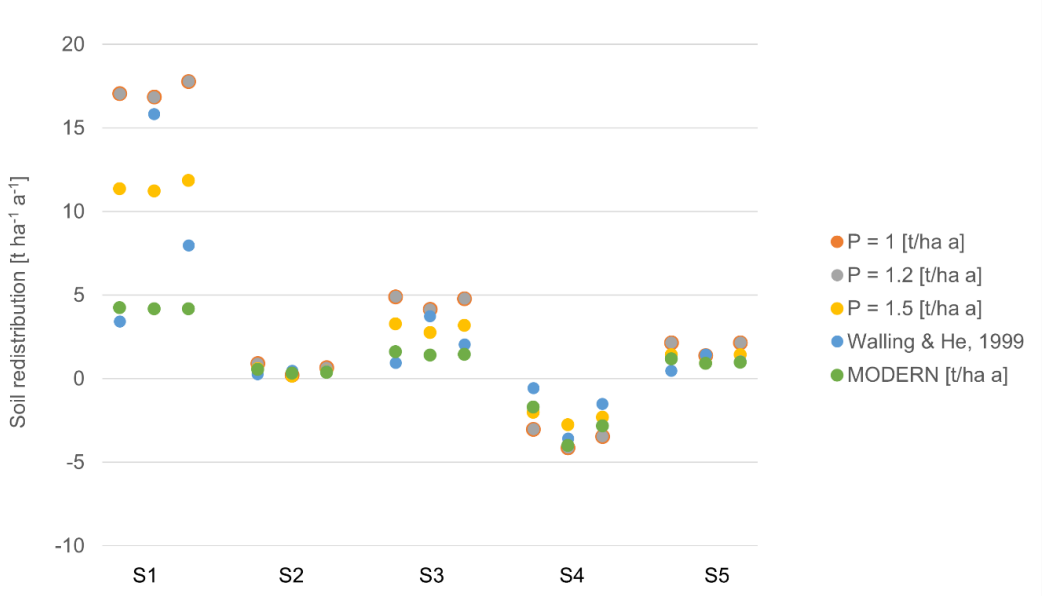

Figure 31: Comparison of soil erosion scenarios based on different reference inventories. At each site from left to right: reference site 1, reference site 2, both reference sites

Negative values show soil erosion and positive values indicate soil accumulation (Alewell et al., 2014). Based on a Shapiro-Wilk test, the data is normally distributed ($p > 0.05$) within the 5 sites independent of the chosen reference sites. A t-test was used to test if there is a

significant difference between the aforementioned three reference scenarios. As the p-value is always higher than 0.05, it can be used as indicator that there is no significant difference between the three reference inventories.

The following section has its emphasis on the combination of both reference sites. Figure 32 shows the different erosion estimations per site based on the calculated erosion rates and the corresponding standard deviation with the different models.

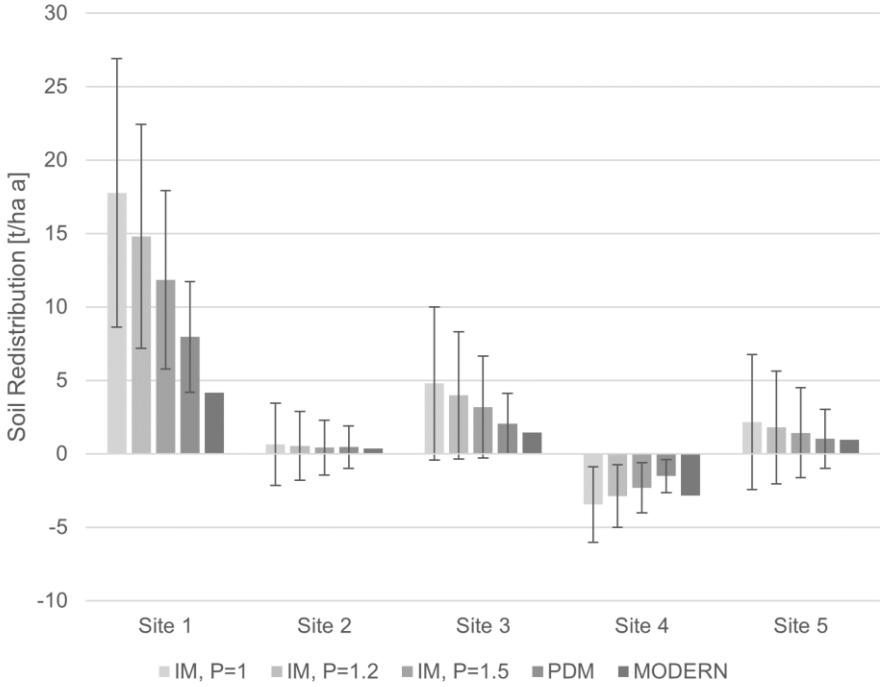

Figure 32: Comparison of soil redistribution based on different models.

In general, the Inventory Method with P = 1 has the highest erosion or accumulation values for all five sites of interest. There is a decreasing trend visible the higher the particle size correction factor is. The Profile Distribution Model shows the lowest amount of soil erosion for site 4, whereas at the other sites MODERN resulted in the lowest material redistribution.

The average soil accumulation at the first site of interest is 11.31 ± 4.83 t ha^{-1} a^{-1}. The lowest was reached with MODERN (4.18 t ha^{-1} a^{-1}), followed by the method of Walling & He (1999) (7.96 ± 3.77), while the highest is almost 18 t ha^{-1} a^{-1} reached with the IM where P = 1. However, this result is strongly influenced by samples SSP57, SSP58 and SSP62. They are from a soil depth of 0 to 5 cm (SSP57 and SSP62) as well as 5 to 10 cm (SSP58) and show a $^{239+240}$Pu activity between 30 to 40 Bq kg^{-1}, which is the highest measured $^{239+240}$Pu activity of all samples. In comparison, the next highest content is around 11.5 Bq kg^{-1} (samples from the first reference site for a soil depth of 0 – 5 cm). Table A7 shows the measured $^{239+240}$Pu activity. In addition, the modelled result for site 1 also has the highest standard deviation and the results need thus to be treated with caution.

Now, if the activity of the aforementioned samples (SSP57, SSP58 and SSP62) would be changed towards values closer to the ones measured with samples from the second pit from this site, the result of the IM for the soil erosion with P = 1 decreases strongly towards 11.3 t ha^{-1} a^{-1} (see Table A 10). The measurement was changed as followed: For sample SSP58 (sampling depth 5 to 10 cm) the measured $^{239+240}$Pu activity of the replicate row was assigned. The average value of the depth 0 to 5 cm was calculated with the samples from the second pit (10.87 ± 0.49 Bq m^{-2}) at site 1 and was then assigned to the SSP57 and SSP62.

This shows the huge influence these three samples have on the overall soil redistribution modelling. If the new $^{239+240}$Pu inventory is used with MODERN, the following soil accumulation results in 3.07 t ha^{-1} a^{-1}.

The modelled values for the second site of interest show soil accumulation as well. However, in comparison with the other sites it has the least amount of accumulation. The average of the three methods is 0.488 ± 0.099 t ha^{-1} a^{-1}. Again, the highest amount was modelled with the IM with P = 1 (0.65 ± 2.8 t ha^{-1} a^{-1}), while the least amount can again be seen in the MODERN data (0.36 t ha^{-1} a^{-1}). The low standard deviation is also visible in Figure 31, where the data points lie almost on top of each other.

The third site of interest has the second highest amount of soil accumulation, with a mean accumulation value of 3.093 ± 1.22 t ha^{-1} a^{-1}. The ranking based on the models is the same as before, with the IM of P = 1 leading to 4.78 ± 5.21 t ha^{-1} a^{-1}, whereas MODERN resulted in an annual amount of 3.09 t ha^{-1}.

It is visible at a first glance that only site 4 is affected by erosion. The mean soil redistribution is -2.595 ± 0.65 t ha^{-1} a^{-1} and again a decreasing trend based on the three particle size factors can be seen. However, here MODERN yield a higher erosion rate with -2.83 t ha^{-1} a^{-1} than PDM (-1.52 ± 1.14 t ha^{-1} a^{-1}) or the IM with P=1.5 (-2.3 ±1.71 t ha^{-1} a^{-1}) , which is in contrast to the other sites.

The fifth site of interest shows a mean accumulation value of 1.475 ± 0.45 t ha^{-1} a^{-1}. The similar pattern as before can be seen. For instance, the IM with P=1 resulted in 2.15 ± 4.6 t ha^{-1} a^{-1}, while MODERN showed an annual accumulation of 0.97 t ha^{-1}.

It can be observed in Figure 31 that there is almost no difference between the scenario with P =1 (orange) and P = 1.2 (grey), independent of the chosen reference. The difference with P = 1.5 is higher. Moreover, the most consistency in the data resulted by using MODERN, as the differences between the three reference inventories is very small. However, in case of site 4, where soil erosion occurs the data points are not in a straight horizontal line. Yet, there is no significant difference between the three different reference scenarios as stated at the beginning of this section.

Figure 40 in the Appendix shows the modelled accumulation or erosion rate based on MODERN. The function S shows the cumulative FRN inventory of the simulated reference profile (Arata et al., 2016b). In comparison with the calculated soil loss, respectively soil gain by Lal et al. (2013), the deposited amount of soil at the first site of interest is smaller when modelled with MODERN. The accumulation is in a range of 0 to 5 cm above the atmosphere – soil border, whereas the Inventory Method results in a thickness layer of around 10 cm. However, for the other sites the values seem almost the same.

4.6.3 Factors potentially affecting soil redistribution

Figure 33 shows the average slope gradient [°] and the mean soil redistribution rate [t ha^{-1} a^{-1}]. The steepest slope gradient was measured at site 1, whereas site 2 has the flattest one. Overall, the highest soil accumulation rate is found at site 1, whereas site 4, which does have the second steepest slope gradient, shows soil erosion. Both of the variables are normally distributed (slope gradient: p= 0.594; mean soil redistribution: p =0.3892). The Pearson correlation resulted in a correlation value of 0.60.

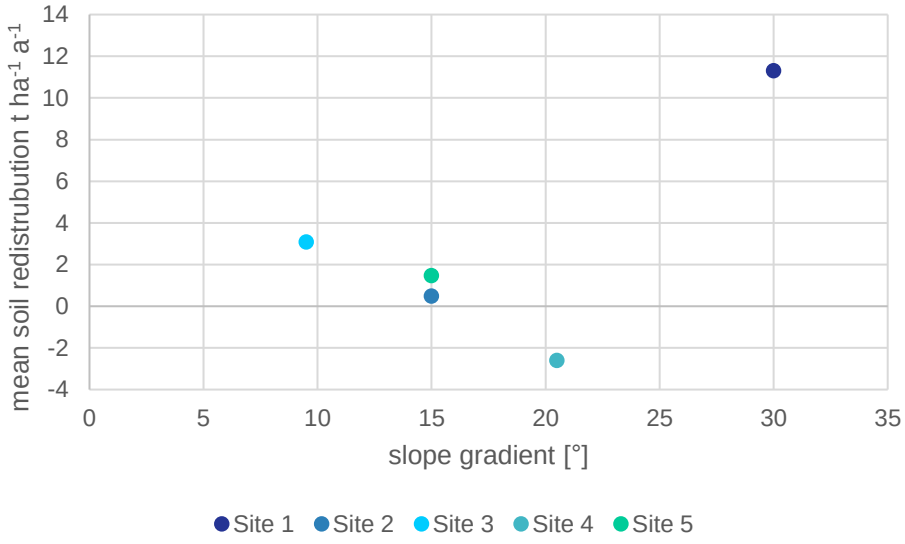

Figure 33: Measured average slope gradient [°] and mean soil redistribution [t ha^{-1} a^{-1}]

To estimate the influence of carbon on the amount of $^{239+240}$Pu in the samples a correlation between these two variables was calculated. A Spearman correlation was used, as only at site 2 and 3 the carbon content was normally distributed ($p > 0.05$), whereas this was not the case at the other sites. Moreover, the $^{239+240}$Pu content was not normally distributed at any site. Table 9 shows the correlation value and Figure 34 shows the relationship for each site. It is visible that rather high correlation values were achieved. Interestingly, site 1 has the second lowest correlation of all sites.

It is clearly visible that the depth 0 to 5 cm has the highest $^{239+240}$Pu content. There is one exception, which is the second site of interest as here a higher $^{239+240}$Pu content was measured

at the depth of 5 to 10 cm. Yet, this site has overall the strongest correlation between the two variables, followed by reference site 2. The lowest correlation is found at the first and third site of interest.

Table 9: Correlation between C [%] and $^{239+240}$Pu activity

Site	Site 1	Site 2	Site 3	Site 4	Site 5	Ref. Site 1	Ref. Site 2
Correlation	0.65	0.94	0.54	0.83	0.78	0.74	0.84

In addition, a correlation between the erosion rate based on the average inventory of each site (see Table 8) with the mean C [%] content of a site was calculated, resulting in a correlation value of 0.9.

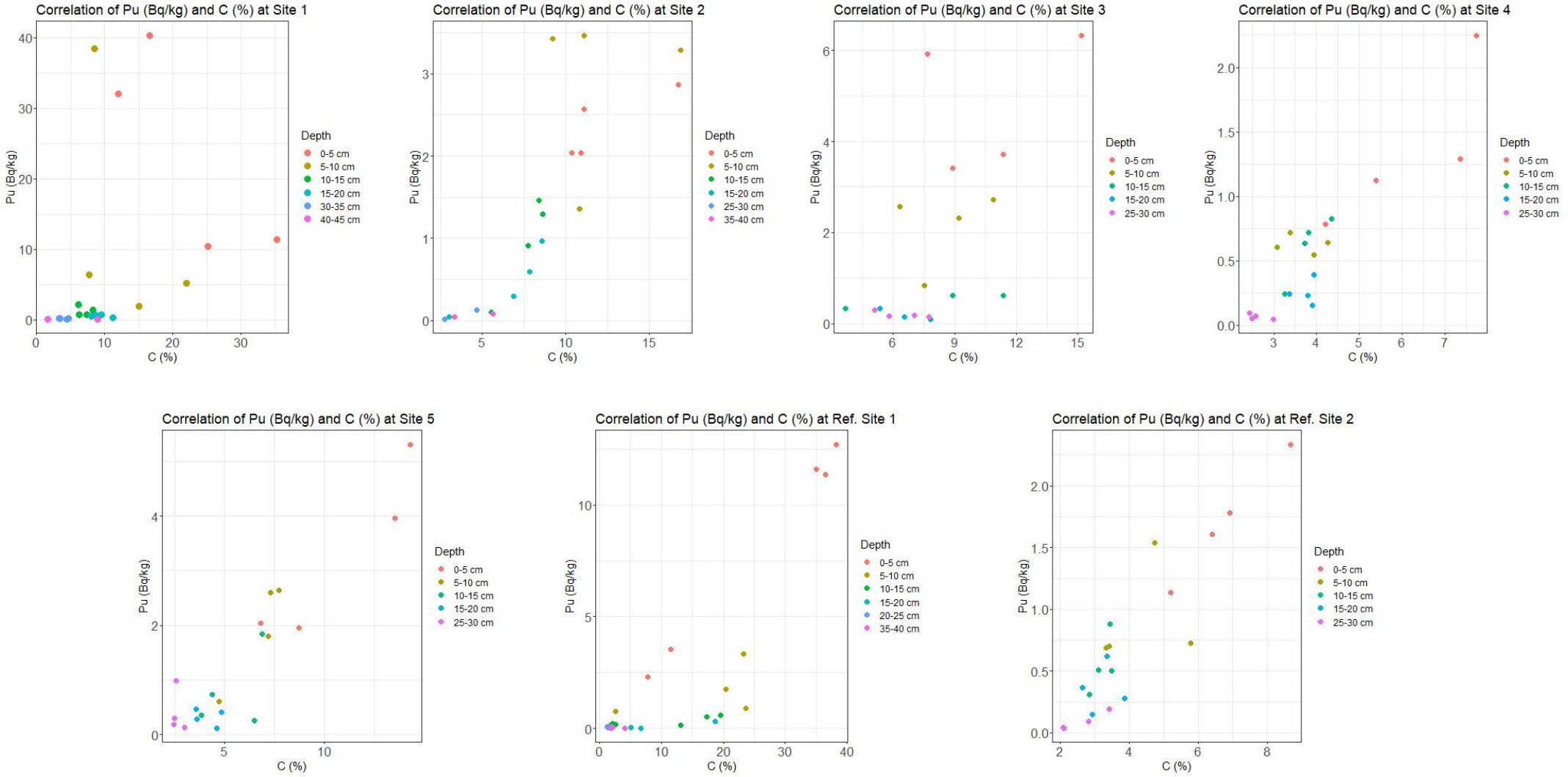

Figure 34: Relationship between Pu [Bq kg^{-1}] and C [%]

5. Discussion

5.1 General soil properties

The soils can be classified as Cambisols. This is a typical soil type in the Iberian Peninsula (Rodeghiero et al., 2011). It can be described as a soil at the beginning of the soil formation characterised by the horizon Bw (Zech et al., 2014). In addition, there is one site (i.e., site 4) that has another soil type, namely an Umbrisol (Zech et al., 2014), which could potentially also be described as a Cambic Umbrisol. For this soil type the thick, dark surface horizon with a high content of organic material is characteristic (FAO, 2014). All sites except reference site 2 which is not located in the Candieira valley and site 4, did have a Rhizic Moder as their humus form, characterised with OR in Table 2 (Jabiol et al., 2013).

There are many similarities between the different sites and yet, each is completely individual. One of the similarities is the bulk density increase with depth (Brady and Weil, 2017). Based on the calculated bulk density, the soils can be described as fine texture mineral soils (1.0 – 1.3 g cm^{-3}), which do have quite a high amount of organic material in the first few centimetres (Bashour and Sayegh, 2007).

5.1.1 Soil pH

All soils can be classified as extremely acidic with a pH < 4.5 (Truog, 1948). Moreover, the parent material of the soils is granite, which is an acidic rock (Olowolafe, 2002). Usually, the resulting pH values of a soil formed out of granite are between 3.5 and 5.5 (Stahr et al., 2016). Thus, the result of the soils being acidic is not surprising. Figure 35 shows the soil pH for the EU countries based on a modelling approach. The arrow indicates the location of the Geopark (the bright spot being the plateau), and it can be seen that the pH values measured in the Candieira valley are slightly more acidic than the ones modelled by Ballabio et al. (2019).

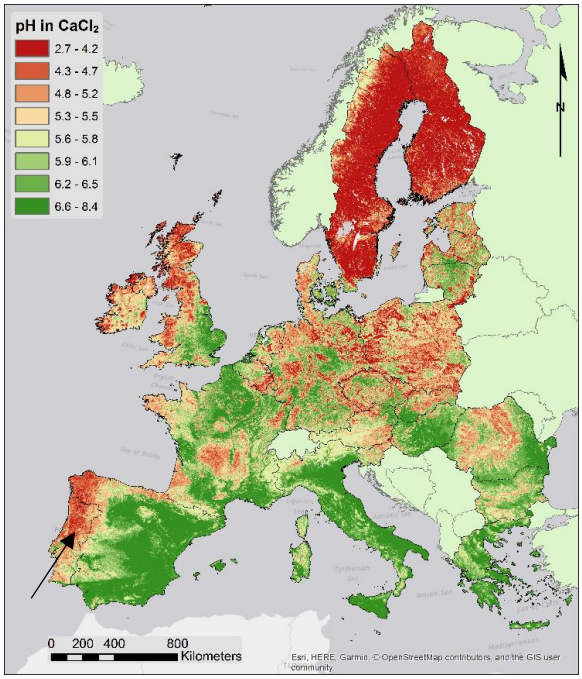

Figure 35: pH distribution of EU soils (Ballabio et al., 2019)

In an undisturbed natural system, a soil's acidity increases with time and the upper horizons are more acidic in comparison with the subsoil due to the soil genesis, which does start at the soil surface (Amelung et al., 2018). Thus, a soil's pH should increase with depth. However, over time it becomes more acidic due to the percolation of water into deeper soil layers (Habte, 1999; Shukla et al., 2013). Yet, this is not the case for the fifth site of interest. Here, a pH

decrease with depth was measured, which can be related to material relocation processes like bioturbation (Amelung et al., 2018). In addition, wildfires can result in a higher soil pH at the soil surface and might thus also lead to such a pH depth distribution. (Chungu et al., 2020)

5.1.2 Relating C, LOI and N to Mediterranean soils

The carbon content and LOI show a similar development for all sites. Generally, there is a high amount of carbon in the first 10 cm of the soils, followed by a decrease with depth. This corresponds with the expectation of a lower C content in deeper soil depths due to the organic material being incorporated into the soil at or near a soils surface. In addition, grasslands are assumed to have a more gradual C decrease with depth (Brady and Weil, 2017).

Figure 36: Example of black dust during sieving

The high C content at the first reference site and the first site of interest is surprising. Even though there is a high variation in the LOI data, the standard deviation is rather small for the C content. Site 1 and reference site 1 were sampled at the same location. Yet, the surroundings of reference site 1 resemble an area, which might evolve into a peatland as the ground was rather soft. The surroundings of the first site of interest did show small channels, where water flowed through. In addition, one soil pit of reference site 1 showed signs of a buried horizon. Another explanation for the overall rather high C content can be linked to the occurrence of wildfires in the area (Rodeghiero et al., 2011). This can be supported by the experience during the sample preparation for the laboratory analysis. During the sieving process, small charcoal pieces were found and most samples had a very black dust cloud (see Figure 36).

The high LOI values indicate a great amount of organic matter in the samples, which can be related to the wildfires occurring in the region. After a wildfire occurs, there can be additional C input from litter of dead plants as well as partly charred material. Yet, this only concerns the first few centimetres (Knicker, 2007).

The N range of the sites is between 0.4 to 1.5%. This corresponds with values found in literature, where the ecosystem development is divided into three phases of which N values above 0.2% are attributed to be found in systems which are characterised as intermediate phase. Here, an increased plant coverage is resulting in a higher C input and surface stabilisation. N values higher than 0.7% are defined to be in mature systems (Ollivier et al., 2011). However, site 1 and the first reference site do have a higher N concentration within the

first 5 cm. Overall, the N content decreases with depth, which can be attributed to the atmospheric N input at the soil surface (Brady and Weil, 2017).

Generally, there is a decrease in the C:N ratio with depth. This is in line with Brady and Weil, (2017). In addition, the calculated ratio in the Ah horizon is around the median range of Brady and Weil (2017), which they stated to be 12:1. Figure 37 shows a modelled C:N ratio for the EU countries and the ratios for this thesis are in line with the modelled one by Ballabio et al. (2019).

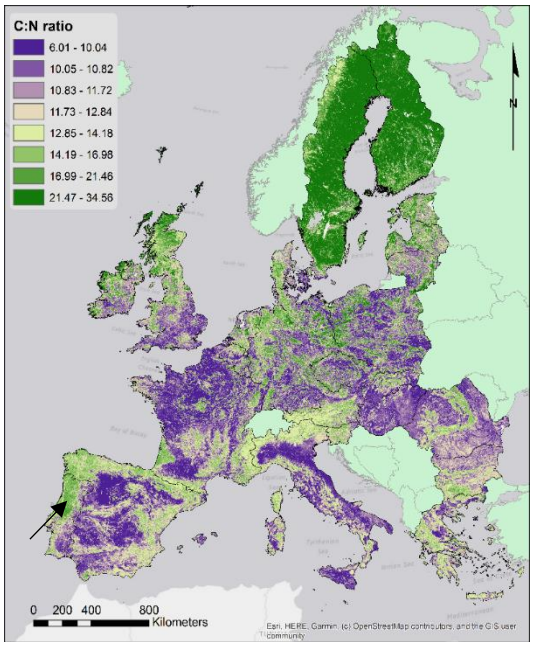

Figure 37: C:N ratio of EU soils (Ballabio et al., 2019). Arrow indicates the location of the Geopark.

5.1.3 Grain size

During weathering, granite can form secondary minerals out of feldspars. These newly formed secondary minerals are more subjective to weathering, leading to further break down. As a result of weathering, fine grained material is washed out by water (Ban et al., 2017). Thus, the resulting high concentration of sand is not unexpected. In addition, soils developed from granitic parent material with a high amount of sand are very vulnerable to soil erosion (Ban et al., 2017). As soil formation starts at a soil's surface, the upper layers are supposed to be more weathered and due to weathering, the grains located closer to the surface should be smaller, compared with soil particles located in deeper soil horizons (Amelung et al., 2018). This is visible by comparing the few top- and subsoil samples, which have a lower amount of sand particles in their topsoil samples. Soils with a high silt content are more prone to erosion than soils with a low clay content or soils with a low amount of organic matter. In addition, they are less likely to be eroded when there is a decrease in the silt fraction independent of an increase in the clay or sand fraction (Wischmeier and Mannering, 1969).

5.1.4 Assessment of oxalate measurements

The expectation for the extracted oxalate values is an increase with depth. Generally, the measurements can be used to see how many weathered products were formed over time. Therefore, a higher concentration can be an indicator for more weathered samples (Dahms et al., 2012). As only top- and subsoil samples were analysed the depth trend can only partly be discussed at the sites where top- and subsoil samples are available. Yet, it is visible that in each of these cases there is at least on element which does have a higher concentration in the subsoil sample. This is against the expectation for an undisturbed soil development.

To set the values into context, they are compared with values obtained by Dollenmeier (2021). In his thesis, he analysed samples from a formerly glaciated region in the Geopark Estrela. The Fe_o values are in the range of 3 to 6 g kg^{-1} (Dollenmeier, 2021). Yet, the values obtained with the top- and subsoil samples from the Candieira valley are a lot lower, with only one sample (subsoil sample from reference site 2) in the range of the obtained data by Dollenmeier, (2021). In contrast, the Mn_o values collected for this thesis are higher with values ranging from 13 to 18 mg kg^{-1}, not including the outliers at reference site 2 (top- and subsoil: 25.53 mg kg^{-1} and 35.68 mg kg^{-1}, respectively) as well as the one from the topsoil sample at site 5 (52.75 mg kg^{-1}). The values measured by Dollenmeier (2021) range from 2.6 to 18.5 mg kg^{-1}, whereas in his data the samples above 12 mg kg^{-1} can be classified as outliers. Moreover, his Al_o values are between 0.95 to 3.33 g kg^{-1}, while the ones for this thesis are between 2.15 to 7.21 g kg^{-1}. Therefore, the values from the Candieira samples are higher. Possible explanations for the higher concentration in the subsoil samples can be related to disturbances such as material relocation processes like bioturbation or lateral redistribution by water (Amelung et al., 2018). The low Fe_o concentration can be attributed to the transformation of the poorly crystalline minerals into more crystalline ones (Slessarev et al., 2022). However, this transformation was not measured and is thus only an assumption.

5.2 Evaluation of the chronosequence

There is no coherent relative age pattern based on the applied weathering indexes as they result in three different scenarios. Yet, a trend is visible. The first and second site of interest were always the most weathered sites, while site 5 has been declared the least weathered by four out of six indexes. Site 3 is assumed to be in the middle of all the sites, which is true for all indexes except the A-Index and the molar ratio of (Ca+K)/Ti, where site 4 is in the middle. Thus, the relative age of the sites is as followed: Sites 1 and 2 are due to a more weathered state assumed to be older in comparison with the other sites, whereas site 5 is classified as youngest soil.

The hypothesis for the relative age distribution of the five sites is based on the assumption of a chronosequence. The idea behind it is that due to the altitude gradient of roughly 450 meters the sites located at lower altitudes should have had more time to evolve and thus show a higher weathering stage compared to sites from higher altitudes. This would result in the following relative age distribution: Site 1 being the youngest, followed in a consecutive order to site 5, which was assumed to be the oldest site. This is clearly not the case as the data shows the exact opposite.

One explanation for this could be related to the strong climate gradient occurring in the Geopark Estrela. As Mora (2010) stated, the amount of precipitation is highly influenced by

altitude. Thus, site 1 and 2 are subjected to more precipitation than for example site 5 is. This does lead to a more weathered soil (Brady and Weil, 2017).

It is important to note that this result does not have to imply that the sites 1 and 2 located at the higher part of the valley were exposed to the atmosphere before the sites further down were. It simply indicates that sites 1 and 2 are more weathered, most likely due to their location at higher altitude and thus more subjected to a higher amount of precipitation. Leading to them being more evolved and thus, termed older in comparison with less evolved soils. Furthermore, it can be an indicator that the glacier retreat occurred at a much faster pace than expected, leading to possibly only a few thousand years difference until all sites were ice free. Thus, a shorter time-span between the retreat at site 5 and site 1 can be another explanation for why there is no clear age trend with altitude. Soils evolve over thousands of years and as stated in Chapter 3.3, their formation depends on many factors. Time is one of the soil formation factors and in combination with climate, one soil can evolve faster than another even though it has been covered by ice for a longer time period than the other soil has. In addition, sites 1 and 2 have a lower pH than the other sites, which supports the idea that these sites are more weathered due to the altitude gradient influencing precipitation (Amelung et al., 2018). Various studies have researched soil formation in deglaciated areas with soil ages up to 600 a (Zech and Wilke, 1977). They concluded among other things that soil evolution is strongly influenced by precipitation (Egli et al., 2006). This supports again the hypothesis of the fast glacier retreat, as soils not only were formed quite fast after the glacier retreat (Egli et al., 2006; Zech and Wilke, 1977), but can also have a higher formation rate due to the higher amount of precipitation.

To test the relationship between grain size and the amount of weathering, a correlation between the median grain size and the average value for each WI and site has been conducted. This is based on the consideration that a more advanced weathering should result in a smaller grain size (Amelung et al., 2018). As shown in Chapter 4.4, a high correlation has been found between the A- and B-Index as well as the CIA. If the emphasis is only on the WI with a high correlation, there is still no equal result visible, as each of the three indexes shows another pattern. Yet, they do show that sites 1 and 2 are more weathered as these sites do have a smaller medium grain size. This can be used as an indicator for a high influence of precipitation or the availability of water in general on the weathering process (Egli et al., 2018).

5.3 Long and mid-term soil redistribution

5.3.1 Soil Formation Modelling to estimate long-term soil erosion

Long-term soil erosion is highly correlated with the median grain size of the samples. This is indicated with a correlation value of almost 1. However, there is no linear increase based on the altitude of the site's location as the third site of interest does have a higher modelled erosion

rate than site 4. Yet, this corresponds with the median grain size of these soils. Site 1 has the lowest median grain size, which can be linked to its location at 1873 m a.s.l. Here, the amount of precipitation is assumed to be highest in comparison with the other sites (Mora, 2010). Based on the WI, this site also has the most weathered soils, which does result in a smaller grain size (Amelung et al., 2018). The range between the modelled erosion rates is very high, whereas it does increase within the lower parts of the valley. Generally, the production rate for Mediterranean soils with an age of 1ka to 10 ka is between 70 and 380 t km^{-2} a^{-1}, whereas younger soils with an age of only 100 years or less can have a soil production rate of up to 1000 t km^{-2} a^{-1} (Egli et al., 2018). As the soils are assumed to be around 15 ka old (Vieira et al., 2021), the soil erosion rate exceeds the soil production rate in almost all cases except site 1, if an annual soil production of 3.8 t ha^{-1} is assumed. Moreover, the yearly calculated soil production based on the model (see Table A11, column sP) is approximately the amount of material which is eroded, leading to the assumption that the soil formation is highly disturbed and not sustainable (Raab et al., 2018). Due to this, the long-term soil formation can also be classified by having regressive phases, where among others the ecosystem services of a soil are lost with erosion (Bajard et al., 2017). In addition, Vieira and Nieuwendam (2020), stated that permafrost in areas higher than 1300 m a.s.l occurs. The thawing of permafrost can lead to slope destabilisation and in turn enhance soil erosion (Zollinger et al., 2015).

There is a statistical correlation with the modelled soil erosion and the WI. Yet, the values are very similar to the ones seen in Table 5, where the correlation between the d_{50} and WI was investigated. An explanation for this can be attributed to the erosion calculation based on the soil formation modelling. Here, d_{50} plays a fundamental part in the equation and as the equation can be used to calculate the long-term soil erosion, the d_{50} value is influencing the calculated correlation between the WI and the erosion values.

5.3.2 Relationship between $\delta^{13}C$ and C content as proxy for mid-term soil erosion

Erosion has no direct influence on the $\delta^{13}C$ value due to the mechanical transport of soil particles as only a differentiation between ^{12}C and ^{13}C is resulting in a change of $\delta^{13}C$ (Guillaume et al., 2015). However, the relationship can still be used as an indirect proxy for soil erosion (Portes et al., 2018, Raab et al., 2018). Generally, different $\delta^{13}C$ relationships can be seen after a soil has been eroded. Due to the removal of material at the soil surface, the $\delta^{13}C$ depth distribution does shift closer to the soil surface (Guillaume et al., 2015). In addition, as material has been lost, the surface layer contains a mixture of new litter input as well as soil organic carbon from the newly exposed surface layer, resulting in a distinguishable isotopic composition between the previous surface layer and the newly exposed one (Häring et al., 2013).

Kohn (2010) stated that the typical range for C_3 plants is between – 20‰ to – 30‰. Thus, the values are in the expected range based on the above ground vegetation. In addition, the expectation for an undisturbed system is to have a decreasing amount of C, while an enrichment of $\delta^{13}C$ occurs with depth (Meusburger et al., 2013). Moreover, the correlation of each site resulted in a negative relationship, which is in line with Raab et al. (2018). They stated, that due to the increase of $\delta^{13}C$ with depth and the decrease of C a negative correlation occurs (Raab et al., 2018). The $\delta^{13}C$ increase can be related among others to isotopic discrimination during the decomposition process or variations in the decomposition rates of various organic compounds with different $\delta^{13}C$ signatures (Balesdent and Mariotti, 1996).

Therefore, the high negative correlation at the two reference sites can be used as an indicator for an undisturbed system. The second site of interest for example indicates in a qualitative way a high amount of disturbances such as erosion (Portes et al., 2018). Another disturbance leading to this correlation is for instance cryoturbation due to permafrost thawing, which can then also result in soil erosion (Zollinger et al., 2015).

By comparing the long- and mid-term trend it becomes evident that site 2 does not have the highest amount of soil erosion based on the long-term modelling. Rather, this site has the second lowest rate with 5.37 t ha^{-1} a^{-1}. In contrast, the correlation value of the fifth site of interest with a value of - 0.79 is similar to the values of the reference sites, and thus does seem not to be affected by erosion. Yet, the long-term soil formation modelling shows an opposite picture, with this site being affected the most with 13.89 t ha^{-1} a^{-1} of erosion. Moreover, based on the chronosequence hypothesis site 4 and 5 should have had more time to evolve, leading to a more stabilised slope and a quasi-steady state of $\delta^{13}C$ and C as well as a clear depth trend (Poage and Feng, 2004; Portes et al., 2018). Even though it has been shown with the WI that this hypothesis is not correct, the two sites do show a correlation closer to -1 instead of 0. Thus, if the result of the WI would be neglected, the correlation value would be in line with the expectation that these sites are more evolved. Maybe due to a better establishment of vegetation, which does stabilise the soil (Cerdà, 1999). This would then result in less erosion. Thus, the mid-term trend based on the correlation of $\delta^{13}C$ with C does not correspond with the long-term data and it is not in line with the data from the weathering indexes.

5.4 Short-term soil redistribution

5.4.1 Estimation of short-term soil erosion based on $^{239+240}Pu$

As there is no significant difference between the chosen reference inventory (e.g., reference 1, reference 2 or a combination with both references), the following chapters emphasis the results based on the $^{239+240}Pu$ inventory containing both references. Moreover, as $^{239+240}Pu$ has been distributed globally (Arata et al., 2016a), it is not surprising that there is no significant

difference between the reference used as FRN inventory as both reference sites are within close proximity and thus having received a similar amount of $^{239+240}$Pu during the fallout.

FRNs are used to quantify the material redistribution of the last 60 years (Arata et al., 2016b). The average ^{240}Pu/^{239}Pu mass ratio of all samples is 0.1577 ± 0.0350. The global fallout of the mid-latitude weapon testing for the northern hemisphere is around 0.18 (Alewell et al., 2017). In addition, Mitchell et al. (1997) and Kelley et al. (1999) found ^{240}Pu/^{239}Pu ratios between 0.14 – 0.24. Therefore, the mass ratio of the samples lies within the expected ratio for FRNs. However, there are 28 samples with a lower mass ratio (see Table A6 – A9). If these are not taken into consideration for the average ^{240}Pu/^{239}Pu mass calculation, the ratio increases to 0.1728 ± 0.0104. Most of them are from below 20 cm, and due to the nature of $^{239+240}$Pu to attach on the fine soil particles at or near the soil surface, the low content of these samples can be explained (Alewell et al., 2014). In addition, all sites show a decreasing $^{239+240}$Pu inventory with depth to some extent. This is in line with the observations made in various other studies, where the highest activity was measured close to the soil surface (e.g. Lal et al. (2013), Zollinger et al. (2015), Portes et al. (2018) or Raab et al. (2018)). The increase of the $^{239+240}$Pu content visible in the subsoil at sites 1, 3 and 5 can be related to material relocation processes such as bioturbation or cryoturbation (Amelung et al., 2018).

Independent of the chosen method, it is evident that only site 4 can be classified as erosive site, as the other sites all indicate material accumulation (see Table 8). The highest amount of material accumulation can be found at the first site of interest, which interestingly has the steepest slope gradient of 30° as well as signs of gully erosion could be seen in the field. This type of erosion is known to be the most severe form of erosion (Verheijen et al., 2009). The extremely high amount of accumulated material is likely connected with the high $^{239+240}$Pu activity found in three of the 22 samples collected at this site. As stated in Chapter 4.6.2, if the activity of these three samples would be changed to be more in line with the one of the replicate samples or the samples from the second soil pit at this site, the amount of accumulation would decrease strongly. A possible explanation for why these samples did yield such a high content can be related to the amount of C at this site. However, as it will be discussed in the next Chapter, this does not seem to be the reason. Similar $^{239+240}$Pu activities have been found in samples from the Chernobyl incident. Yet, if they would have originated from this accident their atomic ratio should be in the range of 0.4 (Mietelski et al., 2002). This is not the case and their atomic ratio of 0.18 clearly indicates the global fallout as the source. A third option for the high $^{239+240}$Pu activity could be attributed to the presence of fungi. Dighton et al. (2008) stated that a significant proportion of the amount of radionuclides in an environment can be accumulated into fungi. But, the amount of $^{239+240}$Pu from the global fallout found in fungi from Spain is still a lot smaller than the amount in the three samples (Mietelski et al., 2002). Therefore, it is most

likely that somewhere during the sampling or the sample preparation an error occurred. It is though surprising that both samples of the depth 0 to 5 cm within one pit yielded a content between 30 and 40 Bq kg^{-1}. If it would have happened between different sites it would look more like a coincidence than it does now.

In addition, by taking the standard deviation into account for the two scenarios (i.e., with and without outliers), the IM with P = 1 at site 1 leads to a decrease of soil accumulation with values of 8.64 or 8.61 t ha^{-1} a^{-1}, respectively. Therefore, by subtracting the standard deviation of the two scenarios, they result in a very similar amount of soil accumulation. Showing that not only the three outlier samples are responsible for the high amount of material accumulation but also that some areas at this site are highly disturbed. Nevertheless, the applied statistical tests did not show a significant difference between the topsoil samples. Even though it does look different in Figure 30 for the depth of 0 to 5 cm, the result can be explained with the huge variation of the $^{239+240}$Pu activity measured at site 1.

The measured $^{239+240}$Pu inventory shows the following decreasing picture: The highest inventory was found at site 1, followed by site 3, site 5, site 2 and lastly, site 4. This clearly does not correspond with the expectation that sites further down the valley (i.e., sites 4 and 5) do have more stabilised slopes, as they had more time to evolve due to the glacier retreat in comparison with sites further up the valley (i.e., sites 1 or 2). Yet, as this hypothesis has already been proven not to be the case it is not surprising that the $^{230+240}$Pu inventory does again show a different picture.

Erosion is influenced by many factors such as the slope gradient, vegetation cover or the amount of precipitation (Amelung et al., 2018). The slope is steepest at site 1 (30°) and site 4 (20.5), while the second and fifth site of interest have the same gradient of 15°. The flattest slope was found at site 3 (9.5°). Note that the slope gradients mentioned here are the average gradient per site. Table 1 shows the measured slope gradients of each pit. Liu et al. (2001), stated that a steep slope increases soil erosion. Thus, the correlation value of 0.6 between soil redistribution and slope gradient seems weaker than expected. Based on Liu et al. (2001), the highest amount of erosion should have been at site 1 and the lowest amount is assumed to be at site 3. In addition, precipitation is highest at site 1 with almost 2400 mm a^{-1}, whereas site 5 has around 450 mm less annual precipitation. This would again correspond to more erosion at site 1. The vegetation cover consisting of grassland and shrubs is the same at all sites.

Figure 38 shows the Lagoa de Peixão (close to the second and third site of interest) in the Candieira valley in 1965 in comparison with a Google Maps image of 2022. Although the image from 1965 is in black and white, it can be seen that the vegetation cover increased over the last 60 years. This should result in a more stabilised soil as various studies have shown (e.g. Cerdà, 1999; Zhongming et al., 2010).

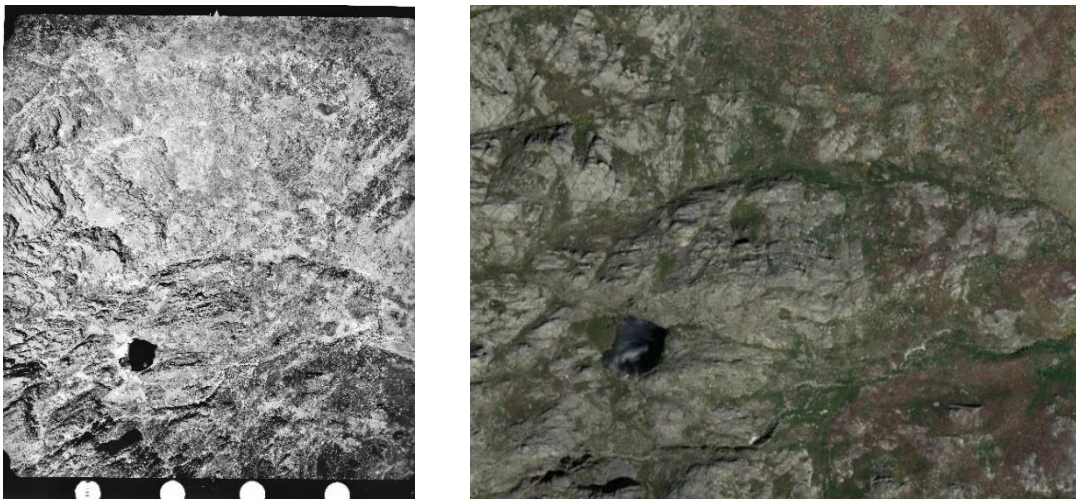

Figure 38: Areal image of the Lagoa de Peixão region in the Candieira valley. Left: Image from 1965 (scale: 1:15'000) by the Instituto Geográfico Portugês, where in the lower right the upper part of the rye fields are visible, right image: Google Maps, 2022.

Additionally, Figure 39 shows the lower part of the Candieira valley in 1941. The image next to it shows the view of the fourth site of interest during the sampling in June, 2021. Again, it is evident that the vegetation in the area did grow. Even though the image from 1941 was taken in winter it can be observed that shrubs became more abundant and the vegetation increased. Thus, despite the frequent occurrence of wildfires, the grass species and small shrubs were able to grow back very fast, resulting in a potential slope stabilisation.

Figure 39: Lower part of the Candieira valley. Left: Image by the geographer Orlando Ribeiro, published in "Contribution to the Study of Pastoreio na Serra da Estrela" in 1941. Right: own image from the sampling in June, 2021.

5.4.2 Relationship between C and soil redistribution based on FRNs

To estimate if the high $^{239+240}$Pu activity measured in the samples form the first site of interest is related to the high C content in the samples, a correlation was conducted. As previously stated, $^{239+240}$Pu does attach to the organic matter (Arata et al., 2016a). Yet, the first site of interest does not have the best correlation values and the three samples with the high $^{239+240}$Pu activity do not have the highest C content at this site, which again is contrary to the expectation. Due to the elaborate laboratory method as well as the sparse amount of sample material left, neither the $^{239+240}$Pu content nor the C [%] concentration were remeasured. Which is why

measurement errors cannot be ruled out. Nevertheless, the general trend that a higher $^{239+240}$Pu activity can be measured in the samples with more C corresponds with the literature such as Chawla et al. (2010), Alewell et al. (2017) or Zhang et al. (2021). But, it does not explain why these three samples do have such a large $^{239+240}$Pu activity.

5.4.3 Comparison of $^{239+240}$Pu inventory based on the different methods

The highest amount of material accumulation was modelled with the IM with P = 1 by Lal et al. (2013), followed by the other two IM scenarios and PDM, while MODERN yielded the smallest amount. This is true for all sites, except site 2, where the PDM resulted in a slightly higher accumulation amount than the IM with P = 1.5. Nevertheless, all five models seem to be most in line at site 2, whereas at the other sites a broad range of material redistribution was modelled. Another exception is site 4, where MODERN resulted in a higher erosion rate then PDM or the IM with P = 1.5.

The difference in the Inventory Method can be explained by the different P factors and thus, the grain size composition of the surface soil. A higher P value assumes a larger grain size. Generally, smaller grain sizes, which in turn have a higher specific area and therefore, a higher $^{239+240}$Pu content, are preferably transported during erosion processes leading to a higher soil redistribution rate, if the particle size factor P is smaller. This can be seen in the decreasing pattern of the IM models with an increasing P factor (Arata et al., 2016a). Based on the rather coarse grain size of the sites, this can lead to two opposite conclusions. Either, the IM with P=1 did lead to an overestimation of the soil redistribution due to the grain size being coarser or the smaller grains have already been transported to another location and thus, the particle size factor of 1.5 is underestimating the amount of soil redistribution. However, based on the PDM and MODERN results, the first case seems more likely, particularly when the high amount of annual precipitation is considered as well.

Another reason for the soil redistribution range can be attributed to the depth distribution of the $^{239+240}$Pu inventory. MODERN for example has a depth distribution similar to a polynomial function, where it follows the incremental measurements, whilst IM is fitted to an exponential depth function. This can result in higher erosion rates with MODERN compared to IM, when only a small inventory change occurs (Arata et al., 2016a). Yet, this did not seem the case with the data from the Geopark Estrela. However, when considering disposition rates, the data corresponds with the one by Arata et al. (2016a). They also had lower deposition rates with MODERN in comparison to the PDM.

5.4.4 Comparison with other FRNs Studies

It is estimated that Portugal has an annual soil erosion of around 2.31 t ha^{-1}, whereas areas within the Central and Northern part of Portugal can have rates up to 20 t ha^{-1} a^{-1}. The Geopark Estrela is located in an area where a soil loss between 5 to 20 t ha^{-1} a^{-1} has been modelled

(Panagos et al., 2015). Thus, the result that the sites can be characterised as material accumulating instead of erosive sites is surprising. However, as this thesis is a follow up master thesis, the soil erosion and accumulation rates can be compared with data from the same region. Table 10 shows the soil accumulation rates by Dollenmeier (2021) for the glaciated research site (S3 and S4) in comparison with the measured soil redistribution rates from the Candieira valley. The second site of interest does fit very well with the accumulation rates of Dollenmeier (2021) at sampling site S3 even though this site is around 10 m higher in altitude. Interestingly, the data from S4 by Dollenmeier (2021), which would be at the same altitude as the second site of interest, does have a very similar $^{239+240}$Pu inventory, yet the accumulation rates are somewhere between the third and fifth site of interest. Moreover, he did not have any soil erosion at the glaciated site, whereas the data from the Candieira valley shows one site with soil erosion (i.e., site 4). However, these rates are a lot lower than the soil erosion rates from the non-glaciated sites of the Geopark Estrela as these are in a the range of 8 to 20 t ha^{-1} a^{-1} (Dollenmeier, 2021). Generally, the measured soil redistribution rates at the second, third and fifth site of interest are in range with the data measured by Dollenmeier (2021). However, the first site of interest is out of range. As stated in Chapter 4.6.2, if the $^{239+240}$Pu activity of the three outlier samples were reduced, an accumulation of 11.3 t ha^{-1} a^{-1} for the IM with P=1 would result. By taking the standard deviation into account and subtracting it, a soil accumulation rate of around 8.6 t ha^{-1} a^{-1} results for IM with P=1. This would still be around twice to three times as much as was measured at S4 by Dollenmeier (2021). But, the PDM leads to an annual accumulation amount of 5.09 t ha^{-1}, which is more in range with the other data. This also supports the idea that the IM with P=1 is overestimating the amount of soil redistribution.

Table 10: Comparison of $^{239+240}$Pu inventory and modelled soil redistribution rates

Site	Altitude [m a.s.l]	Slope [°]	Aspect [°N]	$^{239+240}$Pu inventory [Bq m^{-2}]	IM: P=1 [t ha^{-1} a^{-1}]	IM: P=1.2 [t ha^{-1} a^{-1}]	IM: P=1.5 [t ha^{-1} a^{-1}]	PDM [t ha^{-1} a^{-1}]
Site 1	1873	30	37.5	661.65 ± 477	17.77	14.81	11.85	7.96
Site 2	1645	15	70	176.21 ± 37.12	0.65	0.54	0.43	0.46
Site 3	1582	9.5	226	230.95 ± 66.34	4.79	3.99	3.19	2.05
Site 4	1429.1	20.5	187.5	128.16 ± 23.45	-3.45	-2.88	-2.30	-1.52
Site 5	1412	15	0	195.45 ± 71.20	2.15	1.79	1.43	1.03
S3 by Dollenmeier (2021)	1655	5	90	119.1	0.55	0.46	0.37	0.63
S4 by Dollenmeier (2021)	1645	5	90	179.3	3.36	2.80	2.23	3.98

Although there is not more $^{239+240}$Pu data available for the Geopark Estrela, there are other studies conducted in a similar environment such as Raab et al. (2018), where they studied the Sila Massif upland in Italy. Hence, their research site is also located in the Mediterranean region. Here, the $^{239+240}$Pu inventory of the second site of interest in the Candieira valley is even more similar with the total inventory of the first reference site of Raab et al. (2018). They did measure an inventory of 176 ± 18 Bq m^{-2}. Yet, they did not measure accumulation at any

of their sampling sites. Moreover, their erosion rates are higher than the one measured at the fourth site of interest, as it is again between 10 to 35 t ha^{-1} a^{-1} (Raab et al., 2018). In addition, there are various other researchers, which used $^{239+240}Pu$ as tracer for soil erosion. Loba et al. (2022) mentioned amongst others Alewell et al. (2014), Zollinger et al. (2015) or Arata et al. (2016a) in their review, of which the altitude of the sampling location is mostly in subalpine areas and therefore, similar to the one of the sites in the Geopark. Some of them did result in an accumulation rate, but Arata et al. (2016a) stated that there is a high uncertainty in the data as the temporal dynamics, the source of the material as well as the size of the source area is unknown.

5.5 Comparison of soil redistribution between different time scales

This thesis has an emphasis on the temporal evolution of soil erosion or rather based on the results of soil redistribution. Different patterns can be seen depending on the time scale one views. Overall, temporal evolution can be described by the development of soil redistribution based on the chronosequence. Yet, as the glacier retreat probably occurred a lot faster than expected, this view is not without faults. In addition, it can be characterised by distinguishing between long-term and short-term patterns and how they did change over time. As previously discussed, the long-, mid- and short-term scales do show a completely different picture. Based on the long-term soil formation modelling at site 5, an annual amount of almost 14 t ha^{-1} was calculated to be eroded. However, the relationship between $\delta^{13}C$ and C indicates that site 5 has a stable soil system. Moreover, at this site the short-term soil redistribution of the last 60 years resulted in material accumulation of 1.47 t ha^{-1} a^{-1}. Table 11 shows the combined soil redistribution values per site. Negative values indicate soil erosion, positive soil accumulation.

Table 11: Comparison of long-term to short-term soil redistribution rates. Negative values indicate soil erosion, positive ones material accumulation. Note: due to the qualitative nature of the relationship of $\delta^{13}C$ and C it is only done descriptive. It is assumed that a correlation value above 0.6 equals a stable system.

Site	Long-term [t ha^{-1} a^{-1}]	Mid-term	Short-term [t ha^{-1} a^{-1}]
Site 1	-2.1	Disturbed system	11.31
Site 2	-5.37	Distrubed system	0.49
Site 3	-9.83	Distrubed system	3.09
Site 4	-6.21	Stable system	-2.59
Site 5	-13.89	Stable system	1.47

The expectation was that the amount of annual erosion decreases with time as the soils have had more time to develop a stable soil system. However, because of the rapidly changing environmental conditions after the last glaciation period, increasing moisture availability resulted in a higher biomass production (Allen et al., 1999). The influence of humans on the landscape with deforestation, agriculture and grazing and again a change in climate in the last few decades, prevent a stable soil system from evolving (Huang et al., 2016; Raab et al., 2018). Therefore, old and new disturbances are influencing the data interpretation.

Raab et al. (2018) found in their study researching the Sila Massif upland in Italy that the soil erosion rates increased strongly after the transition from Pleistocene to Holocene. The Sila Massif does have comparable conditions as the Geopark Estrela such as a similar climate and the same soil types with Cambisol and Umbrisol. The soil erosion rate at the Geopark Estrela is almost as high as the soil formation rate is, based on the soil formation modelling. Therefore, an increased erosion rate after the change from one epoch into another due to a warmer and moisture climate could also have happened in Portugal. Yet, the modelled soil erosion is around 2 to 5 times higher depending on the site of interest. This can be related to the coarser medium grain size of the Candieira samples in comparison with the ones from Raab et al. (2018).

The relationship between $\delta^{13}C$ and C content does not correspond with the long-time trend or the short-term pattern. The correlation values indicate that the soils are disturbed, yet this does not have to be because of material accumulation or removal. The relationship can also be affected by wildfires occurring in the region, resulting in a higher C input at the soil surface as well as a new ratio of ^{13}C to ^{12}C (Callegary et al., 2021). Another disturbance can be cryoturbation (Zollinger et al., 2015). Based on Zollinger et al. (2015) the expectation was that mid-term as well as short-term soil redistribution rates are higher in comparison with the long-term ones due to climate warming, leading to for example melting of permafrost. Yet, this is in terms of erosion neither the case for the mid- nor for the short-term soil redistribution.

The Geopark Estrela has been used for different agricultural purposes like sheep grazing or the cultivation of rye. Depending on the intensity, these practices can enhance soil erosion (Ries, 2010). Both of these activities have been conducted in the Candieira valley, which is why they contribute to the expectation to see erosion in the short-term soil redistribution data.

The fourth site of interest, which is the only site that shows to be affected by erosion in the last 60 years does have a very dark soil colour. Wildfires can for example alter the soil colour by charring of the organic matter (Ulery and Graham, 1993). Although it does not have the highest correlation between the $^{239+240}Pu$ activity, the correlation with a value of 0.83 is high and can be used as an indicator that this site is likely to be disturbed by wildfires, resulting in a high C input and possibly responsible for the measured erosion.

The $^{239+240}Pu$ inventory shows that material has been redistributed. Yet, the question remains why there are many areas with material accumulation. In theory, factors such as slope gradient, the land use history and the climatic condition (Ferreira et al., 2022), are leading to the assumptions that these sites should be characterised as erosive sites instead of areas where material accumulates. It is important to keep in mind the $^{239+240}Pu$ measurements are point measurement. Thus, they only represent soil loss or gain at the sampling location (Lal et al., 2013). Therefore, if the sampling locations were located a few meters away from the current

sampling location, a different picture could potentially result. Yet, there is a trend for material accumulation, as both this thesis and Dollenmeier (2021) did find material accumulation in a formerly glaciated area. This can be related to different soil disturbance processes such as anthropogenic influences like wildfires and climate change, leading to unprotected soils as well as longer dry periods, followed by heavy precipitation events (Borrelli et al., 2014; Caon et al., 2014). As a result material is eroded, which might have been accumulated on the sampling locations.

6. Conclusion and Outlook

The aim of this master thesis was to compare the soil redistribution rates over five sites located along an altitude gradient in the Candieira valley, Portugal. Based on the FRNs of $^{239+240}$Pu, soil erosion and accumulation of the last 60 years was reconstructed. Contrary to the assumption that soils located at lower altitude are more stable as they should have had more time to evolve, the results draw a different picture. In addition, the idea of a slow gradual glacier retreat leading to more established soils further down the valley had to be rejected as well based on the result of the weathering indexes.

By comparing long-, mid- and short-term soil redistribution rates, no relationship between the three time scales was visible. Moreover, the hypothesis that the long-term soil erosion rate is smaller in comparison with the short-term one, had to be rejected as well. The long-term soil redistribution concerns a time period of the last 15 ka and is based on soil formation modelling. It showed high erosion rates as well as a high correlation with the soil grain size. Mid-term soil redistribution was only assed qualitatively based on the relationship between δ^{13}C and the total C amount. Yet, it showed that sites 4 and 5, both located at lower altitudes, seem not to be influenced by any soil disturbances. However, the correlation value of site 2, which is close to zero indicates a disturbed soil system. The short-term trend based on the FRNs of $^{239+240}$Pu shows again a different picture. Here, soil accumulation is the dominating pattern, as only site 4 is affected by erosion with a mean annual erosion of 2.59 t ha^{-1}. This is surprising as the samples were collected on steep slopes and wildfires relicts such as charcoal have been found in them. Both of these factors should in theory result in soil erosion. Therefore, it is interesting that at the sampled sites material accumulation was measured. The highest average soil accumulation rate of 11.31 t ha^{-1} a^{-1} or 7.28 t ha^{-1} a^{-1} was found at the steepest slope gradient at site 1, independent of the three samples with a high $^{239+240}$Pu activity being included or not. Followed by site 3 with 3.09 t ha^{-1} a^{-1} and site 5, where an average soil accumulation of 1.47 t ha^{-1} a^{-1} was detected. Site 2 had the smallest mean soil accumulation with 0.49 t ha^{-1} a^{-1} as well as overall the most similar results based on the five models. In addition, it also fitted best in comparison with the data from other FRN studies. Contrary to previous findings, the amount

of soil redistribution did not seem to be directly correlated with the slope gradient as only a correlation value of 0.6 resulted.

Even though there seems to be no relationship between the time scales, the general pattern of the long-term time scale does make sense. The natural tendency of erosion being a function of altitude and grainsize can be seen. Especially the latter is visible with a high correlation value between erosion and d_{50} of the samples. The relationship with altitude is visible indirectly in the weathering indexes, where site 1 and 2 located at higher altitude indicate a more weathered soil. Due to the different patterns visible depending on the time scale one views, it can further be said that the soils are affected by various disturbances leading to material relocation within the soil as well as along the landscape. The high erosion rate from the long-term modelling can be attributed to a change in climate at the Pleistocene to Holocene transition. The current trend shows a high amount of material accumulation, which can become even more enhanced in the near future. This can be due to anthropogenic influences on the landscape itself with sheep cultivation or wildfires and indirectly with the increase of dry and warm summers due to climate change. Soil erosion is expected to occur more often, leading to material being removed at one site and relocated at another. This does not only result in the shaping of a landscape but can also have negative effects in other areas. For example, currently the Geopark Estrela is used as a recreation area. If slopes become less stable, hiking paths need to be adjusted or closed to minimize danger.

To establish a clearer picture of the glacier retreat, the soil development and the disturbances influencing it, further studies are needed. During the sampling in June 2021, ^{10}Be samples for surface exposure dating were collected as well. Yet, at the time of writing, these samples have not been analysed. However, once they are, the time of surface exposure to the atmosphere will be known and can then be used to assess the maximum soil age (Raab et al., 2018). This in turn can be used to evaluate how fast the glacier retreat along the Candieira valley was and, possibly help to support the hypothesis that the glacier retreat occurred faster than originally expected. In addition, further images from past activities in the Candieira valley can be used to better understand the short-term soil redistribution dynamics based on the anthropogenic influence.

This thesis was able to show that there are various disturbances influencing the soil redistribution processes between and within different time scales. The results can thus be used to improve the understanding of the landscape formation and dynamics in the Geopark Estrela.

References

Alewell, C., Meusburger, K., Juretzko, G., Mabit, L., Ketterer, M.E., 2014. Suitability of 239+240Pu and 137Cs as tracers for soil erosion assessment in mountain grasslands. Chemosphere 103, 274–280. https://doi.org/https://doi.org/10.1016/j.chemosphere.2013.12.016

Alewell, C., Pitois, A., Meusburger, K., Ketterer, M., Mabit, L., 2017. Earth-Science Reviews Pu from " contaminant " to soil erosion tracer : Where do we stand ? Earth-Science Rev. 172, 107–123. https://doi.org/10.1016/j.earscirev.2017.07.009

Alewell, C., Ringeval, B., Borrelli, P., Ballabio, C., Robinson, D.A., Panagos, P., 2020. Global phosphorus shortage will be aggravated by soil erosion. Nat. Commun. 11. https://doi.org/10.1038/s41467-020-18326-7

Allen, J.R.M., Brandt, U., Brauer, A., Hubberten, H.-W., Huntley, B., Keller, J., Kraml, M., Mackensen, A., Mingram, J., Negendank, J.F.W., Nowaczyk, N.R., Oberhänsli, H., Watts, W.A., Wulf, S., Zolitschka, B., 1999. Rapid environmental changes in southern Europe during the last glacial period. Nature 400, 740–743. https://doi.org/10.1038/23432

Amelung, W., Blume, H.-P., Fleige, H., Horn, R., Kandeler, E., Kögel-Knabner, I., Kretzschmar, R., Stahr, K., Wilke, B.-M., 2018. Scheffer/Schachtschabel Lehrbuch der Bodenkunde., 17th ed. Springer Berlin Heidelberg.

Arata, L., Alewell, C., Frenkel, E., A'Campo-Neuen, A., Iurian, A.R., Ketterer, M.E., Mabit, L., Meusburger, K., 2016a. Modelling Deposition and Erosion rates with RadioNuclides (MODERN) - Part 2: A comparison of different models to convert 239+240Pu inventories into soil redistribution rates at unploughed sites. J. Environ. Radioact. 162–163, 97–106. https://doi.org/10.1016/j.jenvrad.2016.05.009

Arata, L., Meusburger, K., Frenkel, E., A'Campo-Neuen, A., Iurian, A.R., Ketterer, M.E., Mabit, L., Alewell, C., 2016b. Modelling Deposition and Erosion rates with RadioNuclides (MODERN) - Part 1: A new conversion model to derive soil redistribution rates from inventories of fallout radionuclides. J. Environ. Radioact. 162–163, 45–55. https://doi.org/10.1016/j.jenvrad.2016.05.008

Ayarza, P., Martinez Catalán, J.R., Martinez Garcia, A., Alcalde, J., Andrés, J., Simancas, J.F., Palomeras, I., Marti, D., DeFelipe, I., Juhlin, C., Carbonell, R., 2021. Evolution of the Iberian Massif as deduced from its crustal thickness and geometry of a mid-crustal (Conrad) discontinuity. Solid Earth 12, 1515–1547. https://doi.org/10.5194/se-12-1515-2021

Bajard, M., Poulenard, J., Sabatier, P., Develle, A.-L., Giguet-Covex, C., Jacob, J., Crouzet, C., David, F., Pignol, C., Arnaud, F., 2017. Progressive and regressive soil evolution phases in the Anthropocene. CATENA 150, 39–52. https://doi.org/https://doi.org/10.1016/j.catena.2016.11.001

Bakker, M.M., Govers, G., Rounsevell, M.D.A., 2004. The crop productivity–erosion relationship: an analysis based on experimental work. CATENA 57, 55–76.

https://doi.org/https://doi.org/10.1016/j.catena.2003.07.002

Balesdent, J., Mariotti, A., 1996. Measurement of soil organic matter turnover using 13C natural abundance. Mass Spectrom. soils 41, 83–111.

Ballabio, C., Lugato, E., Fernández-Ugalde, O., Orgiazzi, A., Jones, A., Borrelli, P., Montanarella, L., Panagos, P., 2019. Mapping LUCAS topsoil chemical properties at European scale using Gaussian process regression. Geoderma 355, 113912. https://doi.org/https://doi.org/10.1016/j.geoderma.2019.113912

Ban, J., Moon, S., Lee, S., Lee, J., Seo, Y., 2017. Physical and Chemical Weathering Indices for Biotite Granite and Granitic Weathered Soil in Gyeongju. J. Eng. Geol. 27, 451–462. https://doi.org/https://doi.org/10.9720/kseg.2017.4.451

Bashour, I.I., Sayegh, A.H., 2007. Methods of analysis for soils of arid and semi-arid regions.. FAO, Rome, Beirut, Lebanon.

Borrelli, P., Märker, M., Panagos, P., Schütt, B., 2014. Catena Modeling soil erosion and river sediment yield for an intermountain drainage basin of the Central Apennines , Italy. Catena 114, 45–58. https://doi.org/10.1016/j.catena.2013.10.007

Borrelli, P., Robinson, D.A., Fleischer, L.R., Lugato, E., Ballabio, C., Alewell, C., Meusburger, K., Modugno, S., Schütt, B., Ferro, V., Bagarello, V., Oost, K. Van, Montanarella, L., Panagos, P., 2017. An assessment of the global impact of 21st century land use change on soil erosion. Nat. Commun. 8. https://doi.org/10.1038/s41467-017-02142-7

Brady, N., Weil, R.R., 2017. The nature and properties of soils, Fifteenth. ed, The nature and properties of soils. Pearson, Harlow, England.

Brosens, L., Robinet, J., Pelckmans, I., Ameijeiras-Mariño, Y., Govers, G., Opfergelt, S., Minella, J.P.G., Vanderborght, J., 2021. Have land use and land cover change affected soil thickness and weathering degree in a subtropical region in Southern Brazil? Insights from applied mid-infrared spectroscopy. CATENA 207, 105698. https://doi.org/https://doi.org/10.1016/j.catena.2021.105698

Brouwer, P., 2003. Theory of XRF. Getting acquainted with the principles. PANalytical BV.

Callegary, J.B., Norman, L.M., Eastoe, C.J., Sankey, J.B., Youberg, A., 2021. Preliminary Assessment of Carbon and Nitrogen Sequestration Potential of Wildfire-Derived Sediments Stored by Erosion Control Structures in Forest Ecosystems, Southwest USA. Air, Soil Water Res. 14, 11786221211001768. https://doi.org/10.1177/11786221211001768

Caon, L., Vallejo, V.R., Coen, R.J., Geissen, V., 2014. Effects of wildfire on soil nutrients in Mediterranean ecosystems. Earth-Science Rev. 139, 47–58. https://doi.org/10.1016/j.earscirev.2014.09.001

Cerdà, A., 1999. Parent Material and Vegetation Affect Soil Erosion in Eastern Spain. Soil Sci. Soc.

Am. J. 63, 362–368. https://doi.org/https://doi.org/10.2136/sssaj1999.03615995006300020014x

Cerdan, O., Govers, G., Le Bissonnais, Y., Van Oost, K., Poesen, J., Saby, N., Gobin, A., Vacca, A., Quinton, J., Auerswald, K., Klik, A., Kwaad, F.J.P.M., Raclot, D., Ionita, I., Rejman, J., Rousseva, S., Muxart, T., Roxo, M.J., Dostal, T., 2010. Rates and spatial variations of soil erosion in Europe: A study based on erosion plot data. Geomorphology 122, 167–177. https://doi.org/https://doi.org/10.1016/j.geomorph.2010.06.011

Cerdan, O., Poesen, J., Govers, G., Saby, N., Le Bissonnais, Y., Gobin, A., Vacca, A., Quinton, J., Auerswald, K., Klik, A., Kwaad, F.J.P.M., Roxo, M.J., 2006. Sheet and rill erosion., in: Boardman, J., Poesen, J. (Eds.), Soil Erosion in Europe. Wiley and Sons, Chichester, pp. 501–518.

Chawla, F., Steinmann, P., Pfeifer, H.R., Froidevaux, P., 2010. Atmospheric deposition and migration of artificial radionuclides in Alpine soils (Val Piora, Switzerland) compared to the distribution of selected major and trace elements. Sci. Total Environ. 408, 3292–3302. https://doi.org/10.1016/j.scitotenv.2010.03.012

Chungu, D., Ng'andwe, P., Mubanga, H., Chileshe, F., 2020. Fire alters the availability of soil nutrients and accelerates growth of Eucalyptus grandis in Zambia. J. For. Res. 31, 1637–1645. https://doi.org/10.1007/s11676-019-00977-y

Courchesne, F; Turmel, M.-C., 2008. Soil Sampling and Methods of Analysis, second edi. ed. Taylor & Francis Group, LLC.

Dahms, D., Favilli, F., Krebs, R., Egli, M., 2012. Soil weathering and accumulation rates of oxalate-extractable phases derived from alpine chronosequences of up to 1 Ma in age. Geomorphology 151–152, 99–113. https://doi.org/10.1016/j.geomorph.2012.01.021

De Castro, E., 2021. Estrela UNESCO Global Geopark (Portugal). <https://en.unesco.org/global-geoparks/estrela#> The Estrela UNESCO global Geopark,batholiths in late orogenic stages. Accessed: 30.03.2022

Dighton, J., Tugay, T., Zhdanova, N., 2008. Fungi and ionizing radiation from radionuclides. FEMS Microbiol Lett. 2, 109–120. https://doi.org/10.1111/j.1574-6968.2008.01076.x

Dollenmeier, W., 2021. Determination of soil disturbances in Geopark Estrela (Portugal). University of Zurich.

EEA, 2009. Assessment of the actual soil erosion risk in Southern Europe by combining four sets of factors: soil, climate, slopes, vegetation. Eur. Evironment Agency. <https://www.eea.europa.eu/data-and-maps/figures/soil-erosion-risk-actual>. Accessed: 12.03.2022

Egli, M., Hunt, A.G., Dahms, D., Raab, G., Derungs, C., 2018. Prediction of Soil Formation as a Function of Age Using the Percolation Theory Approach 6, 1–21. https://doi.org/10.3389/fenvs.2018.00108

Egli, M., Lessovaia, S., Chistyakov, K., Inozemzev, S Polekhovsky, Y., Ganyushkin, D., 2015. Microclimate affects soil chemical and mineralogical properties of cold alpine soils of the Altai Mountains (Russia). Journal of Soils and Sediments.

Egli, M., Plötze, M., Tikhomirov, D., Kraut, T., Wiesenberg, G.L.B., Lauria, G., Raimondi, S., 2020. Soil development on sediments and evaporites of the Messinian crisis. CATENA 187, 104368. https://doi.org/https://doi.org/10.1016/j.catena.2019.104368

Egli, M., Tikhomirov, D., Keller, T., Taghizadeh, E., 2021. Geochronology laboratory methods. Zurich.

Egli, M., Wernli, M., Kneisel, C., Haeberli, W., 2006. Melting Glaciers and Soil Development in the Proglacial Area Morteratsch (Swiss Alps): I. Soil Type Chronosequence. Arctic, Antarct. Alp. Res. 38, 499–509. https://doi.org/10.1657/1523-0430(2006)38[499:MGASDI]2.0.CO;2

Espinha Marques, J., Samper, J., Pisani, B. V., Alvares, D., Vieira, G.T., Mora, C., Carvalho, J.M., Chaminé, H.I., Marques, J.M., Sodré Borges, F., 2006. Avaliação de recursos hídricos através de modelação hidrológica: Aplicação do programa VISUAL BALAN v2.0 a uma bacia hidrográfica na Serra da Estrela (Centro de Portugal). Cad. do Lab. Xeol. Laxe 31, 43–65.

FAO, 2014. World reference base for soil resources 2014. International soil classification system for naming soils and creating legends for soil maps, World Soil Resources Reports No. 106.

Ferreira, C., Seifollahi-aghmiuni, S., Destouni, G., Ghajarnia, N., Kalantari, Z., 2022. Science of the Total Environment Soil degradation in the European Mediterranean region : Processes , status and consequences. Sci. Total Environ. 805, 150106. https://doi.org/10.1016/j.scitotenv.2021.150106

Ferreira, N., Iglésias, M., Noronha, F., Pereira, E., Ribeiro, A., Ribeiro, M., 1987. Geologia de los Granitóides y Rocas asociadas del Macizo Hespérico, Granitóides da Zona Centro Ibérica e seu enquadramento geodinâmico. Editorial Rueda, Madrid.

Gomes, H., Loureiro, F., Cezar, L., Castro, E., Vieira, G., 2019. Interpreting Late Pleistocene Paleoenvironments through the geosites of the Estrela Geopark, Central Portugal.

Guillaume, T., Damris, M., Kuzyakov, Y., 2015. Losses of soil carbon by converting tropical forest to plantations : erosion and decomposition estimated by d 13 C. Glob. Chang. Biol. 21, 3548–3560. https://doi.org/10.1111/gcb.12907

Habte, M., 1999. Soil acidity as a constraint to the application of arbuscular mycorrhizal technology, in: Varma, A., Hock, B. (Eds.), Mycorrhiza. Springer Berlin Heidelberg, pp. 557–569.

Häring, V., Fischer, H., Cadisch, G., Stahr, K., 2013. Improved δ13C method to assess soil organic carbon dynamics on sites affected by soil erosion. Eur. J. Soil Sci. 64, 639–650. https://doi.org/https://doi.org/10.1111/ejss.12060

Hu, Yunfeng, Dao, R., Hu, Yang, 2019. Vegetation Change and Driving Factors : Contribution Analysis in the Loess Plateau of China during 2000 – 2015. Sustainability 11, 16.

https://doi.org/10.3390/su11051320

Huang, J., Ji, M., Xie, Y., Wang, S., He, Y., Ran, J., 2016. Global semi-arid climate change over last 60 years. Clim. Dyn. 46, 1131–1150. https://doi.org/10.1007/s00382-015-2636-8

Huggett, R.J., 1998. Soil chronosequences , soil development , and soil evolution : a critical review. Catena 32, 155–172. https://doi.org/https://doi.org/10.1016/S0341-8162(98)00053-8

Hunt, A.G., Ghanbarian, B., 2016. Percolation theory for solute transport in porous media: geochemistry, geomorphology, and carbon cycling. Water Resour. Res. 52, 7444–7459. https://doi.org/https://doi.org/10.1002/2016WR019289

IAEA, 2014. Guidelines for Using Fallout Radionuclides to Assess Erosion and Effectiveness of Soil Conservation Strategies, International Atomic Energy Agency Publication. Vienna, Austria, Vienna, Austria.

Jabiol, B., Zanella, A., Ponge, J.F., Sartori, G., Englisch, M., van Delft, B., de Waal, R., Le Bayon, R.C., 2013. A proposal for including humus forms in the World Reference Base for Soil Resources (WRB-FAO). Geoderma 192, 286–294. https://doi.org/10.1016/j.geoderma.2012.08.002

Jansen, J., 1998. Übersicht der Silikatschutt-Vegetation in den höheren Stufen der Serra da Estrela , Portugal. Port. - Berichte der Reinhold-Tüxen-Gesellschaft 10, 95–124.

Jenny, H., 1941. Factors of Soil Formation: A System of Quantitative Pedology. Dover Publications, INC. New York, Dover, N.Y. https://doi.org/Factors of Soil Formation: A System of Quantitative Pedology

Kelley, J.M., Bond, L.A., Beasley, T.M., 1999. Global distribution of Pu isotopes and 237Np. Sci. Total Environ. 237–238, 483–500. https://doi.org/10.1016/S0048-9697(99)00160-6

Ketterer, M.E., 2015. Standard operating procedure for preparation of soils and sediments for 239+240 Pu activity and 240Pu/239Pu atom ratio measurements -Acid Leaching and Quadrupole ICPMS.

Kneisel, C., Emmert, A., Polich, P., Zollinger, B., Egli, M., 2015. Soil geomorphology and frozen ground conditions at a subalpine talus slope having permafrost in the eastern Swiss Alps. Catena 133, 107–118. https://doi.org/10.1016/j.catena.2015.05.005

Knicker, H., 2007. How does fire affect the nature and stability of soil organic nitrogen and carbon ? A review. Biogeochemistry 85, 91–118. https://doi.org/10.1007/s10533-007-9104-4

Kohn, M.J., 2010. Carbon isotope compositions of terrestrial C3 plants as indicators of (paleo) ecology and (paleo) climate. PNAS 107, 19691–19695. https://doi.org/10.1073/pnas.1004933107

Kronberg, B.I., Nesbitt, H.W., 1981. Quantification of weathering, soil geochemistry and soil fertility. Eur. J. Soil Sci. 32, 453–459. https://doi.org/https://doi.org/10.1111/j.1365-2389.1981.tb01721.x

Lal, R., Tims, S.G., Fifield, L.K., Wasson, R.J., Howe, D., 2013. Nuclear Instruments and Methods in Physics Research B Applicability of 239 Pu as a tracer for soil erosion in the wet-dry tropics of northern Australia. Nucl. Inst. Methods Phys. Res. B 294, 577–583. https://doi.org/10.1016/j.nimb.2012.07.041

Liu, Q., Chen, L., Li, J., 2001. Influences of Slope Gradient on Soil Erosion. Appl. Math. Mech. 22, 510–519. https://doi.org/10.1023/A:1016303213326

Loba, A., Waroszewski, J., Sykuła, M., Kabala, C., 2022. Medium-Term Soil Erosion — A Review. Minerals 12, 1–23. https://doi.org/https://doi.org/10.3390/min12030359

Martín-González, F., 2009. Cenozoic tectonic activity in a Variscan basement: Evidence from geomorphological markers and structural mapping (NW Iberian Massif). Geomorphology 107, 210–225. https://doi.org/10.1016/j.geomorph.2008.12.008

Matisoff, G., Whiting, P.J., 2011. Measuring Soil Erosion Rates Using Natural (7Be , 210Pb) and Anthropogenic Measuring Soil Erosion Rates Using Natural (7 Be , 210 Pb) and Anthropogenic (137 Cs , 239 , 240 Pu) Radionuclides, in: Baskaran, M. (Ed.), Handbook of Environmental Isotope Geochemistry,. Springer Berlin Heidelberg, pp. 487–519. https://doi.org/DOI 10.1007/978-3-642-10637-8_25

Meusburger, K., Mabit, L., Ketterer, M., Park, J., Sandor, T., 2016. A multi-radionuclide approach to evaluate the suitability of 239 + 240Pu as soil erosion tracer. Sci. Total Environ. https://doi.org/10.1016/j.scitotenv.2016.06.035

Meusburger, K., Mabit, L., Park, J.-H., Sandor, T., Alewell, C., 2013. Combined use of stable isotopes and fallout radionuclides as soil erosion indicators in a forested mountain site , South Korea. Biogeosxiences 10, 5627–5638. https://doi.org/10.5194/bg-10-5627-2013

Mietelski, J.W., Baeza, A.S., Guillen, J., Buzinny, M., Tsigankov, N., Gaca, P., Jasinska, M., Tomankiewicz, E., 2002. Plutonium and other alpha emitters in mushrooms from Poland, Spain and Ukraine.pdf. Appl. Radiat. Isot. 56, 717–729.

Mitchell, P.I., León Vintró, L., Dahlgaard, H., Gascó, C., Sánchez-Cabeza, J.A., 1997. Perturbation in the 240Pu/239Pu global fallout ratio in local sediments following the nuclear accidents at Thule (Greenland) and Palomares (Spain). Sci. Total Environ. 202, 147–153. https://doi.org/10.1016/S0048-9697(97)00111-3

Mora, C., 2010. A synthetic map of the climatopes of the serra da estrela (portugal). J. Maps 6, 591–608. https://doi.org/10.4113/jom.2010.1112

Nesbitt, H.W., Young, G.M., 1982. Early Proterozoic climates and plate motions inferred from major element chemistry of Intites 299, 715–717. https://doi.org/10.1038/299715a0

Nunes, A.N., 2011. Soil Erosion Under Different Land Use and Cover Types in a Marginal Area of Portugal, in: Soil Erosion Studies. CEGOT, Departamento de Geografia, Faculdade de Letras, Universidade de Coimbra, Coimbra.

Ollivier, J., Töwe, S., Bannert, A., Hai, B., Kastl, E.M., Meyer, A., Su, M.X., Kleineidam, K., Schloter, M., 2011. Nitrogen turnover in soil and global change. FEMS Microbiol. Ecol. 78, 3–16. https://doi.org/10.1111/j.1574-6941.2011.01165.x

Olowolafe, A.E.A., 2002. Soil parent materials and soil properties in two separate catchment areas on the Jos Plateau , Nigeria. GeoJournal 56, 201–212. https://doi.org/https://doi.org/10.1023/A:1025158121610

Panagos, P., Ballabio, C., Poesen, J., Lugato, E., Scarpa, S., Montanarella, L., Borrelli, P., 2020. A Soil Erosion Indicator for Supporting Agricultural , Environmental and Climate Policies in the European Union. Remote Sens. 12, 1365. https://doi.org/10.3390/rs12091365

Panagos, P., Borrelli, P., Poesen, J., 2019. Science of the Total Environment Soil loss due to crop harvesting in the European Union : A fi rst estimation of an underrated geomorphic process. Sci. Total Environ. 664, 487–498. https://doi.org/10.1016/j.scitotenv.2019.02.009

Panagos, P., Borrelli, P., Poesen, J., Ballabio, C., Lugato, E., Meusburger, K., Montanarella, L., Alewell, C., 2015. The new assessment of soil loss by water erosion in Europe. Environ. Sci. Policy 54, 438–447. https://doi.org/https://doi.org/10.1016/j.envsci.2015.08.012

Pansu, M., Gautheyrou, J., 2006. Handbook of Soil Analysis. Springer Berlin Heidelberg.

Poage, M.A., Feng, X., 2004. A theoretical analysis of steady state δ13C profiles of soil organic matter. Global Biogeochem. Cycles 18. https://doi.org/https://doi.org/10.1029/2003GB002195

Portes, R., Dahms, D., Brandová, D., Raab, G., Christl, M., Kühn, P., Ketterer, M., Egli, M., 2018. Evolution of soil erosion rates in alpine soils of the Central Rocky Mountains using fallout Pu and δ 13 C. Earth Planet. Sci. Lett. 496, 257–269. https://doi.org/10.1016/j.epsl.2018.06.002

Raab, G., Scarciglia, F., Norton, K., Dahms, D., Brandová, D., Castro, R. De, Egli, M., Michael, E., 2018. Denudation variability of the Sila Massif upland (Italy) from decades to millennia using 10 Be and 239 + 240 Pu. L. Degrad. Dev. 1–17. https://doi.org/10.1002/ldr.3120

Ries, J.B., 2010. Methodologies for soil erosion and land degradation assessment in mediterranean-type ecosystems. L. Degrad. Dev. 187, 171–187. https://doi.org/https://doi.org/10.1002/ldr.943

Rijk, I.J.C., Ekblad, A., 2020. Carbon and nitrogen cycling in a lead polluted grassland evaluated using stable isotopes (δ13C and δ15N) and microbial, plant and soil parameters. Plant Soil 449, 249–266. https://doi.org/10.1007/s11104-020-04467-7

Rodeghiero, M., Rubio, A., Díaz-Pinés, E., Romanyà, J., Marañón-Jiménez, S., Levy, G.J., Fernandez-Getino, A.P., Sebastià, M.T., Karyotis, T., Chiti, T., Sirca, C., Martins, A., Madeira, M., Zhiyanski, M., Gristina, L., La Mantia, T., 2011. Soil Carbon in Mediterranean Ecosystems and Related Management Problems, Soil Carbon in Sensitive European Ecosystems: From Science to Land Management. https://doi.org/10.1002/9781119970255.ch8

Salehi, M.H., Hashemi Beni, O., Beigi Harchegani, H., Esfandiarpour Borujeni, I., Motaghia, H.R.,

2011. Refining Soil Organic Matter Determination by Loss-on-Ignition. Pedosph. An Int. J. 21, 473–482. https://doi.org/10.1016/S1002-0160(11)60149-5

Shakesby, R.A., 2011. Earth-Science Reviews Post-wildfire soil erosion in the Mediterranean : Review and future research directions. Earth Sci. Rev. 105, 71–100. https://doi.org/10.1016/j.earscirev.2011.01.001

Shukla, A., Vyas, D., Jha, A., 2013. Soil depth: An overriding factor for distribution of Arbuscular Mycorrhizal fungi. J. Soil Sci. Plant Nutr. 13, 23–33. https://doi.org/10.4067/s0718-95162013005000003

Slessarev, E.W., Chadwick, O.A., Sokol, N.W., Nuccio, E.E., Pett-Ridge, J., 2022. Rock weathering controls the potential for soil carbon storage at a continental scale. Biogeochemistry 157, 1–13. https://doi.org/10.1007/s10533-021-00859-8

Stahr, K., Kandeler, E., Hermann, L., Streck, T., 2016. Bodenkunde und Standortlehre, 3rd ed. utb.

Truog, E., 1948. Lime in relation to availability of plant nutrients. Soil Sci. 65, 1–7. https://doi.org/10.1097/00010694-194801000-00002

Ulery, A.L., Graham, R.C., 1993. Forest Fire Effects on Soil Color and Texture. Soil Sci. Soc. Am. J. 57, 135–140. https://doi.org/https://doi.org/10.2136/sssaj1993.03615995005700010026x

Verheijen, F.G.A., Jones, R.J.A., Rickson, R.J., Smith, C.J., 2009. Tolerable versus actual soil erosion rates in Europe. Earth-Science Rev. 94, 23–38. https://doi.org/https://doi.org/10.1016/j.earscirev.2009.02.003

Vieira, G., Castro, E. De, Gomes, H., Loureiro, F., 2020. The Estrela Geopark—From Planation Surfaces to Glacial Erosion. Springer International Publishing. https://doi.org/10.1007/978-3-319-03641-0

Vieira, G., Jansen, J., Ferreira, N., 2005. Environmental setting of the Serra da Estrela, Portugal : a short-note, in: Correia, P., Bunce, R.G.., Howard, D.C. (Eds.), Landscape Ecology and Management of Atlantic Mountains. IALE.

Vieira, G., Nieuwendam, A., 2020. Glacial and Periglacial Landscapes of the Serra da Estrela. Springer International Publishing. https://doi.org/10.1007/978-3-319-03641-0

Vieira, G., Palacios, D., Andrés, N., Mora, C., Vázquez Selem, L., Woronko, B., Soncco, C., Úbeda, J., Goyanes, G., 2021. Penultimate Glacial Cycle glacier extent in the Iberian Peninsula: New evidence from the Serra da Estrela (Central System, Portugal). Geomorphology 388. https://doi.org/10.1016/j.geomorph.2021.107781

Walling, D.E., He, Q., 1999. Improved Models for Estimating Soil Erosion Rates from Cesium-137 Measurements. J. Environ. Qual. 38, 611–622. https://doi.org/https://doi.org/10.2134/jeq1999.00472425002800020027x

Walling, D.E., Quine, T.A., 1990. Calibration of caesium-137 measurements to provide quantitative

erosion rate data. L. Degrad. Dev. 2, 161–175. https://doi.org/https://doi.org/10.1002/ldr.3400020302

Wischmeier, W.H., Mannering, J. V, 1969. Relation of Soil Properties to its Erodibility. Soil Sci. Soc. Am. J. 33, 131–137. https://doi.org/https://doi.org/10.2136/sssaj1969.03615995003300010035x

Yu, F., Hunt, A.G., 2018. Predicting soil formation on the basis of transport-limited chemical weathering. Geomorphology 301, 21–27. https://doi.org/10.1016/j.geomorph.2017.10.027

Zech, W., Schad, P., Hintermaier-Erhard, G., 2014. Böden der Welt - Ein Bildatlas, 2nd ed. Springer Berlin Heidelberg.

Zech, W., Wilke, B.M., 1977. Vorläufige Ergebnisse einer Bodenchronosequenzstudie im Zillertal. Mitteilungen der Dtsch. Bodenkundlichen Gesellschaft 25, 571–586.

Zhang, W., Hou, X., Zhang, H., Wang, Y., Dang, H., Xing, S., Chen, N., 2021. Level, distribution and sources of plutonium in the northeast and north China. Environ. Pollut. 289, 117967. https://doi.org/https://doi.org/10.1016/j.envpol.2021.117967

Zhang, X., Higgitt, D.L., Walling, D.E., 1990. A preliminary assessment of the potential for using caesium-137 to estimate rates of soil erosion in the Loess Plateau of China 35, 267–276. https://doi.org/10.1080/02626669009492427

Zhongming, W., Lees, B.G., Feng, J., Wanning, L., Haijing, S., 2010. Stratified vegetation cover index: a new way to assess vegetation impact on soil erosion. Catena 83, 87–93. https://doi.org/https://doi.org/10.1016/j.catena.2010.07.006.

Zollinger, B., Alewell, C., Kneisel, C., Meusburger, K., Brandová, D., Kubik, P., 2015. The effect of permafrost on time-split soil erosion using (δ 13 C) in the eastern Swiss Alps 1400–1419. https://doi.org/10.1007/s11368-014-0881-9

Appendix

*Table A 1: Raw data chemical and physical measurements of the sites of interest. Note that top- and subsoil samples were measured twice for C [%], $\delta^{13}C$ and N [%] content, whereas it was not possible to calculate their bulk density (BD). * indicates samples where twice the amount of liquid for the pH measurement was used. A and B are the replicate rows. AB are the top- and subsoil samples.*

Site	Soil Pit	Sample ID	Depth	pH	LOI [%]	C [%]	$\delta^{13}C$ [‰ V-PDB]	N [%]	BD [g cm^{-3}]	Munsel Color dry
1	5A	SSP44	0-5 cm	3.6*	37.62	16.54	-27.14	1.12	0.45	
1	5A	SSP45	5-10 cm	3.51	19.52	8.55	-26.73	0.67	0.89	
1	5A	SSP46	10-15 cm	3.51	14.83	6.10	-26.54	0.44	1.26	
1	5A	SSP47	15-20 cm	3.39	20.21	8.73	-26.22	0.63	0.89	
1	5A	SSP48	30-35 cm	3.76	7.65	3.36	-26.35	0.22	1.18	
1	5A	SSP49	40-45 cm	3.83	20.42	8.90	-26.74	0.65	0.71	
1	5B	SSP50	0-5 cm	3.18	33.78	12.04	-26.53	0.83	0.52	
1	5B	SSP51	5-10 cm	3.51	17.20	7.70	-26.38	0.64	0.91	
1	5B	SSP52	10-15 cm	3.53	14.15	6.31	-26.43	0.42	0.91	
1	5B	SSP53	15-20 cm	3.59	24.62	11.19	-26.07	0.80	0.67	
1	5B	SSP54	30-35 cm	3.68	7.54	3.40	-26.29	0.24	1.12	
1	5B	SSP55	40-45 cm	3.91	3.37	1.62	-26.55	0.12	1.36	
1	5AB	SSP56	Topsoil	3.43	21.63	9.73	-26.18	0.70		10YR 4/2
1	5AB	SSP56	Topsoil			9.70	-26.16	0.70		
1	6A	SSP57	0-5 cm	3.57*	54.31	25.07	-26.81	1.72	0.33	
1	6A	SSP58	5-10 cm	3.58*	48.19	21.97	-26.65	1.65	0.33	
1	6A	SSP59	10-15 cm	3.34	17.87	8.23	-26.25	0.68	0.86	
1	6A	SSP60	15-20 cm	3.61	18.59	9.48	-26.36	0.77	0.69	
1	6A	SSP61	30-35 cm	3.64	10.29	4.69	-26.51	0.37	1.17	
1	6B	SSP62	0-5 cm	3.72*	69.51	35.27	-27.57	2.25	0.19	
1	6B	SSP63	5-10 cm	3.53	31.45	14.99	-26.38	1.21	0.83	
1	6B	SSP64	10-15 cm	3.6	16.08	7.36	-26.53	0.62	0.86	
1	6B	SSP65	15-20 cm	3.62	17.42	8.01	-26.61	0.61	0.86	
1	6B	SSP66	30-35 cm	3.68	9.15	4.42	-26.54	0.30	1.09	
1	6AB	SSP67	Topsoil	3.44	17.16	7.58	-26.51	0.61		10YR 4/1
1	6AB	SSP67	Topsoil			7.51	-26.46	0.60		
2	1A	SSP1	0-5 cm	3.63	20.85	10.34	-27.01	0.77	0.63	
2	1A	SSP2	5-10 cm	3.54	31.22	16.88	-27.29	1.42	0.58	
2	1A	SSP3	10-15 cm	3.59	20.07	8.61	-26.73	0.60	0.84	
2	1A	SSP4	15-20 cm	3.92	15.15	6.85	-27.11	0.44	1.23	
2	1A	SSP5	25 - 30 cm	3.98	10.89	4.65	-27.17	0.31	1.27	
2	1A	SSP6	35 - 40 cm	4.13	8.94	3.33	-27.65	0.29	1.38	
2	1B	SSP7	0-5 cm	3.74	32.00	16.74	-26.74	1.14	0.55	
2	1B	SSP8	5-10 cm	3.78	25.33	10.81	-26.81	0.60	0.78	
2	1B	SSP9	10-15 cm	4.00	11.56	5.51	-26.85	0.37	1.07	
2	1B	SSP10	15-20 cm	4.05	7.33	3.00	-27.36	0.24	1.18	
2	1B	SSP11	25 - 30 cm	4.08	7.25	2.73	-27.59	0.27	1.25	
2	1B	SSP12	35 - 40 cm	4.08	14.98	5.64	-27.95	0.46	1.14	
2	1AB	SSP13	Topsoil	3.50	21.67	10.04	-26.79	0.81		2.5Y 5/2
2	1AB	SSP13	Topsoil			10.54	-26.85	0.85		
2	1AB	SSP14	Subsoil	3.85	9.95	4.05	-27.17	0.39		10YR 4/3
2	1AB	SSP14	Subsoil			4.15	-27.46	0.39		
2	2A	SSP15	0-5 cm	3.49	23.23	11.10	-26.66	1.06	0.60	
2	2A	SSP16	5-10 cm	3.87	20.89	9.20	-26.71	0.89	0.71	
2	2A	SSP17	10-15 cm	3.69	16.34	7.76	-25.95	0.71	0.96	
2	2A	SSP18	15-20 cm	3.57	17.63	7.83	-25.65	0.75	0.83	
2	2B	SSP19	0-5 cm	3.64	26.08	10.93	-26.95	0.95	0.52	
2	2B	SSP20	5-10 cm	3.67	20.02	11.10	-26.53	0.84	0.59	
2	2B	SSP21	10-15 cm	3.77	21.40	8.37	-25.80	0.80	0.88	
2	2B	SSP22	15-20 cm	3.34	19.37	8.55	-25.75	0.86	0.71	
2	2AB	SSP23	Topsoil	3.61	18.37	8.47	-25.94	0.82		10YR 3/1
2	2AB	SSP23	Topsoil			8.61	-25.99	0.84		
3	3A	SSP24	0-5 cm	3.51	32.87	15.17	-26.43	1.16	0.56	
3	3A	SSP25	5-10 cm	3.46	22.90	10.89	-26.12	0.90	0.68	
3	3A	SSP26	10-15 cm	3.50	25.04	11.35	-25.51	0.97	0.80	
3	3A	SSP27	25-30 cm	3.6	13.27	5.81	-25.59	0.48	1.30	
3	3B	SSP28	0-5 cm	3.79	19.62	8.89	-26.40	0.70	0.93	
3	3B	SSP29	5-10 cm	3.61	19.00	9.20	-26.28	0.65	0.87	
3	3B	SSP30	10-15 cm	3.54	18.80	8.91	-25.76	0.76	0.79	
3	3B	SSP31	25-30 cm	3.41	12.92	7.76	-25.68	0.48	1.28	
3	3AB	SSP32	Topsoil	3.39	23.44	11.07	-25.86	0.94		10YR 3/2
3	3AB	SSP32	Topsoil			10.93	-25.82	0.93		
3	4A	SSP33	0-5 cm	3.77	22.79	11.36	-26.72	0.80	0.78	
3	4A	SSP34	5-10 cm	3.76	16.04	7.52	-26.00	0.61	1.15	
3	4A	SSP35	10-15 cm	3.79	9.95	7.83	-25.45	0.41	1.35	
3	4A	SSP36	15-20 cm	3.73	13.43	6.55	-25.78	0.51	1.23	
3	4A	SSP37	25 - 30 cm	3.7	16.06	7.04	-25.84	0.46	1.10	
3	4B	SSP38	0-5 cm	3.91	17.60	7.67	-26.59	0.44	0.83	
3	4B	SSP39	5-10 cm	3.68	13.13	6.32	-26.27	0.40	1.51	
3	4B	SSP40	10-15 cm	3.72	8.58	3.67	-25.70	0.30	1.33	
3	4B	SSP41	15-20 cm	3.81	10.53	5.36	-25.50	0.47	1.28	
3	4B	SSP42	25 - 30 cm	3.82	8.52	5.09	-25.51	0.44	1.33	

Site	Soil Pit	Sample ID	Depth	pH	LOI [%]	C [%]	$\delta^{13}C$ [‰ V-PDB]	N [%]	BD [g cm^{-3}]	Munsel Color dry
3	4AB	SSP43	Topsoil	3.62	12.98	5.89	-26.17	0.49		10YR 3/1
3	4AB	SSP43	Topsoil			5.94	-26.09	0.50		
4	7A	SSP68	0-5 cm	3.44	8.54	4.20	-27.63	0.25	1.01	
4	7A	SSP69	5-10 cm	3.78	8.80	3.95	-26.41	0.22	1.20	
4	7A	SSP70	10-15 cm	3.77	8.26	3.72	-26.14	0.24	1.20	
4	7A	SSP71	15-20 cm	3.75	0.60	3.94	-25.97	0.25	1.19	
4	7A	SSP72	30-35 cm	3.72	6.71	3.24	-25.88	0.20	1.09	
4	7B	SSP73	0-5 cm	3.78	15.75	7.36	-28.07	0.46	0.75	
4	7B	SSP74	5-10 cm	3.76	9.17	4.27	-26.42	0.20	1.07	
4	7B	SSP75	10-15 cm	3.71	9.04	4.36	-26.21	0.29	1.11	
4	7B	SSP76	15-20 cm	3.76	8.06	3.81	-26.02	0.24	1.13	
4	7B	SSP77	30-35 cm	3.72	7.30	3.40	-25.73	0.19	1.05	
4	7AB	SSP78	Topsoil	3.62	10.10	4.84	-26.17	0.31		10YR 3/1
4	7AB	SSP78	Topsoil			4.08	-27.48	0.39		
4	8A	SSP79	0-5 cm	3.69	11.04	5.39	-27.29	0.38	0.90	
4	8A	SSP80	5-10 cm	3.77	7.38	3.08	-26.30	0.15	0.99	
4	8A	SSP81	10-15 cm	3.82	7.36	3.26	-26.05	0.17	1.24	
4	8A	SSP82	15-20 cm	3.75	6.77	3.37	-25.93	0.19	0.95	
4	8A	SSP83	30-35 cm	3.91	7.97	4.06	-25.74	0.18	1.07	
4	8B	SSP84	0-5 cm	3.52	16.02	7.73	-27.69	0.50	0.77	
4	8B	SSP85	5-10 cm	3.63	6.95	3.39	-26.24	0.21	1.13	
4	8B	SSP86	10-15 cm	3.65	7.53	3.81	-26.03	0.23	1.08	
4	8B	SSP87	15-20 cm	3.68	8.35	3.90	-25.89	0.25	1.08	
4	8B	SSP88	30-35 cm	3.64	9.16	4.77	-25.54	0.27	1.04	
4	8AB	SSP89	Topsoil	3.57	7.69	3.85	-26.16	0.26		10YR 4/1
4	8AB	SSP89	Topsoil			3.84	-26.19	0.25		
5	9A	SSP90	0-5 cm	3.8	13.89	6.80	-26.62	0.58	1.14	
5	9A	SSP91	5-10 cm	3.8	10.65	4.70	-26.10	0.30	1.01	
5	9A	SSP92	10-15 cm	3.8	9.95	4.38	-25.64	0.34	1.07	
5	9A	SSP93	15-20 cm	3.9	9.89	4.82	-25.56	0.38	1.02	
5	9A	SSP94	25-30 cm	3.73	6.19	2.98	-25.71	0.21	1.38	
5	9B	SSP95	0-5 cm	3.91	17.86	8.74	-26.80	0.65	0.75	
5	9B	SSP96	5-10 cm	3.83	15.37	7.29	-26.52	0.53	0.72	
5	9B	SSP97	10-15 cm	3.71	14.03	6.50	-25.74	0.37	1.04	
5	9B	SSP98	15-20 cm	3.72	7.92	4.59	-25.50	0.36	0.96	
5	9B	SSP99	25-30 cm	3.72	6.09	2.49	-25.68	0.19	1.22	
5	9AB	SSP100	Topsoil	3.74	9.00	3.98	-25.96	0.32		10YR 3/1
5	9AB	SSP100	Topsoil			3.65	-25.99	0.30		
5	10A	SSP101	0-5 cm	4.36	28.91	13.55	-26.65	1.03	0.44	
5	10A	SSP102	5-10 cm	4.37	15.06	7.19	-26.65	0.56	0.78	
5	10A	SSP103	10-15 cm	4.35	14.89	6.86	-26.34	0.52	0.68	
5	10A	SSP104	15-20 cm	4.31	5.80	3.60	-26.09	0.28	1.14	
5	10A	SSP105	25-30 cm	4.02	5.30	2.44	-25.82	0.19	1.42	
5	10B	SSP106	0-5 cm	4.39	28.63	14.32	-26.95	0.99	0.43	
5	10B	SSP107	5-10 cm	4.32	17.55	7.74	-26.48	0.67	0.71	
5	10B	SSP108	10-15 cm	4.03	7.17	3.82	-25.93	0.28	1.55	
5	10B	SSP109	15-20 cm	4.2	7.72	3.54	-26.02	0.22	1.24	
5	10B	SSP110	25-30 cm	4.1	5.21	2.57	-25.88	0.19	1.27	
5	10B	SSP111	Topsoil	4.19	12.02	5.14	-26.08	0.34		10YR 4/1
5	10B	SSP111	Topsoil			5.38	-26.13	0.33		

*Table A 1.2: Raw data chemical and physical measurements of the reference sites. Note that top- and subsoil samples were measured twice for C [%], δ13C and N [%] content, whereas it was not possible to calculate their bulk density (BD). * indicates samples where twice the amount of liquid for the pH measurement was used. A and B are the replicate rows. AB are the top- and subsoil samples.*

Site	Soil Pit	Sample ID	Depth	pH	LOI [%]	C [%]	$\delta^{13}C$ [‰ V-PDB]	N [%]	BD [g cm^{-3}]	Munsel Color dry
Reference Site 1	R1A	SSP112	0-5 cm	3.08*	77.36	38.31	-27.03	2.10	0.33	
Reference Site 1	R1A	SSP113	5-10 cm	3.17*	48.55	23.33	-27.21	1.50	0.48	
Reference Site 1	R1A	SSP114	10-15 cm	3.33	35.78	17.28	-26.63	1.21	0.45	
Reference Site 1	R1A	SSP115	15-20 cm	3.25	38.49	18.64	-27.03	1.40	1.03	
Reference Site 1	R1A	SSP116	35-40cm	3.86	9.40	4.12	-27.26	0.24	0.22	
Reference Site 1	R1B	SSP117	0-5 cm	3.12*	76.99	36.57	-27.34	2.02	0.33	
Reference Site 1	R1B	SSP118	5-10 cm	3.06	47.08	20.46	-27.49	1.41	0.45	
Reference Site 1	R1B	SSP119	10-15 cm	3.31	41.06	19.53	-26.92	1.44	0.77	
Reference Site 1	R1B	SSP120	15-20 cm	3.62	13.37	5.12	-26.98	0.54	1.32	
Reference Site 1	R1B	SSP121	35-40cm	3.93	5.14	2.09	-27.41	0.13		
Reference Site 1	R1ABC	SSP122	Topsoil	3.44	19.23	8.38	-27.22	0.81		10YR 3/1
Reference Site 1	R1ABC	SSP122	Topsoil			8.60	-27.27	0.81		
Reference Site 1	R1ABC	SSP123	Subsoil	3.87	8.50	3.23	-27.47	0.23	0.25	10YR 5/3
Reference Site 1	R1ABC	SSP123	Subsoil			3.30	-27.50	0.23		
Reference Site 1	R1C	SSP124	0-5 cm	3.12*	78.90	35.10	-27.11	1.82	0.35	
Reference Site 1	R1C	SSP125	5-10 cm	3.27*	50.79	23.66	-27.24	1.56	0.53	
Reference Site 1	R1C	SSP126	10-15 cm	3.37	29.74	13.10	-26.96	0.98	0.73	
Reference Site 1	R1C	SSP127	15-20 cm	3.73	16.09	6.72	-26.73	0.58	1.36	
Reference Site 1	R1C	SSP128	35-40cm	3.96	5.57	1.89	-27.55	0.10	0.57	
Reference Site 1	R2A	SSP129	0-5 cm	2.87	24.16	11.56	-26.09	0.63	1.25	
Reference Site 1	R2A	SSP130	5-10 cm	3.38	3.50	1.73	-25.77	0.08	1.32	
Reference Site 1	R2A	SSP131	10-15 cm	3.46	4.12	2.04	-25.85	0.14	1.39	
Reference Site 1	R2A	SSP132	15-20 cm	3.76	2.64	1.34	-26.06	0.08	1.39	
Reference Site 1	R2A	SSP133	20-25 cm	3.74	3.23	1.23	-26.13	0.06	0.82	
Reference Site 1	R2B	SSP134	0-5 cm	3.08	17.41	7.76	-25.88	0.50	1.05	
Reference Site 1	R2B	SSP135	5-10 cm	3.18	6.28	2.61	-26.08	0.17	1.25	
Reference Site 1	R2B	SSP136	10-15 cm	3.45	5.88	2.52	-25.51	0.12	1.28	
Reference Site 1	R2B	SSP137	15-20 cm	3.71	2.79	1.18	-25.97	0.09	1.34	
Reference Site 1	R2B	SSP138	20-25 cm	3.78	3.61	1.93	-26.36	0.16		
Reference Site 1	R2AB	SSP139	Topsoil	3.17	6.22	2.47	-25.75	0.12	0.90	10YR 5/2
Reference Site 1	R2AB	SSP139	Topsoil			2.47	-25.81	0.12		
Reference Site 2	R3A	SSP140	0-5 cm	3.88	12.47	5.19	-26.95	0.19	1.17	
Reference Site 2	R3A	SSP141	5-10 cm	3.78	7.34	3.32	-25.89	0.16	1.20	
Reference Site 2	R3A	SSP142	10-15 cm	3.78	6.69	2.84	-25.69	0.11	1.42	
Reference Site 2	R3A	SSP143	15-20 cm	3.9	6.86	2.92	-25.74	0.15	1.15	
Reference Site 2	R3A	SSP144	25-30 cm	4.25	7.02	2.09	-25.59	0.16	0.98	
Reference Site 2	R3B	SSP145	0-5 cm	4.09	15.08	6.89	-26.82	0.30	1.18	
Reference Site 2	R3B	SSP146	5-10 cm	3.67	7.13	3.40	-25.73	0.10	1.22	
Reference Site 2	R3B	SSP147	10-15 cm	3.71	6.91	3.09	-25.83	0.10	1.23	
Reference Site 2	R3B	SSP148	15-20 cm	3.83	5.66	2.64	-25.85	0.13	1.30	
Reference Site 2	R3B	SSP149	25-30 cm	4.28	7.14	2.11	-25.50	0.16		
Reference Site 2	R3AB	SSP150	Topsoil	3.77	9.45	4.18	-25.68	0.18		10YR 4/1
Reference Site 2	R3AB	SSP150	Topsoil			4.20	-26.13	0.17		
Reference Site 2	R3AB	SSP151	Subsoil	4.08	7.54	2.39	-25.45	0.12	0.94	
Reference Site 2	R3AB	SSP151	Subsoil			2.36	-25.49	0.12		
Reference Site 2	R4A	SSP152	0-5 cm	4	15.43	6.39	-26.34	0.26	1.24	2.5Y 5/2
Reference Site 2	R4A	SSP153	5-10 cm	3.78	7.99	5.77	-25.72	0.20	1.12	
Reference Site 2	R4A	SSP154	10-15 cm	3.7	7.70	3.47	-25.60	0.13	1.15	
Reference Site 2	R4A	SSP155	15-20 cm	3.75	8.28	3.86	-25.66	0.19	1.13	
Reference Site 2	R4A	SSP156	25-30 cm	3.87	8.96	3.42	-25.80	0.22	0.79	
Reference Site 2	R4B	SSP157	0-5 cm	3.87	16.79	8.65	-26.77	0.36	1.10	
Reference Site 2	R4B	SSP158	5-10 cm	3.61	9.59	4.72	-25.81	0.18	1.09	
Reference Site 2	R4B	SSP159	10-15 cm	3.68	7.52	3.43	-25.61	0.13	1.20	
Reference Site 2	R4B	SSP160	15-20 cm	3.74	7.73	3.34	-25.70	0.16	1.21	
Reference Site 2	R4B	SSP161	25-30 cm	3.8	7.45	2.81	-25.78	0.14		
Reference Site 2	R4AB	SSP162	Topsoil	3.62	9.95	4.43	-25.93	0.21		10YR 4/1
Reference Site 2	R4AB	SSP162	Topsoil			4.41	-25.96	0.22		

Table A 2.1: Oxid values of the sites of interest per soil pit

Site_Pit	mean K_2O [%]	sd K_2O [%]	mean MgO [%]	sd MgO [%]	mean Al_2O_3 [%]	sd Al_2O_3 [%]	mean SiO_2 [%]	sd SiO_2 [%]	mean TiO_2 [%]	sd TiO_2 [%]
Site 1_P5										
0-5 cm	2.82	0.12	0.63	0.01	11.58	0.06	44.46	1.44	0.19	0.00
5-10 cm	3.80	0.08	0.58	0.02	13.33	0.77	57.90	0.59	0.18	0.01
10-15 cm	3.96	0.10	0.53	0.04	13.94	0.90	62.23	1.00	0.18	0.01
15-20 cm	3.49	0.19	0.62	0.02	14.86	0.03	52.98	1.83	0.21	0.00
30-35 cm	4.83	0.61	0.53	0.10	16.12	1.63	65.54	3.01	0.15	0.01
40-45 cm	4.45	0.95	0.59	0.06	16.13	1.45	61.18	5.46	0.15	0.03
OB	3.50	0.00	0.62	0.00	14.64	0.00	54.34	0.00	0.21	0.00
Site1_P6										
0-5 cm	1.26	0.52	0.57	0.14	6.14	2.51	24.22	8.23	0.18	0.07
5-10 cm	2.42	0.40	0.73	0.00	10.53	1.44	41.12	7.07	0.28	0.01
10-15 cm	3.69	0.05	0.55	0.04	12.52	0.32	60.11	0.83	0.18	0.02
15-20 cm	3.61	0.11	0.53	0.05	12.05	0.42	59.01	2.20	0.19	0.02
30-35 cm	4.20	0.44	0.51	0.07	14.33	1.79	65.62	2.29	0.16	0.02
OB	3.64	0.00	0.40	0.00	12.06	0.00	59.98	0.00	0.17	0.00
Site2_P1										
0-5 cm	2.91	0.18	0.55	0.02	11.19	0.18	54.19	6.06	0.14	0.01
5-10 cm	2.82	0.17	0.50	0.03	10.36	1.05	52.54	2.61	0.13	0.00
10-15 cm	3.94	0.70	0.54	0.07	14.18	2.13	60.47	0.82	0.14	0.01
15-20 cm	3.83	0.30	0.46	0.02	13.55	0.17	65.60	3.79	0.11	0.01
25 - 30 cm	4.77	0.04	0.57	0.02	15.94	0.12	63.96	1.54	0.14	0.00
35 - 40 cm	4.00	0.64	0.52	0.02	14.45	1.79	62.81	0.80	0.12	0.01
OB	3.15	0.00	0.50	0.00	11.36	0.00	57.72	0.00	0.13	0.00
UB	4.17	0.00	0.55	0.00	14.92	0.00	64.99	0.00	0.15	0.00
Site2_P2										
0-5 cm	3.16	0.02	0.67	0.00	11.61	0.40	54.26	0.54	0.23	0.01
5-10 cm	3.33	0.04	0.73	0.01	12.71	0.17	56.86	0.44	0.28	0.00
10-15 cm	3.64	0.13	0.69	0.02	13.33	0.34	58.08	1.90	0.23	0.00
15-20 cm	3.52	0.13	0.69	0.02	12.94	0.36	58.24	0.67	0.24	0.01
OB	3.48	0.00	0.70	0.00	13.01	0.00	58.73	0.00	0.23	0.00
Site3_P3										
0-5 cm	3.04	0.39	0.51	0.00	10.10	0.89	55.59	4.96	0.14	0.01
5-10 cm	3.20	0.12	0.52	0.05	10.48	0.22	59.18	2.53	0.15	0.02
10-15 cm	3.22	0.24	0.53	0.01	10.74	0.05	58.88	2.00	0.15	0.01
25-30 cm	3.88	0.06	0.50	0.03	12.00	0.16	65.79	0.11	0.11	0.01
OB	3.08	0.00	0.57	0.00	11.10	0.00	57.88	0.00	0.16	0.00
Site3_P4										
0-5 cm	3.38	0.07	0.53	0.02	10.68	0.14	59.88	2.87	0.12	0.01
5-10 cm	3.66	0.02	0.47	0.02	10.82	0.24	65.45	1.85	0.11	0.01
10-15 cm	4.37	0.14	0.47	0.05	12.83	0.64	68.44	1.70	0.11	0.01
15-20 cm	4.37	0.56	0.55	0.06	13.67	1.73	64.49	1.12	0.12	0.02
25 - 30 cm	4.47	0.76	0.55	0.07	13.82	1.82	64.27	0.35	0.11	0.02
OB	3.78	0.00	0.44	0.00	11.68	0.00	66.51	0.00	0.12	0.00
Site4_P7										
0-5 cm	4.30	0.76	0.53	0.03	13.51	1.55	64.13	1.29	0.10	0.00
5-10 cm	3.91	0.07	0.44	0.00	13.27	0.12	69.07	0.22	0.10	0.00
10-15 cm	4.24	0.44	0.53	0.08	14.87	1.40	66.77	2.13	0.11	0.01
15-20 cm	4.05	0.15	0.46	0.00	14.10	0.31	72.28	3.10	0.10	0.00
30-35 cm	4.74	0.22	0.56	0.05	16.16	0.58	65.89	0.76	0.12	0.00
OB	4.69	0.00	0.67	0.00	16.97	0.00	61.99	0.00	0.13	0.00
Site4_P8										
0-5 cm	3.74	0.11	0.47	0.00	12.29	0.49	65.18	2.05	0.09	0.00
5-10 cm	4.67	0.11	0.50	0.03	15.81	0.27	66.14	0.08	0.11	0.00
10-15 cm	4.65	0.02	0.53	0.04	16.31	0.15	65.36	0.08	0.11	0.00
15-20 cm	4.41	0.37	0.49	0.04	15.28	1.14	67.17	2.66	0.11	0.01
30-35 cm	4.32	0.42	0.52	0.03	15.28	1.32	66.24	1.69	0.11	0.01
OB	3.93	0.00	0.45	0.00	13.89	0.00	69.32	0.00	0.10	0.00
Site5_P9										
0-5 cm	3.46	0.45	0.48	0.07	10.25	1.58	64.55	0.09	0.12	0.01
5-10 cm	3.82	0.01	0.47	0.02	11.11	0.22	66.74	2.27	0.12	0.01
10-15 cm	3.66	0.32	0.42	0.07	11.49	0.79	67.68	3.09	0.13	0.03
15-20 cm	3.89	0.02	0.45	0.01	12.15	0.25	69.45	0.64	0.12	0.01
25-30 cm	3.72	0.01	0.39	0.01	11.45	0.16	73.38	0.19	0.09	0.00
OB	3.77	0.00	0.42	0.00	11.77	0.00	70.17	0.00	0.10	0.00
Site5_P10										
0-5 cm	2.55	0.03	0.51	0.01	8.99	0.30	52.94	0.56	0.16	0.02
5-10 cm	2.89	0.02	0.41	0.02	9.37	0.05	66.54	1.58	0.12	0.01
10-15 cm	3.40	0.49	0.43	0.03	10.81	1.24	69.83	1.34	0.12	0.00
15-20 cm	3.88	0.21	0.41	0.03	11.79	0.75	71.80	0.13	0.12	0.01
25-30 cm	3.96	0.01	0.43	0.04	12.79	0.10	72.48	0.43	0.12	0.01
OB	3.87	0.00	0.45	0.00	11.91	0.00	66.72	0.00	0.14	0.00

Table A 2.2: Oxid values of the reference sites per soil pit

Site_Pit	mean K_2O [%]	sd K_2O [%]	mean MgO [%]	sd MgO [%]	mean Al_2O_3 [%]	sd Al_2O_3 [%]	mean SiO_2 [%]	sd SiO_2 [%]	mean TiO_2 [%]	sd TiO_2 [%]
R1_P1										
0-5 cm	0.47	0.03	0.34	0.01	2.65	0.21	11.93	1.01	0.08	0.01
5-10 cm	1.96	0.12	0.59	0.02	10.69	0.31	33.92	1.75	0.24	0.00
10-15 cm	2.38	0.25	0.61	0.09	12.02	0.89	43.57	4.99	0.27	0.03
15-20 cm	2.70	0.37	0.58	0.02	12.66	1.08	55.92	10.72	0.30	0.03
35-40cm	5.24	0.70	0.53	0.00	17.08	0.53	65.06	0.52	0.14	0.01
OB	2.80	0.00	0.60	0.00	12.53	0.00	59.84	0.00	0.28	0.00
UB	5.39	0.00	0.57	0.00	17.50	0.00	62.63	0.00	0.15	0.00
R1_P2										
0-5 cm	3.86	0.14	0.44	0.08	10.15	0.47	59.20	4.08	0.13	0.01
5-10 cm	5.47	0.17	0.49	0.00	15.17	0.14	68.47	0.97	0.14	0.00
10-15 cm	5.72	0.04	0.51	0.02	15.59	0.28	67.48	1.14	0.14	0.00
15-20 cm	5.67	0.13	0.52	0.01	15.75	0.18	69.68	0.09	0.13	0.00
20-25 cm	5.77	0.08	0.41	0.05	16.12	0.47	68.57	0.79	0.14	0.00
OB	5.45	0.00	0.43	0.00	14.74	0.00	67.79	0.00	0.14	0.00
R2_P3										
0-5 cm	4.25	0.03	0.62	0.09	13.46	0.76	63.40	3.17	0.30	0.02
5-10 cm	5.11	0.43	0.56	0.08	13.68	1.47	68.45	2.40	0.33	0.04
10-15 cm	5.68	0.02	0.59	0.01	14.69	0.13	66.74	0.14	0.36	0.01
15-20 cm	5.46	0.07	0.67	0.05	15.26	0.42	66.55	1.15	0.37	0.02
25-30 cm	5.34	0.08	0.76	0.02	17.21	0.08	62.48	0.31	0.37	0.00
OB	4.63	0.00	0.57	0.00	13.11	0.00	67.92	0.00	0.32	0.00
UB	4.56	0.00	0.59	0.00	14.80	0.00	66.54	0.00	0.31	0.00
R2_P4										
0-5 cm	4.14	0.02	0.65	0.06	13.16	0.84	60.46	2.36	0.31	0.01
5-10 cm	5.61	0.07	0.68	0.05	14.78	0.11	64.73	0.81	0.37	0.00
10-15 cm	5.46	0.05	0.61	0.03	14.80	0.20	65.96	0.42	0.38	0.00
15-20 cm	5.14	0.45	0.63	0.04	14.17	0.89	66.85	1.51	0.37	0.00
25-30 cm	5.05	0.41	0.79	0.16	15.25	1.65	65.12	3.44	0.43	0.06
OB	5.41	0.00	0.72	0.00	15.14	0.00	63.30	0.00	0.38	0.00

Table A 3.1: Mean values and standard deviation of weathering indexes of the sites of interest per soil pit

Site_Pit	mean (Ca+K)/Ti	sd (Ca+K)/Ti	Mean A Index	sd A Index	mean B Index	sd B Index	mean CIA	sd CIA	mean WIP	sd WIP	mean (Na+K)/Ti	sd (Na+K)/Ti
Site 1_P5												
0-5 cm	26.281	0.675	0.877	0.003	0.382	0.000	61.818	0.011	47.756	0.559	57.816	0.370
5-10 cm	35.428	1.343	0.889	0.005	0.397	0.010	60.291	1.041	59.438	0.970	73.530	3.077
10-15 cm	38.227	1.118	0.891	0.007	0.383	0.001	61.669	0.121	59.264	3.202	75.463	0.448
15-20 cm	28.023	2.046	0.868	0.004	0.359	0.004	64.084	0.403	56.448	1.318	60.238	2.322
30-35 cm	54.256	2.692	0.884	0.013	0.416	0.008	58.412	0.792	77.375	10.340	117.598	6.656
40-45 cm	55.438	21.352	0.877	0.001	0.404	0.036	59.594	3.554	74.756	17.093	127.458	51.508
OB	29.200	0.000	0.873	0.000	0.364	0.000	63.557	0.000	56.840	0.000	63.104	0.000
Site1_P6												
0-5 cm	12.944	0.191	0.883	0.009	0.407	0.037	59.272	3.729	26.119	7.684	34.628	3.286
5-10 cm	15.313	2.005	0.878	0.003	0.375	0.008	62.489	0.762	42.405	4.736	34.538	2.897
10-15 cm	36.001	4.138	0.899	0.001	0.430	0.001	56.961	0.051	62.982	1.513	82.969	10.892
15-20 cm	33.060	2.300	0.901	0.006	0.434	0.002	56.615	0.236	61.539	2.654	76.158	4.532
30-35 cm	45.877	0.744	0.895	0.014	0.436	0.003	56.373	0.273	73.447	9.648	109.630	1.587
OB	36.405	0.000	0.902	0.000	0.445	0.000	55.490	0.000	63.600	0.000	86.952	0.000
Site2_P1												
0-5 cm	35.841	0.530	0.898	0.008	0.402	0.003	59.841	0.285	49.855	1.670	80.848	0.560
5-10 cm	36.379	1.754	0.903	0.005	0.420	0.013	57.969	1.269	49.441	2.611	84.943	4.764
10-15 cm	48.150	4.466	0.888	0.012	0.403	0.001	59.725	0.094	64.356	10.188	106.343	8.031
15-20 cm	59.278	8.235	0.899	0.004	0.406	0.005	59.436	0.496	62.219	2.412	130.593	12.714
25 - 30 cm	60.164	0.223	0.882	0.001	0.410	0.006	58.979	0.605	75.046	0.928	128.065	3.859
35 - 40 cm	56.143	2.734	0.890	0.010	0.399	0.004	60.088	0.435	64.619	9.350	122.289	4.640
OB	41.536	0.000	0.903	0.000	0.421	0.000	57.881	0.000	54.841	0.000	97.508	0.000
UB	48.264	0.000	0.889	0.000	0.390	0.000	61.012	0.000	64.802	0.000	100.693	0.000
Site2_P2												
0-5 cm	23.748	0.959	0.892	0.004	0.384	0.010	61.621	1.014	50.640	0.467	49.240	1.684
5-10 cm	20.634	0.213	0.890	0.000	0.359	0.001	64.064	0.102	50.031	0.828	39.952	0.644
10-15 cm	26.914	0.926	0.891	0.001	0.383	0.004	61.703	0.402	55.487	2.258	53.741	2.103
15-20 cm	25.571	2.413	0.889	0.004	0.368	0.020	63.217	2.028	53.385	2.814	50.676	5.805
OB	25.465	0.000	0.892	0.000	0.378	0.000	62.172	0.000	54.258	0.000	52.131	0.000
Site3_P3												
0-5 cm	39.93	7.87	0.91	0.00	0.42	0.00	58.03	0.29	48.92	5.24	83.42	15.899
5-10 cm	36.85	5.23	0.91	0.00	0.42	0.00	58.40	0.21	50.24	1.48	75.32	10.594
10-15 cm	37.59	0.12	0.91	0.00	0.41	0.02	58.95	1.53	50.56	3.13	77.15	0.541
25-30 cm	63.50	4.09	0.91	0.00	0.42	0.01	58.17	0.52	58.83	0.48	128.01	7.699
OB	33.88	0.00	0.90	0.00	0.40	0.00	60.34	0.00	49.12	0.00	70.05	0.000

Site_Pit	mean (Ca+K)/Ti	sd (Ca+K)/Ti	Mean A Index	sd A Index	mean B Index	sd B Index	mean CIA	sd CIA	mean WIP	sd WIP	mean (Na+K)/Ti	sd (Na+K)/Ti
Site3_P4												
0-5 cm	48.12	4.38	0.91	0.00	0.43	0.01	56.82	1.27	54.41	1.92	102.15	11.439
5-10 cm	55.49	2.21	0.92	0.00	0.44	0.01	56.10	0.67	57.19	0.15	115.58	5.725
10-15 cm	70.61	1.66	0.91	0.01	0.43	0.00	57.01	0.15	65.81	2.84	142.23	1.730
15-20 cm	62.55	0.28	0.90	0.01	0.42	0.00	58.05	0.47	67.31	9.53	128.71	1.542
25 - 30 cm	69.98	0.96	0.90	0.01	0.42	0.01	58.29	0.63	67.73	10.76	141.89	0.441
OB	56.24	0.00	0.91	0.00	0.43	0.00	56.80	0.00	59.84	0.00	119.90	0.000
Site4_P7												
0-5 cm	75.72	10.96	0.90	0.01	0.44	0.01	55.61	0.58	71.63	10.55	169.07	20.905
5-10 cm	66.26	0.21	0.91	0.00	0.42	0.00	58.45	0.31	63.11	0.40	144.21	1.115
10-15 cm	66.13	1.15	0.89	0.01	0.42	0.01	58.26	0.70	71.22	8.65	150.59	6.114
15-20 cm	67.31	0.37	0.90	0.00	0.42	0.00	58.26	0.03	67.38	1.65	152.66	2.827
30-35 cm	69.59	2.76	0.88	0.00	0.43	0.01	57.41	0.54	79.99	4.55	160.65	8.184
OB	62.52	0.00	0.87	0.00	0.42	0.00	57.58	0.00	82.82	0.00	150.77	0.000
Site4_P8												
0-5 cm	69.27	4.29	0.91	0.00	0.43	0.00	56.86	0.18	61.62	2.13	151.48	11.543
5-10 cm	75.67	0.31	0.89	0.00	0.44	0.00	56.05	0.38	81.64	0.23	181.78	4.465
10-15 cm	75.67	2.09	0.88	0.00	0.43	0.01	56.99	0.74	81.35	1.42	181.83	9.019
15-20 cm	68.60	1.76	0.89	0.01	0.42	0.00	58.03	0.07	73.66	5.80	156.30	5.027
30-35 cm	66.43	0.50	0.89	0.01	0.42	0.00	58.11	0.48	73.42	7.63	154.06	2.632
OB	70.57	0.00	0.90	0.00	0.42	0.00	57.90	0.00	67.01	0.00	164.25	0.000
Site5_P9												
0-5 cm	51.56	0.36	0.92	0.01	0.48	0.00	51.86	0.15	60.64	8.95	114.40	3.344
5-10 cm	57.38	2.07	0.92	0.00	0.48	0.01	52.12	1.03	65.73	0.99	127.36	4.357
10-15 cm	52.01	6.02	0.92	0.01	0.46	0.00	54.49	0.46	62.29	5.45	115.65	13.706
15-20 cm	57.28	4.74	0.91	0.00	0.46	0.01	54.20	0.97	66.89	0.87	130.53	12.866
25-30 cm	71.26	0.85	0.92	0.00	0.47	0.00	53.18	0.50	65.78	0.37	170.95	3.352
OB	65.01	0.00	0.92	0.00	0.46	0.00	53.96	0.00	65.38	0.00	150.17	0.000
Site5_P10												
0-5 cm	33.17	3.12	0.92	0.00	0.46	0.01	53.61	1.09	46.47	0.98	67.10	10.699
5-10 cm	45.12	2.85	0.93	0.00	0.46	0.01	54.11	0.52	50.17	0.56	96.76	4.977
10-15 cm	51.94	4.86	0.92	0.01	0.45	0.01	54.54	0.96	58.05	9.45	112.68	16.114
15-20 cm	56.86	1.72	0.92	0.00	0.46	0.00	53.74	0.12	65.62	4.46	124.89	1.242
25-30 cm	60.15	4.52	0.91	0.00	0.45	0.01	55.29	0.88	67.75	2.62	137.49	3.711
OB	48.74	0.00	0.91	0.00	0.46	0.00	53.61	0.00	65.92	0.00	105.52	0.000

Table A 3.2: Mean values and standard deviation of weathering indexes of the reference sites per soil pit

Site_Pit	mean (Ca+K)/Ti	sd (Ca+K)/Ti	mean A Index	sd A Index	Mean B Index	sd B Index	mean CIA	sd CIA	mean WIP	sd WIP	mean (Na+K)/Ti	sd (Na+K)/Ti
R1_P1												
0-5 cm	10.577	0.615	0.894	0.001	0.450	0.013	54.997	1.298	13.946	0.613	41.472	2.141
5-10 cm	13.911	0.877	0.854	0.002	0.316	0.009	68.370	0.858	33.735	0.490	31.331	0.275
10-15 cm	15.044	0.478	0.868	0.015	0.328	0.008	67.178	0.841	40.027	3.093	33.482	2.081
15-20 cm	15.552	0.952	0.888	0.012	0.360	0.014	64.045	1.408	47.724	5.853	36.905	2.935
35-40cm	65.382	6.422	0.877	0.002	0.408	0.014	59.193	1.383	80.041	7.303	134.873	7.035
OB	17.159	0.000	0.897	0.000	0.364	0.000	63.571	0.000	48.326	0.000	39.555	0.000
UB	59.727	0.000	0.871	0.000	0.411	0.000	58.942	0.000	82.677	0.000	123.201	0.000
R1_P2												
0-5 cm	49.875	4.433	0.915	0.001	0.452	0.009	54.784	0.892	57.195	0.620	98.303	6.305
5-10 cm	65.640	1.180	0.894	0.001	0.446	0.004	55.449	0.396	82.664	2.122	133.628	1.636
10-15 cm	70.087	1.866	0.891	0.003	0.450	0.005	54.977	0.473	86.525	0.255	142.715	2.970
15-20 cm	76.214	2.732	0.893	0.001	0.451	0.001	54.949	0.058	87.263	0.277	158.409	0.883
20-25 cm	71.698	1.053	0.889	0.004	0.444	0.001	55.589	0.092	86.968	1.438	146.122	3.558
OB	66.526	0.000	0.896	0.000	0.449	0.000	55.111	0.000	70.160	11.238	86.670	47.105
R2_P3												
0-5 cm	25.188	1.680	0.896	0.009	0.388	0.009	61.209	0.938	58.113	0.809	42.635	3.070
5-10 cm	26.865	0.646	0.902	0.012	0.427	0.006	57.272	0.575	70.083	5.998	47.340	1.163
10-15 cm	27.465	0.496	0.895	0.001	0.439	0.001	56.144	0.068	78.806	0.357	49.371	0.435
15-20 cm	25.317	1.566	0.891	0.004	0.425	0.014	57.502	1.389	77.409	1.904	46.604	3.711
25-30 cm	25.264	0.156	0.871	0.001	0.382	0.000	61.844	0.001	73.353	0.417	44.024	0.223
OB	25.328	0.000	0.905	0.000	0.409	0.000	59.142	0.000	62.386	0.000	43.165	0.000
UB	25.428	0.000	0.892	0.000	0.376	0.000	62.402	0.000	61.635	0.000	43.499	0.000
R2_P4												
0-5 cm	24.076	0.761	0.894	0.009	0.400	0.011	60.049	1.068	58.748	0.767	42.038	0.946
5-10 cm	25.954	0.246	0.891	0.000	0.436	0.007	56.413	0.659	78.339	1.530	46.620	0.823
10-15 cm	25.153	0.123	0.893	0.002	0.432	0.003	56.814	0.344	77.032	1.675	46.071	1.457
15-20 cm	23.895	1.960	0.897	0.007	0.419	0.012	58.149	1.226	70.757	7.639	42.251	4.594
25-30 cm	20.416	1.153	0.887	0.015	0.392	0.005	60.766	0.515	68.788	6.148	35.560	1.830
OB	24.766	0.000	0.887	0.000	0.434	0.000	56.561	0.000	78.915	0.000	46.553	0.000

Table A 4: Raw data of oxalate extraction

Site	Sample ID	Fe_o 1 [mg kg^{-1}]	Fe_o 2 [mg kg^{-1}]	mean Fe_o [mg kg^{-1}]	sd Fe_o [mg kg^{-1}]	Mn_o 1 [mg kg^{-1}]	Mn_o 2 [mg kg^{-1}]	mean Mn_o [mg kg^{-1}]	sd Mn_o [mg kg^{-1}]	Al_o 1 [mg kg^{-1}]	Al_o 2 [mg kg^{-1}]	mean Al_o [mg kg^{-1}]	sd Al_o [mg kg^{-1}]
Site 1 Topsoil	SSP56	1003.00	962.00	982.50	20.50	15.44	15.28	15.36	0.08	3305.50	3149.00	3227.25	78.25
Site 1 Topsoil	SSP67	567.50	506.50	537.00	30.50	14.73	13.62	14.17	0.55	2214.50	1784.50	1999.50	215.00
Site 2 Topsoil	SSP13	761.80	753.50	757.65	4.15	15.99	15.31	15.65	0.34	3923.00	3836.00	3879.50	43.50
Site 2 Subsoil	SSP14	80.95	71.80	76.38	4.58	11.92	14.10	13.01	1.09	6305.00	5555.00	5930.00	375.00
Site 2 Topsoil	SSP23	1687.50	1749.00	1718.25	30.75	20.71	20.06	20.38	0.32	4338.50	4217.50	4278.00	60.50
Site 3 Topsoil	SSP32	976.00	1066.50	1021.25	45.25	15.27	15.58	15.42	0.15	3219.00	3212.00	3215.50	3.50
Site 3 Topsoil	SSP43	392.80	457.90	425.35	32.55	13.68	13.71	13.70	0.01	1973.50	2123.00	2048.25	74.75
Site 4 Topsoil	SSP78	864.50	877.50	871.00	6.50	14.10	13.99	14.04	0.05	2595.50	2614.00	2604.75	9.25
Site 4 Topsoil	SSP89	492.10	482.95	487.53	4.57	13.16	12.92	13.04	0.12	1735.50	1650.50	1693.00	42.50
Site 5 Topsoil	SSP100	329.55	333.15	331.35	1.80	32.06	35.33	33.69	1.64	1131.79	1146.83	1388.25	39.25
Site 5 Topsoil	SSP111	679.00	605.00	642.00	37.00	75.80	67.85	71.83	3.98	1427.50	1349.00	4572.75	198.75
Ref. S1 Topsoil	SSP122	332.15	365.10	348.63	16.48	14.31	13.79	14.05	0.26	4374.00	4771.50	4572.75	198.75
Ref. S1 Subsoil	SSP123	46.63	45.86	46.24	0.38	13.57	13.16	13.36	0.20	2723.00	2602.00	2662.50	60.50
Ref. S1 Topsoil	SSP139	116.80	105.45	111.13	5.68	27.41	19.25	23.33	4.08	447.35	390.49	418.92	28.43
Ref. S2 Topsoil	SSP150	1974.50	1875.00	1924.75	49.75	29.71	29.60	29.65	0.05	2518.00	2504.50	2511.25	6.75
Ref. S2 Subsoil	SSP151	4192.50	3871.00	4031.75	160.75	35.99	35.38	35.69	0.31	7245.00	7185.00	7215.00	30.00
Ref. S2 Topsoil	SSP162	1868.00	1765.00	1816.50	51.50	21.56	21.29	21.43	0.14	2202.00	2071.50	2136.75	65.25

Table A 5: Grain size distribution in percentage

Depth	Sample ID	<2000 µm [%]	<1000 µm [%]	<500 µm [%]	<250 µm [%]	<125 µm [%]	<63 µm [%]	<45 µm [%]	<32 µm [%]	<25 µm [%]	<20 µm [%]	<15 µm [%]
S1 Topsoil	SSP56	100	95.6	93.2	87.2	75.3	56	47.1	38.9	38.5	36.6	31.8
S2 Topsoil	SSP13	100	93.8	84.4	69.9	54.7	41.7	37.7	33.7	33.3	31.6	28.7
S2 Subsoil	SSP14	100	87.6	74.9	59.0	42.8	29.3	23.8	19.2	17.8	16.7	14.7
S3 Topsoil	SSP32	100	94.1	66.1	52.7	38.8	27.9	24.4	21.6	21.2	20.2	18.4
S4 Topsoil	SSP78	100	86.8	75.6	60.1	44.7	32	27.6	24.8	23.8	22.2	20.6
S5 Topsoil	SSP100	100	72.2	57.1	43.2	31.4	23.3	21.2	19.3	18.4	17.4	15.9
R1 Topsoil	SSP122	100	93.6	88.4	77.8	64.9	53.6	49.3	44.5	42.9	40.2	36.7
R1 Subsoil	SSP123	100	88.5	76.2	57.5	37.1	21	16.7	13.1	12.5	11.2	9.3
R2 Topsoil	SSP150	100	89.8	77.7	62.4	53.5	39.4	33.4	27.8	26.6	24.9	22.4
R2 Subsoil	SSP151	100	84.6	74.9	64.5	51.5	38.3	33.3	28.3	27.7	26	23.8

Depth	Sample ID	<10 µm [%]	<8 µm [%]	<7 µm [%]	<6 µm [%]	<5 µm [%]	<4 µm [%]	<3 µm [%]	<2 µm [%]	<1.5 µm [%]	<1 µm [%]
S1 Topsoil	SSP56	26.2	24.3	23.2	21.4	19.2	16.6	14.4	11.9	9.9	8.7
S2 Topsoil	SSP13	24.6	22.5	21.5	20.3	18.5	16.1	13	9.9	7.8	6.2
S2 Subsoil	SSP14	11.5	9.8	9.1	8.3	7.1	5.7	4.4	2.8	2.1	1.2
S3 Topsoil	SSP32	16.1	15.1	14.4	13.6	12.6	11.5	9.8	8.2	7	4.7
S4 Topsoil	SSP78	18.1	16.7	15.7	14.6	13.5	12.1	10.4	8.8	7.5	6.2
S5 Topsoil	SSP100	14.4	13.3	12.6	12	11.5	10.8	9.7	8.3	7.5	6.1
R1 Topsoil	SSP122	33.5	31	29.4	28	26.1	23.1	19.9	16.4	14.9	12.3
R1 Subsoil	SSP123	7.3	6	5.4	4.7	4.1	3.6	2.8	1.8	1.6	0.8
R2 Topsoil	SSP150	18.5	16.8	15.8	14.6	13.3	12.2	10.9	8.8	7.9	6
R2 Subsoil	SSP151	20.4	18.4	17.3	16.1	14.8	12.8	10.6	7.7	6.5	4.4

Table A 6: Raw data of the $^{239+240}$Pu measurements (Batch 1)

Batch 1			Measured activites and isotopic ratios										Activity corrected to standard IAEA-447			
Sample ID	Depth	Site	^{242}Pu		^{239}Pu activity		^{240}Pu activity		$^{239+240}$Pu activity		^{240}Pu/^{239}Pu		$^{239+240}$Pu activity		^{240}Pu/^{239}Pu	
			CPS	RSD [%]	Bq kg^{-1}	RSD [%]	Bq kg^{-1}	RSD [%]	Bq kg^{-1}	RSD [%]	mass ratio	RSD [%]	Bq kg^{-1}	RSD [%]	mass ratio	RSD [%]
SSP1	0-5 cm	2	14553.85	1.80	1.09	3.67	0.69	12.43	1.78	12.84	0.17	12.71	2.04	12.94	0.17	12.75
SSP2	5-10 cm	2	35829.02	1.50	1.75	3.00	1.13	5.22	2.88	5.83	0.17	5.64	3.28	6.05	0.17	5.66
BLK1			30227.77	1.00	0.00	0.00	0.00	0.00	0.00	0.00	0.00	0.00	0.00	0.00	0.00	0.00
SSP3	10-15 cm	2	52866.67	1.00	0.69	2.15	0.45	4.51	1.13	4.90	0.17	4.79	1.29	5.16	0.18	4.81
SSP4	15-20 cm	2	30596.65	1.50	0.17	6.77	0.09	15.87	0.26	17.19	0.15	17.12	0.29	17.41	0.15	17.11
SSP5	25 - 30 cm	2	50062.43	1.30	0.08	6.63	0.04	17.75	0.11	18.90	0.12	18.86	0.12	19.50	0.13	18.77
SSP6	35 - 40 cm	2	28166.89	1.00	0.03	11.94	0.01	62.21	0.04	63.34	0.05	63.33	0.04	70.19	0.05	65.21
STD1			20929.06	3.50	2.48	4.03	1.77	5.09	4.25	5.47	0.19	4.21	4.85	5.70	0.19	4.22
SSP7	0-5 cm	2	41942.13	1.70	1.54	2.20	0.97	4.81	2.51	5.01	0.17	4.71	2.87	5.26	0.17	4.73
SSP8	5-10 cm	2	44024.87	1.50	0.73	3.72	0.46	8.34	1.19	9.00	0.17	8.88	1.35	9.16	0.17	8.90
SSP9	10-15 cm	2	34747.86	1.90	0.06	9.10	0.04	22.58	0.09	24.27	0.17	24.20	0.10	25.00	0.17	23.91
SSP10	15-20 cm	2	24388.45	1.60	0.03	9.73	0.01	44.33	0.04	45.36	0.13	45.33	0.05	47.58	0.13	44.48
NC1			48338.05	1.60	0.05	7.77	0.03	23.75	0.08	24.94	0.19	24.89	0.09	25.78	0.19	24.47
SSP11	25 - 30 cm	2	43452.89	2.20	0.01	14.76	0.01	51.65	0.02	53.67	0.13	53.63	0.02	62.31	0.14	50.46
SSP12	35 - 40 cm	2	24717.99	1.50	0.06	9.91	0.01	43.83	0.07	44.91	0.07	44.88	0.08	46.74	0.07	45.07
SSP15	0-5 cm	2	52751.24	1.20	1.37	2.86	0.88	4.37	2.25	5.08	0.17	4.94	2.57	5.33	0.17	4.96
SSP16	5-10 cm	2	35130.75	2.00	1.83	3.77	1.17	5.48	3.01	6.34	0.17	6.02	3.43	6.54	0.17	6.04
SSP17	10-15 cm	2	43574.42	1.50	0.49	3.18	0.31	6.09	0.80	6.70	0.17	6.53	0.91	6.91	0.17	6.55
BLK2			28145.65	2.30	0.00	0.00	0.00	0.00	0.00	0.00	0.00	0.00	0.00	0.00	0.00	0.00
SSP18	15-20 cm	2	32226.42	3.00	0.33	3.72	0.20	10.15	0.52	10.39	0.16	9.95	0.60	10.56	0.16	9.96
SSP19	0-5 cm	2	46731.92	2.30	1.08	3.78	0.70	5.50	1.79	6.27	0.18	5.83	2.04	6.47	0.18	5.85
SSP20	5-10 cm	2	35198.38	1.50	1.86	1.80	1.17	4.37	3.04	4.48	0.17	4.22	3.46	4.75	0.17	4.24
SSP21	10-15 cm	2	45485.96	2.10	0.80	2.64	0.49	5.61	1.28	5.83	0.16	5.44	1.46	6.06	0.16	5.46
STD2			24225.19	2.30	2.75	3.55	1.92	5.14	4.67	5.81	0.19	5.33	5.33	6.02	0.19	5.35
SSP22	15-20 cm	2	35476.59	2.60	0.54	5.02	0.31	11.69	0.85	12.46	0.15	12.18	0.96	12.59	0.15	12.22
SSP24	0-5 cm	3	34966.56	1.80	3.38	3.33	2.16	2.69	5.54	3.88	0.17	3.44	6.32	4.20	0.17	3.46
SSP25	5-10 cm	3	32364.92	2.40	1.46	4.16	0.93	4.92	2.39	5.98	0.17	5.48	2.72	6.20	0.17	5.50
SSP26	10-15 cm	3	35253.30	1.30	0.35	4.30	0.19	10.18	0.54	10.98	0.15	10.90	0.61	11.14	0.15	10.92
SSP27	25-30 cm	3	36678.42	2.20	0.12	7.15	0.03	24.80	0.14	25.71	0.06	25.62	0.16	26.42	0.06	25.78
SSP28	0-5 cm	3	40532.57	2.00	1.81	3.05	1.18	3.52	2.99	4.21	0.18	3.70	3.41	4.50	0.18	3.72
SSP29	5-10 cm	3	35685.25	2.50	1.24	3.61	0.79	6.59	2.04	7.09	0.17	6.63	2.32	7.27	0.17	6.65
SSP30	10-15 cm	3	45471.34	3.40	0.33	4.81	0.21	9.53	0.54	10.12	0.17	9.53	0.61	10.29	0.17	9.54
SSP31	25-30 cm	3	32188.31	0.90	0.10	5.97	0.04	19.62	0.14	20.49	0.10	20.47	0.15	20.99	0.10	20.45
BLK3			38366.47	2.00	0.00	0.00	0.00	0.00	0.00	0.00	0.00	0.00	0.00	0.00	0.00	0.00
SSP33	0-5 cm	3	46300.84	1.90	2.00	2.62	1.25	4.07	3.25	4.45	0.17	4.02	3.71	4.73	0.17	4.04
SSP34	5-10 cm	3	43136.73	2.30	0.46	4.19	0.28	9.48	0.74	10.11	0.17	9.84	0.84	10.26	0.17	9.86
SSP35	10-15 cm	3	47223.17	2.40	0.07	5.64	0.02	21.63	0.09	22.23	0.09	22.10	0.10	23.21	0.09	22.07
SSP36	15-20 cm	3	44760.71	1.40	0.10	3.77	0.03	22.64	0.13	22.91	0.09	22.87	0.15	23.47	0.09	22.88
STD3			27610.52	1.70	2.78	3.36	1.95	4.62	4.74	5.46	0.19	5.19	5.41	5.69	0.19	5.21
SSP37	25 - 30 cm	3	36717.39	1.50	0.12	4.09	0.05	24.25	0.17	24.54	0.10	24.50	0.19	24.93	0.10	24.50
SSP38	0-5 cm	3	37585.09	1.90	3.20	2.76	1.99	6.39	5.19	6.69	0.17	6.42	5.92	6.88	0.17	6.45
SSP39	5-10 cm	3	33835.15	3.00	1.38	4.46	0.87	6.35	2.25	7.16	0.17	6.50	2.57	7.34	0.17	6.52
SSP40	10-15 cm	3	29097.00	1.60	0.18	6.60	0.12	13.20	0.30	14.67	0.17	14.58	0.34	14.87	0.17	14.57
NC2			33330.79	4.20	0.04	10.85	0.02	25.35	0.07	27.25	0.15	26.93	0.08	28.39	0.15	26.54
DUP1/SSP6	35 - 40 cm	2	21904.15	3.00	0.01	21.91	0.01	127.64	0.02	129.47	0.14	129.43	0.02	142.67	0.16	119.27
DUP2/SSP12	35 - 40 cm	2	24622.14	1.90	0.04	11.26	0.01	35.55	0.05	37.24	0.09	37.19	0.06	39.35	0.09	36.98
DUP3/SSP34	5-10 cm	3	38491.90	2.80	0.44	5.64	0.27	13.59	0.71	14.45	0.17	14.17	0.81	14.57	0.17	14.20
DUP4/SSP28	0-5 cm	3	48556.19	0.50	1.81	2.35	1.18	3.83	2.98	4.47	0.18	4.44	3.40	4.75	0.18	4.46

Table A 7: Raw data of the $^{239+240}$Pu measurements (Batch 2)

Batch 2			Measured activites and isotopic ratios										Activity corrected to standard IAEA-447			
Sample ID	Depth	Site	^{242}Pu		^{239}Pu activity		^{240}Pu activity		$^{239+240}$Pu activity		^{240}Pu/^{239}Pu		$^{239+240}$Pu activity		^{240}Pu/^{239}Pu	
			CPS	RSD [%]	Bq kg^{-1}	RSD [%]	Bq kg^{-1}	RSD [%]	Bq kg^{-1}	RSD [%]	mass ratio	RSD [%]	Bq kg^{-1}	RSD [%]	mass ratio	RSD [%]
SSP41	15-20 cm	3	30263.09	2.00	0.21	4.03	0.09	19.50	0.30	19.81	0.11	19.71	0.34	20.02	0.11	19.74
SSP42	25 - 30 cm	3	38550.89	1.50	0.24	2.75	0.02	33.03	0.27	33.11	0.03	33.08	0.30	33.97	0.02	33.63
BLK4			45054.76	1.90	0.00	0.00	0.00	0.00	0.00	0.00	0.00	0.00	0.00	0.00	0.00	0.00
SSP44	0-5 cm	1	42323.24	1.20	5.45	2.00	3.64	2.59	9.09	3.05	0.18	2.80	10.38	3.44	0.18	2.81
SSP45	5-10 cm	1	45191.69	2.00	2.69	3.28	1.91	5.85	4.61	6.40	0.19	6.08	5.26	6.60	0.19	6.11
SSP46	10-15 cm	1	40258.90	1.70	0.76	2.62	0.52	6.82	1.27	7.10	0.19	6.90	1.45	7.29	0.19	6.92
SSP47	15-20 cm	1	34615.16	2.70	0.38	5.95	0.25	9.40	0.63	10.79	0.18	10.44	0.72	10.95	0.18	10.46
STD4			22319.37	1.60	2.79	2.88	1.96	5.54	4.76	6.03	0.19	5.82	5.43	6.24	0.19	5.84
SSP48	30-35 cm	1	46185.76	1.90	0.10	7.35	0.07	14.13	0.18	15.81	0.19	15.70	0.20	16.14	0.19	15.61
SSP49	40-45 cm	1	52534.29	1.20	0.08	7.60	0.04	28.92	0.11	29.88	0.12	29.86	0.13	30.48	0.12	29.73
SSP50	0-5 cm	1	40814.19	1.80	5.90	2.48	4.05	2.92	9.95	3.38	0.19	2.86	11.36	3.73	0.19	2.87
SSP51	5-10 cm	1	56189.89	1.00	1.00	2.33	0.69	6.87	1.70	7.19	0.19	7.12	1.93	7.37	0.19	7.14
NC3			43501.97	3.60	0.05	8.41	0.03	19.73	0.07	21.14	0.15	20.84	0.08	22.17	0.15	20.55
SSP52	10-15 cm	1	32713.70	3.20	0.42	6.11	0.27	11.46	0.70	12.58	0.18	12.17	0.79	12.72	0.18	12.19
SSP53	15-20 cm	1	42575.71	2.10	0.27	3.42	0.19	6.64	0.46	7.17	0.19	6.85	0.52	7.41	0.19	6.86
SSP54	30-35 cm	1	43700.50	2.50	0.12	9.24	0.08	16.98	0.20	19.18	0.18	19.01	0.22	19.47	0.18	18.94
SSP55	40-45 cm	1	39076.06	1.90	0.08	10.08	0.04	17.40	0.12	20.02	0.15	19.93	0.14	20.54	0.16	19.80
SSP57	0-5 cm	1	40280.13	1.20	21.07	1.70	14.21	2.16	35.28	2.47	0.18	2.16	40.29	2.94	0.18	2.17
BLK5			38364.65	1.90	0.00	0.00	0.00	0.00	0.00	0.00	0.00	0.00	0.00	0.00	0.00	0.00
SSP58	5-10 cm	1	40309.81	1.50	20.00	2.05	13.69	2.27	33.69	2.66	0.18	2.20	38.48	3.10	0.18	2.21
SSP59	10-15 cm	1	45125.30	2.00	1.11	3.94	0.75	6.71	1.86	7.52	0.18	7.25	2.12	7.69	0.18	7.27
SSP60	15-20 cm	1	38309.96	1.90	0.33	4.34	0.19	10.28	0.52	10.99	0.16	10.83	0.59	11.16	0.16	10.84
SSP61	30-35 cm	1	38826.07	1.90	0.12	6.48	0.08	19.89	0.20	20.83	0.18	20.75	0.23	21.10	0.18	20.67
STD5			18601.82	1.60	2.74	2.72	1.99	5.92	4.72	6.32	0.20	6.11	5.39	6.51	0.20	6.13
SSP62	0-5 cm	1	46031.86	3.10	16.74	4.11	11.27	3.74	28.02	4.62	0.18	3.42	32.00	4.88	0.18	3.44
SSP63	5-10 cm	1	38223.13	2.30	3.32	3.55	2.26	4.36	5.58	5.13	0.18	4.58	6.37	5.37	0.18	4.60
SSP64	10-15 cm	1	44776.92	1.50	0.42	3.09	0.25	8.43	0.67	8.86	0.16	8.73	0.77	9.03	0.16	8.75
SSP65	15-20 cm	1	44700.89	1.60	0.17	4.59	0.08	17.47	0.26	17.99	0.13	17.92	0.29	18.22	0.13	17.92
SSP66	30-35 cm	1	47698.44	1.00	0.06	13.44	0.04	25.32	0.11	28.65	0.18	28.63	0.12	29.29	0.18	28.31
SSP68	0-5 cm	4	36942.32	1.70	0.42	3.80	0.27	6.04	0.69	6.93	0.17	6.72	0.78	7.15	0.17	6.74
SSP69	5-10 cm	4	48820.33	1.80	0.31	3.76	0.17	8.59	0.48	9.20	0.15	9.02	0.54	9.40	0.15	9.04
SSP70	10-15 cm	4	41764.17	1.70	0.42	3.28	0.14	6.62	0.56	7.19	0.09	6.99	0.63	7.42	0.09	7.01
SSP71	15-20 cm	4	45174.83	3.00	0.28	4.10	0.07	18.45	0.35	18.66	0.06	18.41	0.39	18.90	0.06	18.50
BLK6			31202.29	1.30	0.00	0.00	0.00	0.00	0.00	0.00	0.00	0.00	0.00	0.00	0.00	0.00
SSP72	30-35 cm	4	38309.19	4.00	0.03	12.84	0.02	43.19	0.04	44.88	0.16	44.70	0.05	47.04	0.16	43.44
SSP73	0-5 cm	4	43803.70	1.60	0.69	3.14	0.44	7.57	1.13	8.04	0.17	7.88	1.29	8.21	0.17	7.90
SSP74	5-10 cm	4	44791.28	4.90	0.33	6.45	0.23	13.15	0.56	13.80	0.18	12.90	0.64	13.95	0.18	12.92
SSP75	10-15 cm	4	32914.23	1.40	0.49	3.13	0.24	10.99	0.72	11.34	0.13	11.25	0.83	11.48	0.13	11.28
STD6			10784.89	2.20	2.70	4.74	1.92	5.83	4.62	7.19	0.19	6.84	5.27	7.36	0.19	6.87
SSP76	15-20 cm	4	42119.31	1.40	0.13	5.97	0.08	19.25	0.20	20.11	0.17	20.06	0.23	20.37	0.17	19.99
SSP77	30-35 cm	4	43943.71	2.20	0.04	7.24	0.01	29.68	0.05	30.47	0.08	30.39	0.06	32.93	0.08	30.36
SSP79	0-5 cm	4	39046.44	1.00	0.59	4.32	0.39	5.00	0.99	6.53	0.18	6.45	1.12	6.74	0.18	6.47
SSP80	5-10 cm	4	38141.69	2.60	0.33	5.37	0.20	11.30	0.53	12.24	0.17	11.96	0.61	12.39	0.17	11.98
NC4			43126.56	2.90	0.04	9.84	0.03	20.90	0.07	22.92	0.17	22.73	0.08	24.04	0.17	22.34
DUP5/SSP41	15-20 cm	3	41333.99	1.50	0.16	4.65	0.09	10.31	0.25	11.21	0.14	11.11	0.28	11.48	0.14	11.10
DUP6/SSP55	40-45 cm	1	43956.95	0.90	0.08	4.49	0.05	16.92	0.13	17.49	0.16	17.46	0.15	17.94	0.16	17.34
DUP7/SSP66	30-35 cm	1	37973.16	2.80	0.07	9.14	0.05	18.12	0.11	20.10	0.18	19.90	0.13	20.70	0.19	19.68
DUP8/SSP72	30-35 cm	4	44642.08	1.90	0.03	11.16	0.01	44.04	0.04	45.39	0.15	45.35	0.04	47.84	0.15	44.04

Table A 8: Raw data of the $^{239+240}$Pu measurements (Batch 3)

Batch 3			Measured activites and isotopic ratios										Activity corrected to standard IAEA-447			
Sample ID	Depth	Site	^{242}Pu		^{239}Pu activity		^{240}Pu activity		$^{239+240}$Pu activity		^{240}Pu/^{239}Pu		$^{239+240}$Pu activity		^{240}Pu/^{239}Pu	
			CPS	RSD [%]	Bq kg^{-1}	RSD [%]	Bq kg^{-1}	RSD [%]	Bq kg^{-1}	RSD [%]	mass ratio	RSD [%]	Bq kg^{-1}	RSD [%]	mass ratio	RSD [%]
SSP81	10-15 cm	4	29395.99	2.40	0.14	5.37	0.08	9.22	0.22	10.39	0.16	10.11	0.25	10.71	0.16	10.09
SSP82	15-20 cm	4	33458.75	2.20	0.14	6.30	0.08	22.21	0.22	22.98	0.15	22.87	0.24	23.23	0.15	22.83
BLK7			37780.24	1.60	0.00	0.00	0.00	0.00	0.00	0.00	0.00	0.00	0.00	0.00	0.00	0.00
SSP83	30-35 cm	4	37796.56	2.20	0.07	3.72	0.02	52.65	0.09	52.73	0.07	52.69	0.10	54.23	0.07	52.91
SSP84	0-5 cm	4	27790.67	0.70	1.20	2.79	0.77	9.92	1.97	10.29	0.17	10.26	2.25	10.41	0.17	10.30
SSP85	5-10 cm	4	45523.07	1.50	0.39	3.18	0.24	6.09	0.63	6.70	0.17	6.53	0.72	6.92	0.17	6.54
SSP86	10-15 cm	4	37373.40	1.60	0.38	4.68	0.25	8.94	0.63	9.97	0.18	9.84	0.72	10.13	0.18	9.86
STD7			18147.94	2.00	2.66	4.65	1.85	2.83	4.52	5.06	0.19	4.65	5.16	5.31	0.19	4.67
SSP87	15-20 cm	4	30755.15	1.30	0.09	10.78	0.05	28.33	0.14	30.28	0.14	30.26	0.15	30.74	0.14	30.13
SSP88	30-35 cm	4	42966.42	1.40	0.04	7.04	0.02	30.73	0.06	31.50	0.11	31.47	0.07	32.86	0.11	31.20
SSP90	0-5 cm	5	38480.94	1.20	1.10	2.42	0.69	4.37	1.79	4.85	0.17	4.70	2.04	5.11	0.17	4.71
SSP91	5-10 cm	5	38948.89	1.60	0.33	5.54	0.21	7.86	0.53	9.48	0.17	9.35	0.61	9.67	0.17	9.36
NC5			38591.85	4.80	0.04	19.50	0.03	15.56	0.07	24.48	0.20	24.01	0.08	25.96	0.21	23.45
SSP92	10-15 cm	5	43484.97	1.10	0.39	2.82	0.25	7.38	0.64	7.83	0.17	7.75	0.73	8.02	0.17	7.76
SSP93	15-20 cm	5	36630.36	1.30	0.22	5.94	0.14	17.05	0.36	18.01	0.16	17.96	0.41	18.17	0.17	17.97
SSP94	25-30 cm	5	32311.29	2.10	0.07	7.60	0.04	14.16	0.12	15.93	0.16	15.79	0.13	16.50	0.17	15.66
SSP95	0-5 cm	5	31660.67	2.20	1.03	3.48	0.67	5.92	1.71	6.51	0.18	6.13	1.95	6.71	0.18	6.15
SSP96	5-10 cm	5	43110.56	2.50	1.39	4.14	0.89	7.24	2.28	7.96	0.17	7.56	2.60	8.12	0.17	7.59
BLK8			37791.37	2.30	0.00	0.00	0.00	0.00	0.00	0.00	0.00	0.00	0.00	0.00	0.00	0.00
SSP97	10-15 cm	5	35751.19	1.10	0.15	3.38	0.08	29.92	0.22	30.09	0.14	30.07	0.25	30.35	0.14	30.04
SSP98	15-20 cm	5	45536.31	1.70	0.06	6.72	0.04	19.67	0.10	20.72	0.17	20.65	0.12	21.35	0.17	20.43
SSP99	25-30 cm	5	31874.93	1.10	0.16	3.38	0.10	12.95	0.26	13.34	0.18	13.29	0.29	13.56	0.18	13.27
SSP101	0-5 cm	5	44495.72	1.00	2.14	2.24	1.33	4.51	3.47	4.94	0.17	4.83	3.96	5.19	0.17	4.85
STD8			20503.53	1.60	2.73	2.72	1.96	3.76	4.69	4.35	0.19	4.05	5.35	4.64	0.19	4.07
SSP102	5-10 cm	5	27923.93	3.50	0.96	4.74	0.62	6.02	1.57	6.82	0.17	5.85	1.80	7.01	0.17	5.87
SSP103	10-15 cm	5	34488.82	1.40	0.98	3.04	0.63	5.97	1.62	6.55	0.17	6.40	1.84	6.75	0.17	6.42
SSP104	15-20 cm	5	30560.34	0.90	0.15	7.16	0.10	16.92	0.24	18.35	0.18	18.33	0.28	18.58	0.18	18.29
SSP105	25-30 cm	5	36171.92	1.40	0.11	5.10	0.05	24.94	0.16	25.42	0.12	25.38	0.18	25.80	0.12	25.32
SSP106	0-5 cm	5	44872.55	2.30	2.81	2.86	1.84	3.05	4.65	3.49	0.18	2.62	5.31	3.84	0.18	2.64
SSP107	5-10 cm	5	47514.37	1.80	1.41	2.41	0.91	5.50	2.32	5.73	0.18	5.44	2.65	5.95	0.18	5.46
SSP108	10-15 cm	5	42063.45	1.70	0.22	3.28	0.09	16.39	0.31	16.63	0.11	16.54	0.35	16.83	0.11	16.56
SSP109	15-20 cm	5	36712.98	2.10	0.26	5.70	0.14	18.32	0.41	19.07	0.15	18.96	0.46	19.22	0.15	18.98
SSP110	25-30 cm	5	26066.43	1.90	0.52	3.30	0.35	9.49	0.86	9.87	0.18	9.68	0.98	10.02	0.18	9.71
BLK9			33445.28	1.80	0.00	0.00	0.00	0.00	0.00	0.00	0.00	0.00	0.00	0.00	0.00	0.00
SSP112	0-5 cm	R1	7072.63	1.60	6.65	3.58	4.48	3.31	11.12	4.61	0.18	4.32	12.70	4.87	0.18	4.34
SSP113	5-10 cm	R1	27705.01	2.20	1.76	3.48	1.17	5.55	2.93	6.18	0.18	5.77	3.34	6.38	0.18	5.79
SSP114	10-15 cm	R1	37814.47	2.60	0.29	4.94	0.18	11.60	0.47	12.33	0.17	12.06	0.53	12.49	0.17	12.07
SSP115	15-20 cm	R1	22223.73	2.50	0.16	4.80	0.11	23.53	0.27	23.89	0.19	23.76	0.31	24.08	0.19	23.71
STD9			21512.67	1.90	2.73	3.55	1.91	5.82	4.64	6.55	0.19	6.26	5.30	6.74	0.19	6.29
SSP116	35-40cm	R1	45675.65	1.80	0.01	16.50	0.01	62.03	0.02	64.16	0.19	64.13	0.02	71.68	0.20	58.47
SSP117	0-5 cm	R1	17990.05	1.90	5.99	2.69	3.95	3.30	9.94	3.81	0.18	3.30	11.35	4.13	0.18	3.32
SSP118	5-10 cm	R1	20302.86	2.00	0.93	3.86	0.62	8.34	1.56	8.97	0.18	8.75	1.77	9.12	0.18	8.77
SSP119	10-15 cm	R1	14750.34	2.20	0.33	6.96	0.19	17.04	0.52	18.28	0.16	18.14	0.59	18.41	0.16	18.17
NC6			39774.27	1.50	0.09	6.38	0.07	17.76	0.16	18.81	0.20	18.75	0.17	19.17	0.21	18.61
DUP9/SSP97	10-15 cm	5	29480.23	1.40	0.12	5.10	0.09	25.24	0.21	25.71	0.19	25.67	0.24	25.96	0.19	25.57
DUP10/SSP104	15-20 cm	5	22738.90	2.00	0.16	7.18	0.09	24.88	0.25	25.82	0.16	25.74	0.29	26.03	0.16	25.71
DUP11/SSP107	5-10 cm	5	24521.47	2.40	1.41	3.92	0.90	9.41	2.30	9.91	0.17	9.61	2.63	10.04	0.17	9.65
DUP12/SSP115	15-20 cm	R1	16085.64	2.90	0.16	6.48	0.10	14.00	0.27	15.16	0.17	14.88	0.30	15.38	0.17	14.85

Table A 9: Raw data of the $^{239+240}$Pu measurements (Batch 4)

Batch 4			Measured activites and isotopic ratios										Activity corrected to standard IAEA-447			
Sample ID	Depth	Site	^{242}Pu		^{239}Pu activity		^{240}Pu activity		$^{239+240}$Pu activity		^{240}Pu/^{239}Pu		$^{239+240}$Pu activity		^{240}Pu/^{239}Pu	
			CPS	RSD [%]	Bq kg^{-1}	RSD [%]	Bq kg^{-1}	RSD [%]	Bq kg^{-1}	RSD [%]	mass ratio	RSD [%]	Bq kg^{-1}	RSD [%]	mass ratio	RSD [%]
SSP120	15-20 cm	R1	29002.7	2.4	0.0344	10.0	0.0220	34.8	0.0564	36.1	0.1731	36.0	0.062138011	37.52638825	0.178059195	35.17660843
SSP121	35-40cm	R1	26275.33	1.60	0.04	8.85	0.00	117.01	0.04	117.33	0.01	117.32	0.05	153.69	0.01	141.32
BLK10			40080.94	0.90												
SSP124	0-5 cm	R1	26351.95	2.50	6.10	3.75	4.05	4.30	10.15	5.13	0.18	4.48	11.59	5.37	0.18	4.50
SSP125	5-10 cm	R1	36022.37	1.60	0.48	4.96	0.31	10.52	0.79	11.52	0.17	11.41	0.90	11.66	0.17	11.44
SSP126	10-15 cm	R1	20048.00	1.10	0.08	6.89	0.03	42.61	0.12	43.15	0.11	43.14	0.13	43.87	0.11	43.04
SSP127	15-20 cm	R1	24859.74	2.80	0.01	22.08	0.00	73.15	0.01	76.36	0.09	76.31	0.01	92.18	0.10	73.45
STD10			21147.46	2.00	2.78	3.36	1.97	3.28	4.74	4.25	0.19	3.75	5.42	4.54	0.19	3.76
SSP128	35-40cm	R1	18333.86	1.20	0.01	15.25	0.00	124.71	0.01	125.63	0.06	125.62	0.01	152.98	0.06	128.38
SSP129	0-5 cm	R1	22178.07	2.70	1.90	4.26	1.22	6.85	3.11	7.61	0.17	7.11	3.55	7.78	0.17	7.14
SSP130	5-10 cm	R1	36765.11	1.30	0.08	11.28	0.05	22.24	0.13	24.90	0.17	24.87	0.14	25.39	0.17	24.68
SSP131	10-15 cm	R1	32518.85	2.20	0.12	6.96	0.08	23.90	0.20	24.80	0.18	24.70	0.22	25.07	0.18	24.60
NC8			35838.32	4.80	0.04	11.55	0.02	35.33	0.06	36.85	0.17	36.54	0.07	38.05	0.18	35.82
SSP132	15-20 cm	R1	34505.68	3.20	0.03	17.89	0.02	33.55	0.05	37.89	0.15	37.75	0.05	39.81	0.16	36.86
SSP133	20-25 cm	R1	45896.77	2.20	0.04	9.75	0.02	31.28	0.06	32.69	0.17	32.61	0.07	34.00	0.17	31.94
SSP134	0-5 cm	R1	28630.49	2.80	1.22	4.03	0.80	3.69	2.01	4.69	0.18	3.76	2.30	4.96	0.18	3.78
SSP135	5-10 cm	R1	35147.90	2.70	0.40	4.11	0.26	11.42	0.66	11.84	0.17	11.52	0.75	11.98	0.17	11.55
SSP136	10-15 cm	R1	40588.43	1.80	0.10	10.46	0.05	15.31	0.15	18.45	0.14	18.36	0.17	18.86	0.14	18.30
BLK11			40733.53	3.10	0.00	0.00	0.00	0.00	0.00	0.00	0.00	0.00	0.00	0.00	0.00	0.00
SSP137	15-20 cm	R1	51676.75	2.60	0.04	11.30	0.02	25.04	0.06	27.35	0.18	27.22	0.07	28.64	0.18	26.62
SSP138	20-25 cm	R1	24747.95	2.90	0.05	15.77	0.03	21.60	0.08	26.58	0.17	26.42	0.08	27.62	0.17	26.02
SSP140	0-5 cm	R2	44686.26	2.80	0.61	4.03	0.39	8.10	1.00	8.60	0.17	8.13	1.14	8.77	0.17	8.16
SSP141	5-10 cm	R2	33474.38	2.40	0.37	4.24	0.23	11.94	0.61	12.45	0.17	12.21	0.69	12.59	0.17	12.23
STD11			18729.87	1.80	2.76	3.33	1.96	5.22	4.72	5.92	0.19	5.64	5.38	6.13	0.19	5.67
SSP142	10-15 cm	R2	33449.57	4.50	0.17	8.24	0.10	15.18	0.27	16.68	0.16	16.06	0.31	16.90	0.16	16.04
SSP143	15-20 cm	R2	43182.38	2.60	0.08	7.00	0.05	28.22	0.13	28.96	0.19	28.84	0.15	29.39	0.19	28.60
SSP144	25-30 cm	R2	28660.85	2.40	0.03	14.89	0.01	41.67	0.04	44.19	0.10	44.12	0.04	47.27	0.10	43.54
SSP145	0-5 cm	R2	35483.79	3.20	0.95	5.12	0.62	7.61	1.56	8.59	0.18	7.98	1.78	8.75	0.18	8.00
SSP146	5-10 cm	R2	24556.22	2.00	0.38	6.04	0.24	16.03	0.61	17.01	0.17	16.89	0.70	17.13	0.17	16.92
SSP147	10-15 cm	R2	43456.46	1.10	0.27	4.92	0.17	13.64	0.45	14.46	0.17	14.42	0.51	14.62	0.17	14.43
SSP148	15-20 cm	R2	46674.26	1.10	0.20	7.48	0.12	16.24	0.32	17.84	0.17	17.81	0.37	18.03	0.17	17.80
SSP149	25-30 cm	R2	33836.39	1.10	0.02	14.94	0.01	33.52	0.04	36.68	0.14	36.66	0.04	39.86	0.15	35.52
SSP152	0-5 cm	R2	38427.94	2.30	0.86	3.40	0.55	5.50	1.41	6.04	0.17	5.59	1.61	6.26	0.17	5.61
BLK12			29191.77	1.70	0.00	0.00	0.00	0.00	0.00	0.00	0.00	0.00	0.00	0.00	0.00	0.00
SSP153	5-10 cm	R2	33539.92	2.10	0.39	4.97	0.25	7.98	0.64	9.16	0.17	8.92	0.73	9.34	0.17	8.93
SSP154	10-15 cm	R2	35971.04	2.10	0.26	5.15	0.18	7.88	0.44	9.18	0.19	8.94	0.50	9.38	0.19	8.94
SSP155	15-20 cm	R2	30943.12	5.50	0.15	7.57	0.10	19.40	0.25	20.08	0.18	19.31	0.28	20.31	0.18	19.27
SSP156	25-30 cm	R2	44895.66	1.50	0.10	6.57	0.07	22.35	0.17	23.25	0.18	23.20	0.19	23.57	0.18	23.08
STD12			27771.86	2.70	2.72	3.89	1.90	4.19	4.62	5.04	0.19	4.25	5.28	5.28	0.19	4.27
SSP157	0-5 cm	R2	38427.10	4.10	1.24	6.47	0.81	8.03	2.04	9.46	0.18	8.52	2.33	9.60	0.18	8.55
SSP158	5-10 cm	R2	41603.00	1.40	0.82	2.87	0.53	4.62	1.35	5.25	0.17	5.06	1.54	5.50	0.17	5.08
SSP159	10-15 cm	R2	36013.07	2.50	0.49	5.50	0.29	12.65	0.77	13.57	0.16	13.33	0.88	13.69	0.16	13.37
SSP160	15-20 cm	R2	27923.52	1.80	0.34	3.16	0.20	13.62	0.55	13.87	0.16	13.75	0.62	14.00	0.16	13.77
SSP161	25-30 cm	R2	37652.44	2.50	0.05	10.11	0.03	36.69	0.09	37.97	0.17	37.89	0.10	38.76	0.18	37.37
NC9			35449.20	3.10	0.04	12.49	0.02	28.67	0.07	31.12	0.15	30.96	0.07	32.27	0.16	30.48
DUP13/SSP155	15-20 cm	R2	38270.46	3.30	0.16	6.67	0.10	18.79	0.26	19.67	0.17	19.39	0.29	19.88	0.17	19.35
DUP14/SSP149	25-30 cm	R2	28955.40	1.60	0.03	17.77	0.01	33.64	0.04	38.01	0.14	37.98	0.04	40.83	0.14	36.95
DUP15/SSP133	20-25 cm	R1	34436.20	2.80	0.03	12.81	0.02	17.33	0.06	21.37	0.20	21.18	0.06	23.05	0.21	20.59

Table A 10: Comparison of material redistribution at site 1 with (top) and without (bottom) the three outlier samples. The change in redistribution can be seen in replicates 3 and 4

with outliers	**Lal et al., 2013**		**IM: P =1**	**IM: P = 1.2**	**IM: P = 1.5**	**PDM**
Replicates	**L=soil loss (cm)**	**t ha^{-1} yr^{-1}**	**t ha^{-1} yr^{-1}**	**t ha^{-1} yr^{-1}**	**t ha^{-1} yr^{-1}**	**t ha^{-1} yr^{-1}**
1	7.81	6.10	11.77	9.81	7.85	5.87
2	7.36	11.34	13.37	11.15	8.92	5.53
3	18.02	39.22	31.37	26.14	20.91	13.55
4	9.14	13.97	14.59	12.15	9.72	6.87
Average	10.58	17.66	17.77	14.81	11.85	7.96
SD	5.02	14.74	9.14	7.61	6.09	3.77

without outliers	**Lal et al., 2013**		**IM: P =1**	**IM: P = 1.2**	**IM: P = 1.5**	**PDM**
Replicates	**L=soil loss (cm)**	**t ha^{-1} yr^{-1}**	**t ha^{-1} yr^{-1}**	**t ha^{-1} yr^{-1}**	**t ha^{-1} yr^{-1}**	**t ha^{-1} yr^{-1}**
1	7.81	6.10	11.77	9.81	7.85	5.87
2	7.36	11.34	13.37	11.15	8.92	5.53
3	7.29	15.87	12.69	10.58	8.46	5.48
4	4.63	7.07	7.38	6.15	4.92	3.48
Average	6.77	10.09	11.30	9.42	7.54	5.09
SD	1.45	4.47	2.70	2.25	1.80	1.09

Table A 11: Input and output parameters for long-term soil formation modelling

Site	**part**	**I**	**erosion**	**Age Soil (a)**	**sP [m yr^{-1}]**	**sDE (Model; m)**	**Empirical data soil depth (m)**
S1	0.00005	1.53	0.00025	15000	0.00025	0.454	0.45
S2	0.00015	1.23	0.00057	15000	0.00057	0.400	0.4
S3	0.00023	1.04	0.00091	15000	0.00091	0.306	0.3
S4	0.00017	1.00	0.00059	15000	0.00059	0.352	0.35
S5	0.00037	1.04	0.00139	15000	0.00139	0.300	0.3

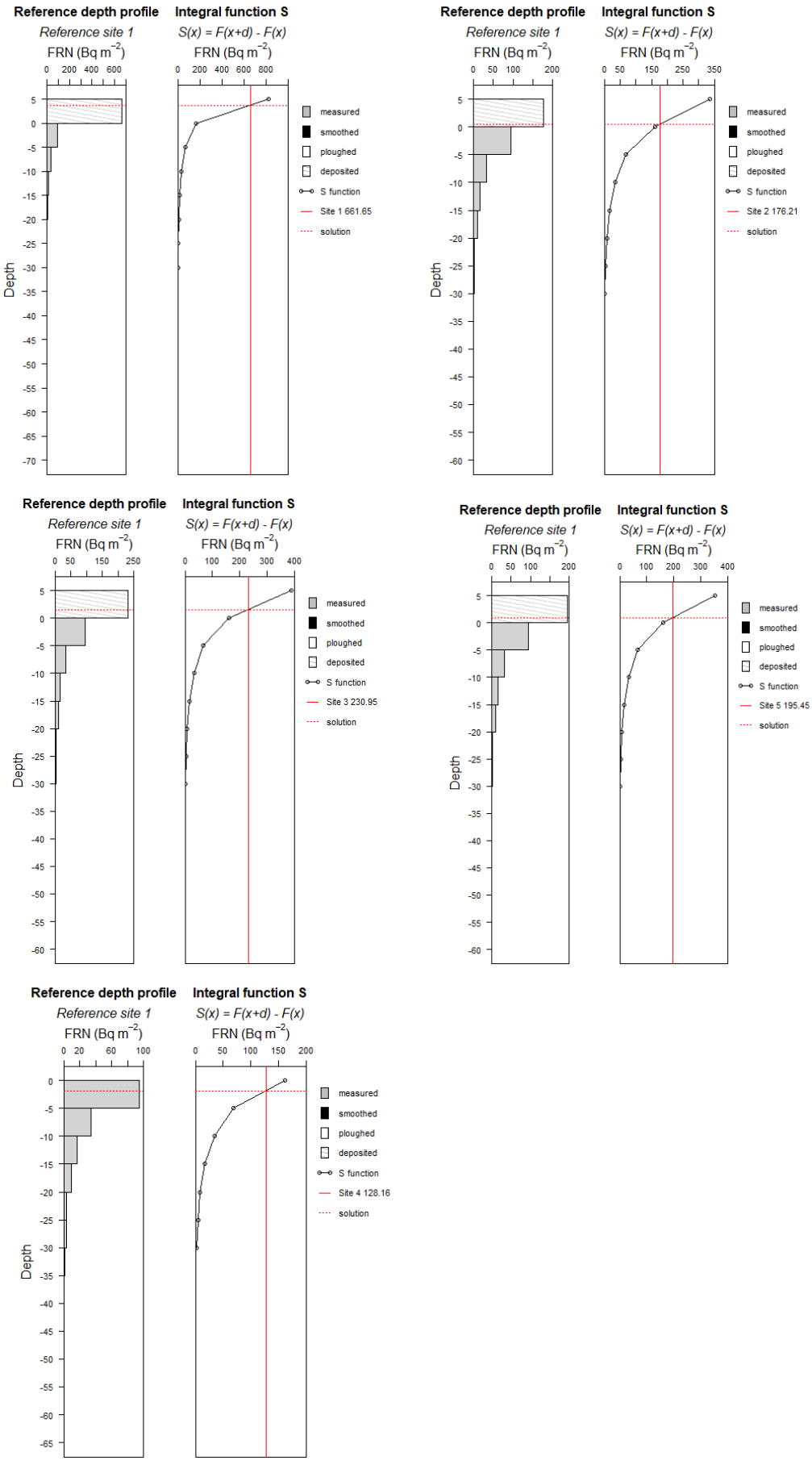

Figure 40: Modelled accumulation or erosion (last image) rate based on MODERN method.

R Codes

MODERN

```
install.packages("modeRn", repos = NULL, type="source")
# load the library
library("modeRn")

# creates a reference profile composed of 6 layers of thickness 5 cm (here: 2x3.16, da Abstand zw. Ref1 und Ref 2 10 cm dh. 2* 5 cm schritte also 6.32*2)

RDP = createReferenceProfile(FRNinv = c(94.49, 33.98, 16.59, 9.58, 3.16, 3.16), thickness =

 5, name = 'Reference sites', falloutTime = 1963, refTime = '2021-06-08', massDepth = 260.18)

plot(RDP)

# creates sampling layers of thickness 40 cm for site 1

S1 = createSamplingProfile(FRNinv = 661.65, thickness = 40, name = 'Site 1',

      falloutTime = 1963, refTime = '2021-6-08', massDepth =256.68)

# creates sampling layers of thickness 30 cm for site 2

S2 = createSamplingProfile(FRNinv = 176.21, thickness = 30 , name = 'Site 2',

      falloutTime = 1963, refTime = '2021-06-08', massDepth = 189.04)

# creates sampling layers of thickness 30 cm for site 3

S3 = createSamplingProfile(FRNinv = 230.95, thickness = 30, name = 'Site 3',

      falloutTime = 1963, refTime = '2021-06-08', massDepth = 164.65)

# creates sampling layers of thickness 35 cm for site 4

S4 = createSamplingProfile(FRNinv = 128.16, thickness = 35, name = 'Site 4',

      falloutTime = 1963, refTime = '2021-06-08', massDepth = 317.76)

# creates sampling layers of thickness 30 cm for site 5

S5 = createSamplingProfile(FRNinv = 195.45, thickness = 30, name = 'Site 5',

      falloutTime = 1963, refTime = '2021-06-08', massDepth = 187.88)

# creates smoothed layers below the reference profile

RDP_smooth1 = addSmoothedLayers(RDP, S1)

plot(RDP_smooth1, main = 'Simulated depth profile')

RDP_smooth2 = addSmoothedLayers(RDP, S2)

plot(RDP_smooth2, main = 'Simulated depth profile')

RDP_smooth3 = addSmoothedLayers(RDP, S3)

plot(RDP_smooth3, main = 'Simulated depth profile')

RDP_smooth4 = addSmoothedLayers(RDP, S4)

plot(RDP_smooth4, main = 'Simulated depth profile')

RDP_smooth5 = addSmoothedLayers(RDP, S5)

plot(RDP_smooth5, main = 'Simulated depth profile')

# sampling profiles with eroded layers Site 1

MODERN_S1 = MODERN(RDP_smooth1, S1)

plot(MODERN_S1)

print(MODERN_S1)

ER1 <-yearlyEDRates(MODERN_S1, samplingTime = 2021, falloutTime = 1963, massDepth = 256.68, sampleDepth = 40)

show(ER1)

# sampling profiles with eroded layers Site 2

MODERN_S2 = MODERN(RDP_smooth2, S2)

plot(MODERN_S2)

print(MODERN_S2)
```

```
ER2 <-yearlyEDRates(MODERN_S2, samplingTime = 2021, falloutTime = 1963, massDepth = 189.04, sampleDepth = 30)
show(ER2)
# sampling profiles with eroded layers Site 3
MODERN_S3 = MODERN(RDP_smooth3, S3)
plot(MODERN_S3)
print(MODERN_S3)
ER3 <-yearlyEDRates(MODERN_S3, samplingTime = 2021, falloutTime = 1963, massDepth = 164.65, sampleDepth = 30)
show(ER3)
# sampling profiles with eroded layers Site 4
MODERN_S4 = MODERN(RDP_smooth4, S4)
plot(MODERN_S4)
print(MODERN_S4)
ER4 <-yearlyEDRates(MODERN_S4, samplingTime = 2021, falloutTime = 1963, massDepth = 317.76, sampleDepth = 35)
show(ER4)
# sampling profiles with eroded layers Site 5
MODERN_S5 = MODERN(RDP_smooth5, S5)
plot(MODERN_S5)
print(MODERN_S5)
ER5 <-yearlyEDRates(MODERN_S5, samplingTime = 2021, falloutTime = 1963, massDepth = 187.88, sampleDepth = 30)
show(ER5)
#with Deposition Site 1
RDP_depS1 = addDepositionLayers(RDP_smooth1, 661.65, 1)
MODERN_S1 = MODERN(RDP_depS1, S1)
plot(MODERN_S1)
print(MODERN_S1)
yearlyEDRates(MODERN_S1, samplingTime = 2021, falloutTime = 1963, massDepth = 256.68, sampleDepth = 40)
#with Deposition Site 2
RDP_depS2 = addDepositionLayers(RDP_smooth2, 176.21, 1)
MODERN_S2 = MODERN(RDP_depS2, S2)
plot(MODERN_S2)
print(MODERN_S2)
yearlyEDRates(MODERN_S2, samplingTime = 2021, falloutTime = 1963, massDepth = 189.04, sampleDepth = 40)
#with Deposition Site 3
RDP_depS3 = addDepositionLayers(RDP_smooth3, 230.95, 1)
MODERN_S3 = MODERN(RDP_depS3, S3)
plot(MODERN_S3)
print(MODERN_S3)
yearlyEDRates(MODERN_S3, samplingTime = 2021, falloutTime = 1963, massDepth = 164.65, sampleDepth = 30)
#with Deposition Site 5
RDP_depS5 = addDepositionLayers(RDP_smooth5, 195.45, 1)
MODERN_S5 = MODERN(RDP_depS5, S5)
plot(MODERN_S5)
print(MODERN_S5)
yearlyEDRates(MODERN_S5, samplingTime = 2021, falloutTime = 1963, massDepth = 187.88, sampleDepth = 30)
```

Soil formation modelling based on Egli et al., 2018

```
rm(list=ls())

####initial parameter----

input<-read.csv("C:/Users/samira/OneDrive/Dokumente/Studium/Master/Masterarbeit/RCodes/R-
Code_SoilDevelopment/Input_Portugal1.csv",sep=";",header=T)

####

canDoAll<-function(part,I,erosion,yearMax){

####compute----

year<-1:yearMax

 soilDepth<-numeric()
 soilProd<-numeric()
 soilDepthEr<-numeric()

 soilDepth[1]<-part*(year[1]/(part/I))^0.53
 soilDepth[2]<-part*(year[2]/(part/I))^0.53

 soilProd[1]<-NA
 soilProd[2]<-I*(1/1.87)*(part/soilDepth[2])^.87

 soilDepthEr[1]<-NA
 soilDepthEr[2]<-soilDepth[1]

 for(i in 3:max(year)){
 soilDepth[i]<-part*(year[i]/(part/I))^0.53
 soilProd[i]<-I*(1/1.87)*(part/soilDepthEr[(i-1)])^0.87
 soilDepthEr[i]<-soilDepthEr[(i-1)]+(soilProd[i])-(erosion)}


results<-data.frame(year=year,sP=soilProd,sDE=soilDepthEr) }
 return(results)

all<-data.frame(Site=NA, ProfileName=NA, part=NA, I=NA, erosion=NA, yearMax=NA, year=NA, sP=NA, sDE=NA)

for(i in 1:nrow(input)){
print(i)
 results<-canDoAll(input$part[i],input$I[i],input$erosion[i],input$yearMax[i])
 resI<-results[results$year==input$yearMax[i],]
 all<-rbind(all,cbind(input[i,],resI))
}

all<-all[-1,]
all.df<-all
write.csv(all.df, "C:/Users/samira/OneDrive/Dokumente/Studium/Master/Masterarbeit/RCodes/R-Code_SoilDevelopment/Output/V1.txt")
```

Acknowledgment

There are many people who supported me during the process of writing this thesis.

First and foremost, I would like to thank my supervisor Prof. Dr. Markus Egli, who supported me from the start whereas it was during the field work or in the lab as well as guiding me through the data interpretation, quickly answering all my questions and giving motivating feedback.

Another important part in this thesis had Dr. Gonçalo Vieria as he not only had various sampling locations in mind but also knew how to get there and which sites would be most suitable for the research question. In addition, he connected me with various people who did and still do work in the Geopark. Among others with José Conde. He is the one to thank for the lovely old pictures of the Geopark, as he searched through the archive to find them as well as he gave useful insights about the past agricultural use of the area.

The Plutonium measurements would not have been possible without the help of Dr. Dmitry Tikhomirov, who not only showed me how to do each step of the sample preparation but also explained the chemistry basics behind it. In addition, he also measurement the samples and adapted them to the used standard, which I am very grateful for.

I would like to thank all the people working in the laboratory, amongst others Yves Brügger, who supported me with many tasks such as changing the XRF samples, explaining different methods as well as doing the oxalate measurement.

And lastly, everyone unmentioned who helped me with proof-reading, who gave thought-provoking insights or just had time for a coffee break.

Personal Declaration

I hereby declare that the submitted Thesis is the result of my own, independent work. All external sources are explicitly acknowledged in the Thesis.

27.04.2022, Uerikon

Name

Date, Place